**Universidade do Minho**
Escola de Medicina

João Vítor Lemos Afonso

# Interplay between adipose-derived stem cells and inflammatory mediators: impact on neurite outgrowth and vascular morphogenesis

janeiro de 2021

João Vítor Lemos Afonso **Interplay between adipose-derived stem cells and inflammatory mediators: impact on neurite outgrowth and vascular morphogenesis**

Uminho | 2021

**Universidade do Minho**
Escola de Medicina

João Vítor Lemos Afonso

# Interplay between adipose-derived stem cells and inflammatory mediators: impact on neurite outgrowth and vascular morphogenesis

Dissertação de Mestrado
Mestrado em Ciências da Saúde

Trabalho Efetuado sob a orientação do
**Doutor António José Braga Osório Gomes Salgado**
e do
**Doutor Nuno André Martins Silva**

janeiro de 2021

# ACKNOWLEDGMENTS

Quero começar por agradecer aos meus orientadores, António Salgado e Nuno Silva, por terem acreditado e apostado em mim, permitindo-me crescer como pessoa e como cientista neste mestrado. Foi um orgulho ser vosso orientando e partilhar estes anos convosco.

Quero também deixar um especial obrigado a todos os colegas e amigos do laboratório. Ciência faz-se em equipa. E sem vocês não estava onde estou nem tinha crescido como cresci. Agradeço também aos grandes amigos que fiz neste mestrado, especialmente à Joana, à Bruna, ao Tiago e à Gisela, e meus amigos de fora, especialmente à Bárbara, por todo o apoio que me deram e por todos os bons momentos que me fizeram passar. Levo-vos para a vida! Quero também deixar um grande obrigado ao meu amor, Rita. És das pessoas que mais contribui para eu ser quem sou e estar onde estou. Acho que nunca te vou conseguir retribuir todo o amor, apoio, carinho e paciência que tens para mim. Obrigado do fundo do coração! Por fim, quero agradecer à minha família, a qual tenho orgulho de pertencer. Sempre acreditaram em mim e tentaram dar-me as melhores condições possíveis para eu ser o melhor ser humano possível. Obrigado por tudo!

Agradeço ao Doutor Nuno Sousa, Presidente da Escola de Medicina da Universidade do Minho, Professor Jorge Correia-Pinto, Presidente do Instituto do Investigação de Vida e Saúde (ICVS), ao Doutor João Bessa, Coordenador do Domínio de Neurociências, e à Professora Doutora Patrícia Maciel, Diretora do Mestrado em Ciências da Saúde pelo apoio institucional.

The work presented in this thesis was performed in the Life and Health Sciences Research Institute (ICVS), University of Minho. Financial support was provided by grants from Prémios Santa Casa Neurociências - Prize Melo e Castro for Spinal Cord Injury Research (MC-04/17); PORTUGAL 2020 Partnership Agreement, through the European Regional Development Fund (ERDF) FEDER, through the Competitiveness Internationalization Operational Programme (POCI), and by National funds, through the Foundation for Science and Technology (FCT), under the scope of the projects TUBITAK/0007/2014; PTDC/DTP-FTO/5109/2014; POCI-01-0145-FEDER-029206; POCI-01-0145-FEDER-031392; PTDC/MED-NEU/31417/2017; NORTE-01-0145-FEDER-029968; UIDB/50026/2020 and UIDP/50026/2020. ICVS Scientific Microscopy Platform, member of the national infrastructure PPBI - Portuguese Platform of Bioimaging (PPBI-POCI-01-0145-FEDER-022122; and by the projects NORTE-01-0145-FEDER-000013 and NORTE-01-0145-FEDER-000023, supported by Norte Portugal Regional Operational Programme (NORTE 2020), under the PORTUGAL 2020 Partnership Agreement, through the European Regional Development Fund (ERDF).

## STATEMENT OF INTEGRITY

I hereby declare having conducted this academic work with integrity. I confirm that I have not used plagiarism or any form of undue use of information or falsification of results along the process leading to its elaboration.

I further declare that I have fully acknowledged the Code of Ethical Conduct of the University of Minho.

**RESUMO - Interação entre células estaminais derivadas de tecido adiposo e mediadores inflamatórios: impacto no crescimento de neurites e na morfogénese vascular**

A lesão da medula espinal (SCI) é uma condição que impede a comunicação entre o cérebro e o resto do corpo, resultando em comorbidades que diminuem a qualidade de vida dos pacientes. Após a lesão primária, vários processos bioquímicos danificam a medula espinal resultando numa variedade de eventos patológicos que dificultam a recuperação. Para além da perda neural, também ocorre um dano vascular extenso. Na procura de novas terapias, as células estaminais derivadas do tecido adiposo (ASCs) têm mostrado resultados promissores por modularem vários processos regenerativos, a nível parácrino e não-parácrino. Contudo, as ASCs ainda não desenvolveram uma reparação satisfatória. Para aumentar o potencial regenerativo destas células, vários investigadores estão a tentar precondicioná-las com diferentes estímulos, tais como moléculas inflamatórias. Enquanto está descrito que estímulos pró-inflamatórios levam a um fenótipo mais imunomodulatório das ASCs, pouco se sabe sobre os efeitos desta estimulação a um nível neural e vascular. Assim, neste trabalho, pretendeu-se perceber como é que moléculas pró e anti-inflamatórias podiam influenciar o potencial angiogénico e neuroregenerativo das ASCs em três níveis: contacto indireto, direto e secretoma.

Para isso, desenvolveu-se um sistema que avalia parâmetros morfológicos de estruturas semelhantes a vasos produzidas por células endoteliais da veia umbilical humanas (HUVECs). Com este sistema, a estimulação pró-inflamatória com lipopolisacarideo (LPS) e interferão- γ (IFN- γ) aumentou o potencial vascular do secretoma das ASCs. Porém, este efeito não se observou na co-cultura indireta. No ensaio de contacto direto não houve formação destas estruturas. A estimulação com IL-10 não alterou o comportamento das ASCs. Explantes de gânglios da raiz dorsal (DRG) foram usados para avaliar o potencial neuroregenerativo das ASCs. Não foram observadas diferenças entre os grupos estimulados e não estimulados relativamente à área de neurites, ao seu tamanho e padrão de arborização. Contudo, o secretoma de ASCs conseguiu induzir o crescimento de neurites em contraste com o grupo controlo. Observaram-se resultados semelhantes para o ensaio de contacto direto, que estimulou o maior grau de crescimento. O ensaio de contacto indireto também levou a um crescimento robusto de neurites. Para saber quais moléculas podiam ser moduladas por estes fatores, realizou-se uma análise de expressão genética de vários fatores relacionados com os processos estudados. Apesar de alguns genes serem diferentemente expressos, não se observou um fenótipo claro. Em suma, este projeto mostrou que as ASCs podem ser moduladas por moléculas inflamatórias, mas o estímulo apropriado para fazer um melhoramento máximo destas células ainda precisa de ser clarificado.

**Palavras-chave:** Células estaminais derivadas do tecido adiposo, Crescimento de neurites, Morfogénese vascular, Pré-condicionamento inflamatório, Secretoma.

## ABSTRACT - Interplay between adipose-derived stem cells and inflammatory mediators: impact on neurite outgrowth and vascular morphogenesis

Spinal cord injury (SCI) is a condition that hampers the communication between the brain and the rest of the body, resulting in several comorbidities that decrease the patient's life quality. After the primary injury, several biochemical processes occur that damage the spinal cord resulting in a variety of interconnected pathological events that hinder the chance of recovery. Besides the neural loss, SCI also leads to a strong vascular damage. In the search for new therapies, adipose-derived stem cells (ASCs) have shown promising results due to their ability to modulate several processes related to repair, both at a paracrine and non-paracrine level. However, up until today, ASCs were unable to elicit a completely satisfactory repair. Thus, to promote a regenerative enhancement of ASCs, several researchers are trying to precondition these cells with different stimuli, for example, with inflammatory mediators. While it is well reported that pro-inflammatory stimuli alter ASCs to a more immunomodulatory profile, few reports show the effects of this stimulation at a neural and vascular level. Therefore, in this work, we aimed to understand how classical pro-inflammatory and anti-inflammatory molecules could influence the angiogenic and neuroregenerative potential of ASCs on three different levels: indirect contact, secretome and direct contact.

To do that, a system that evaluated morphological parameters of vessel-like structures created by human umbilical vein endothelial cells (HUVECs) was established. With this system, pro-inflammatory stimulation with lipopolysaccharide (LPS) and interferon-γ (IFN-γ) enhanced the vascular potential of ASCs secretome. However, this effect was lost in the indirect co-culture. No vessel-like structures were formed in direct contact assay. Stimulation with IL-10 did not alter ASCs behavior. Dorsal root ganglia explants were used to evaluate the neuroregenerative potential of ASCs. No differences between stimulated and unstimulated groups were found regarding neurite area, length and arborization pattern. However, the secretome of ASCs could induce neurite growth in contrast to the control. In the direct cell contact assay, the results were similar. Moreover, direct contact stimulated the highest neurite outgrowth. Nonetheless, indirect contact also elicited a robust formation of neurites. In order to understand which molecular players were being modulated by these factors, gene expression analysis was done to several molecules related to vascularization and axonal growth. Although it was possible to discover some altered expressed genes, no clear phenotype was observed. Overall, this project showed that ASCs are able to be modulated by inflammatory molecules but the appropriate stimuli to fully enhance these cells still needs to be further clarified.

**Keywords**: Adipose-derived stem cells, Inflammatory pre-conditioning, Neurite outgrowth, Secretome, Vascular morphogenesis.

# TABLE OF CONTENTS

# ABBREVIATIONS

## A

**Ang-1:** Angiopoietin 1.

**ASCs**: Adipose tissue-derived stem/stromal cells.

## B

**BBB:** Blood-brain barrier.

**BDNF:** Brain-derived neurotrophic factor.

**bFGF**: Basic fibroblast growth factor.

**BM-MSCs**: Bone marrow mesenchymal stem cells.

**BSCB:** Blood-spinal cord barrier.

## C

**CD**: Cluster of differentiation.

**CNS**: Central nervous system.

**CXCL**: Chemokine C-X-C ligand.

## D

**d:** Cohen's d.

**DAPI**: 4′,6-Diamidino-2-phenylindole dihydrochloride.

**DMEM**: Dulbecco Modified Eagle Medium.

**DRG**: Dorsal root ganglia.

## E

**ECM**: Extracellular matrix.

**EGM**: Endothelial growth medium.

**EGS**: Endothelial growth supplement.

## F

**FBS**: Fetal Bovine Serum.

**FGF-2**: Fibroblast growth factor 2.

## G

**GADPH:** Glyceraldehyde 3-phosphate dehydrogenase.

## H

**HUVECs:** Human umbilical vein endothelial cells.

**HBSS:** Hank's Balanced Salt Solution buffer.

## I

**IFN-γ**: Interferon-gamma.

**IL**: Interleukin.

## L

**LPS**: Lipopolysaccharides.

## M

**MSCs**: Mesenchymal stem/stromal cells.

## N

**NBCS**: Newborn Calf Serum.

**NGF:** Nerve growth factor.

**NSCs**: Neural stem cells.

**NVU**: Neurovascular unit.

## P

**P**: Passage.

**p:** p-value.

**PBS**: Phosphate-buffered saline.

**PBS-T**: Phosphate-buffered saline with 0.3 % Triton.

**PenStrep**: Penicillin/Streptomycin.

**PFA**: Paraformaldehyde.

**PNS**: Peripheral nervous system.

**PPIA:** Peptidylprolyl isomerase A.

## Q

**qPCR**: Quantitative polymerase chain reaction.

## S

**SCI**: Spinal cord injury.

**SD:** Standard deviation.

## T

**TLR**: Toll-like receptor.

**TNF-α**: Tumor necrosis factor-alpha.

**Trypsin-EDTA**: Trypsin-ethylenediaminetetraacetic acid.

## U

**UM-MSCs**: Umbilical cord mesenchymal stem cells.

## V

**VEGF**: Vascular endothelial growth factor.

**VWF**: Von Willebrand Factor.

## Others

**α-MEM**: Minimum Essential Medium – alpha.

**$\eta^2$:** eta-square.

**$\omega^2$:** omega-square.

**3D**: Three dimensional.

# LIST OF TABLES

# LIST OF FIGURES

# 1. Introduction

## 1.1 Nervous system

The nervous system is responsible for the communication, control, and coordination of the different body parts. In humans, the nervous system is composed of two branches: the central nervous system (CNS) and the peripheral nervous system (PNS). The latter is composed of nerves that are connected to the CNS, transmitting signals to and from different body regions (Barker & Cicchetti, 2012; Stanfield, 2012).

On the other hand, the CNS is composed by the brain and the spinal cord (**Figure 1A**) (Barker & Cicchetti, 2012; Stanfield, 2012). Although the multitude of brain functions range from cognition processes to motor control, its main function is to process and integrate the information coming from different stimuli (the environment or own organism) and react with appropriate responses to the rest of the body to ensure homeostasis (Barker & Cicchetti, 2012; Stanfield, 2012).

Complementing this body processor, the spinal cord acts as a bridge between the brain and the rest of the body, being responsible for the transmission of nerve signals to and from the periphery (Barker & Cicchetti, 2012; Stanfield, 2012).

## 1.2 Spinal cord

The spinal cord is a tubular structure that serves as a communication line between the brain and the peripheral nerves. More specifically, it transmits sensorial information from the sensory neurons to the brain, and also sends nerve signals through motor neurons from the brain to the body (Barker & Cicchetti, 2012; Stanfield, 2012). Furthermore, the spinal cord also presents brain-independent reflexes and neural circuits, termed central pattern generators, responsible for rhythmic movement control (Silva *et al.*, 2014).

Anatomically, in humans, the spinal cord extends from the medulla oblongata (at the base of the brain) to the first lumbar vertebra (Barker & Cicchetti, 2012; Silva *et al.*, 2014). Additionally, the spinal cord is segmented, with two pairs of nerve roots emerging both dorsally and ventrally, at each segment, making the connection to the PNS (Barker & Cicchetti, 2012; Stanfield, 2012). These roots are classified according to their functional and anatomical characterizations (**Figures 1A** and **1B**).

On one hand, dorsal nerve roots are composed of afferent sensory neurons with cell bodies grouped in ganglia, generating structures designated dorsal root ganglia (DRG) (Barker & Cicchetti, 2012; Stanfield, 2012). On the other hand, ventral roots are responsible for carrying the efferent motor

neuron axons that enervate the different body parts and whose cell bodies are located in the spinal cord (**Figure 1C**) (Barker & Cicchetti, 2012; Stanfield, 2012). Each dorsal root merges with the corresponding ventral root originating 31 symmetric pairs of spinal nerves (Stanfield, 2012).

Each segment of the spinal cord and its corresponding spinal nerves are designated according to its corresponding location in the vertebral column. In humans, this results in 8 pairs of cervical nerves (enervating the neck, shoulder, arm, and hand), 12 pairs of thoracic nerves (enervating the chest and the abdomen region), 5 pairs of lumbar nerves (associated with the hip, legs, and feet), 5 pairs of sacral nerves (that supplies the genital area) and 1 coccygeal nerve (enervating the skin over the coccyx) (**Figures 1A** and **1B**) (Silva *et al.*, 2014; Stanfield, 2012). Because the spinal cord is smaller than the vertebral column, all nerves below the second pair of lumbar nerves become a nerve bundle, termed *cauda equina,* emerging from the spinal cord to innervate the corresponding segments (**Figure 1A**) (Barker & Cicchetti, 2012; Stanfield, 2012).

Furthermore, in the spinal cord, neurons are organized in two distinct regions: white and gray matter (**Figure 1C**) (Stanfield, 2012). The first is mainly composed of axons, being found in the most external zone of the spinal cord, appearing white due to the presence of myelin (Stanfield, 2012). The white matter also presents an organization according to the class to which the neuron belongs (e.g. pain, sensation, touch, motor) (Barker & Cicchetti, 2012; Stanfield, 2012).

The gray matter is concentrated inside the spinal cord within a butterfly-shaped region, being composed of cell bodies, interneurons, dendrites of efferent neurons, and axon terminals of afferent neurons (Stanfield, 2012). Moreover, the gray matter is also divided into ventral and dorsal sides with two horns in each region. Dorsal horns are the structures where afferent neurons synapse with interneurons or sensory neurons, while ventral horns accommodate the dendrites and soma of the efferent neurons (Stanfield, 2012).

Besides neurons, the spinal cord is also composed of glial cells. These non-neuronal cells can be divided into astrocytes, who support neuronal functions, oligodendrocytes, responsible for axon myelination, and microglia, which are specialized embryonic-derived macrophages that are part of the CNS immune system (Barker & Cicchetti, 2012; Stanfield, 2012).

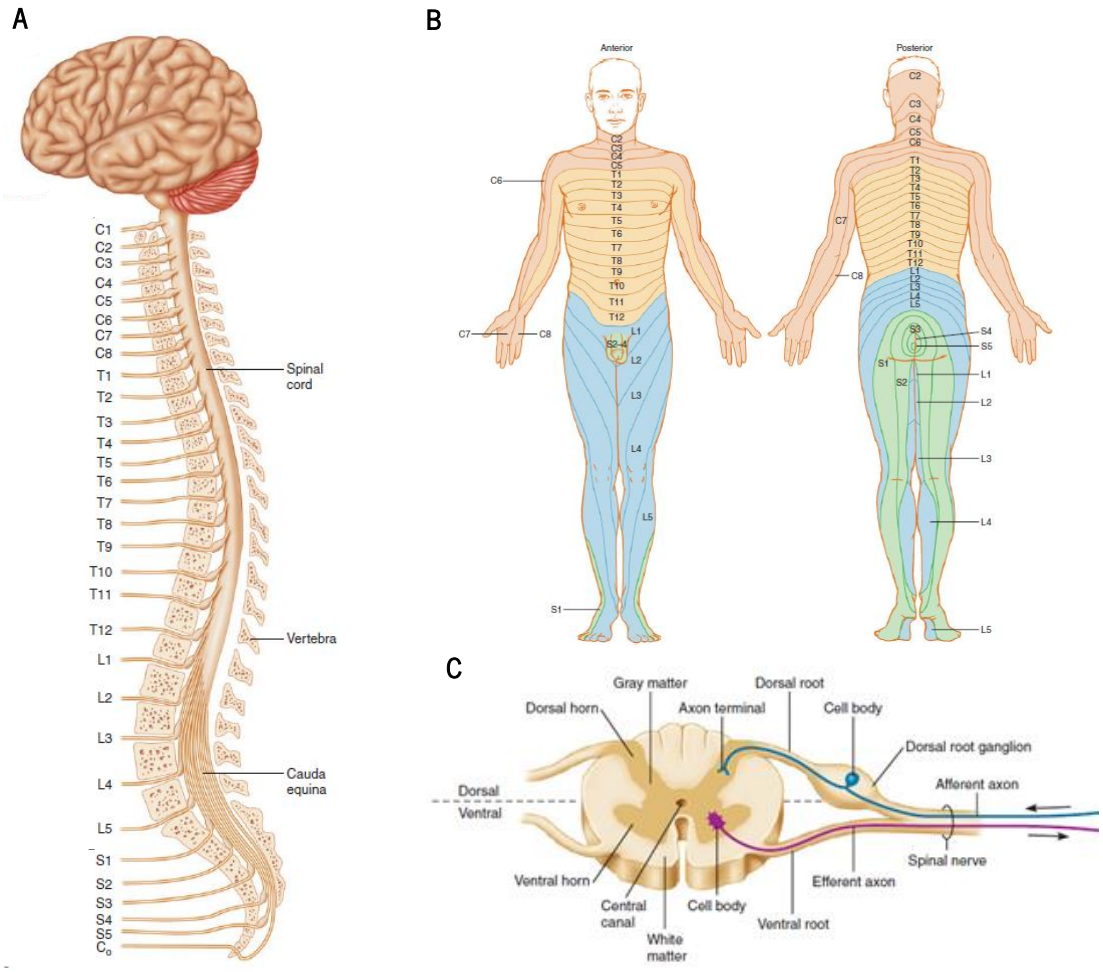


**Figure 1: Central nervous system (CNS) basic representation. (A)** CNS basic anatomy depicting the brain, the spinal cord, and its corresponding levels; **(B)** Human dermatome showing how different nerve levels affect different body regions; **(C)** Transversal section of the spinal cord highlighting the gray and white matter, the roots, the horns, and the efferent and afferent neurons. All figures were adapted from Stanfield. (Stanfield, 2012).

## 1.2.1 Spinal cord protection and blood supply

The spinal cord has several layers of protection. The first layer is the vertebral column, which is composed of vertebrae and intervertebral discs and offers physical protection to the spinal cord (Stanfield, 2012). Additionally, three membranes termed meninges protect the spinal cord and have an analogous structural organization to the cranial meninges. Namely, these are dura mater, arachnoid mater and pia mater (**Figure 2A**) (Stanfield, 2012). The final layer of protection to the spinal cord is the blood-spinal cord barrier (BSCB) (**Figure 2B**). Similar to the blood-brain barrier (BBB), this component offers selective permeability between the CNS and the bloodstream (Barker & Cicchetti, 2012; Stanfield, 2012). This allows the protection from potentially harmful substances while playing a role in nutrient and metabolic transport (Stanfield, 2012; Wilhelm *et al.*, 2016). In order to achieve this high degree of selectivity, CNS endothelial cells have a low number of membrane fenestrations, restricting the free transcellular molecule transport (Bartanusz *et al.*, 2011). Moreover, paracellular transport is

also limited due to the high number of tight junctions present between these cells (Bartanusz *et al.*, 2011). Additionally, these cells also feature an enzymatic barrier that metabolizes biologically active substances such as catecholamines, acetylcholine, and some peptides (Wilhelm *et al.*, 2016). Therefore, specialized transporters are needed to allow different molecules to cross these barriers (Wilhelm *et al.*, 2016).

Additionally, endothelial cells from the BSCB are involved by a basement membrane, pericytes, and astrocytic endfeet processes (Bartanusz *et al.*, 2011). The basement membrane is mainly composed of proteoglycans and laminins (Bartanusz *et al.*, 2011). While this component is not well studied, it seems to offer structural support by providing a matrix where cells can anchor and also contribute to the barrier function of endothelial cells (Bartanusz *et al.*, 2011; Xu *et al.*, 2019). Pericytes also have an important role on these cells, by influencing angiogenesis, barrier formation and maintenance, affecting blood flow regulation, and clearing of some possible hazardous molecules (Armulik *et al.*, 2010; Winkler *et al.*, 2011). Finally, although astrocytes feature a wide heterogeneity, their common function is to support the development and maintenance of the CNS barriers (Alvarez *et al.*, 2013). Besides secreting molecules like vascular endothelial growth factor (VEGF) and angiopoietin 1 (Ang-1), which are necessary for angiogenesis, vascular stabilization, and permeability control, astrocytes also play a role in CNS metabolism, mediating glucose and water transport between CNS and the blood (Alvarez *et al.*, 2013; Bartanusz *et al.*, 2011).

Besides these principal components of the BSCB and the BBB, other cells also may participate in the modulation of the aforementioned functions, namely microglia, oligodendroglia, vascular smooth muscle cells, and neurons (Winkler *et al.*, 2011). This cross-communication occurring between the different cell types contributes to the maintenance of the CNS homeostasis. This unit composed of neuronal and non-neuronal cells is termed neurovascular unit (NVU) (Alvarez *et al.*, 2013; Bartanusz *et al.*, 2011; Winkler *et al.*, 2011).

Although the general structure and molecular composition of the two barriers are similar, there are some differences between the BBB and BSCB. For instance, although pericytes present a higher vessel coverage in the CNS than in the periphery, the spinal cord has less pericyte coverage than the brain (12 to 32 % less) (Armulik *et al.*, 2010; Winkler *et al.*, 2011). Coupled with this, spinal cord endothelial cells show decreased expression of tight and adherence junctions, which overall contributes to the higher permeability of the BSCB (Bartanusz *et al.*, 2011; Wilhelm *et al.*, 2016). Moreover, there are also regional differences inside the spinal cord. For example, the gray matter has a higher capillary density than the white matter, which can be attributed to the higher synaptic activity and metabolic demand of

neuron cell bodies (Wilhelm *et al.*, 2016). Further differences are found among the different types of blood vessels. These are divided into arteries, capillaries, and veins and while all types exhibit barrier function, the related biochemical and biophysical properties seem to be more expressed in capillaries than in larger vessels. Moreover, venules present a looser arrangement of junctional strands than capillaries (Wilhelm *et al.*, 2016).

Another key feature of the BSCB to keep in mind is the vessel distribution along the cord (**Figure 2C**). Regarding arterial supply, the spinal cord is mainly irrigated by three longitudinal arteries: one anterior spinal artery and a pair of posterior spinal arteries, all branching from the vertebral artery (Felten *et al.*, 2016; Tran & Yao, 2018). Furthermore, below the cervical region, blood flow in these longitudinal arteries is reinforced by radicular arteries (Felten *et al.*, 2016). Moreover, the posterior spinal arteries and the anterior spinal artery reconnect forming an arterial vasocorona, encircling the spinal cord and supplying blood to its peripheral parts (Felten *et al.*, 2016). Additionally, longitudinal arteries branches of the central arteries penetrate the spinal cord, delivering oxygen and nutrients to the gray and white matter (Felten *et al.*, 2016). On the other hand, spinal cord venous drainage is less complex than the arterial system. A net of veins perforates the spinal cord uniformly and symmetrically, draining intramedullary blood to the posterior and anterior spinal veins. In turn, these veins drain into the plexus situated in the pia mater and the epidural space, and then to the rest of the major body veins (Felten *et al.*, 2016; Tran & Yao, 2018).

## 1.3 Spinal cord injury

Spinal cord injury (SCI) is a condition where the spinal cord is damaged either by a force, termed traumatic SCI, or by an internal insult, like ischemia or auto-inflammatory diseases, termed non-traumatic SCI. Traumatic SCI is the most common, with falls and road accidents representing its major underlying causes (James *et al.*, 2019). Overall, SCI incidence is higher in elder people (>70 years), although there is a peak of incidence in cervical lesions in males between 20 and 40 years (James *et al.*, 2019). Moreover, it is estimated that around 27 million people suffer from this condition, with more than 900 thousand new cases appearing every year all around the globe (James *et al.*, 2019). Considering just Portugal, over 90 thousand patients are living with SCI, with 2 thousand new cases occurring every year (James *et al.*, 2019).

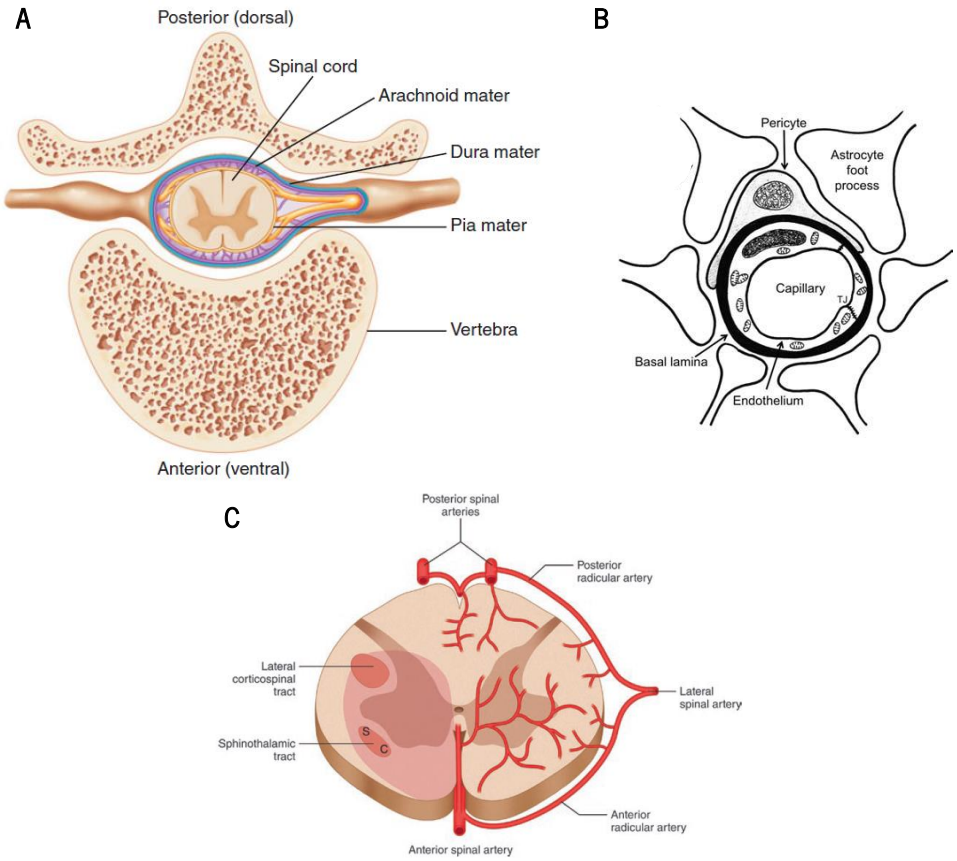


**Figure 2: Spinal cord protection and blood supply. (A)** Schematics of bone and membrane protection of the spinal cord, highlighting the vertebrae and the 3 meninges: dura mater, arachnoid mater and pia matter; **(B)** Blood-spinal cord barrier, with emphasis on the pericytes, astrocytes, basal lamina (basement membrane), presence of tight junctions and lack of fenestrations; **(C)** Schematics of a transversal view of the spinal cord arterial distribution. **(A)** Adapted from Stanfield (Stanfield, 2012); **(B)** Adapted from Bartanusz *et al.* (Bartanusz *et al.*, 2011); **(C)** Adapted from Kaiser *et al.* (Kaiser *et al.*, 2019).

As the spinal cord plays an important role in the communication between the brain and the rest of the body, damage to this organ will affect several body functions. Usually, this is translated into loss or decreased function on the organs below the injury. Moreover, the extent of these lost functions is correlated with the injury level as well as with its severity (Silva *et al.*, 2014).

The most visible consequence of SCI is the loss of motor and sensory functions. Despite the daily problems triggered by these disabilities, several other consequences occur in patients' life. For instance, several SCI patients develop respiratory and cardiac disturbances, as well as a loss of bowel and bladder control and altered sexual function (Silva *et al.*, 2014). Coupled with this, up to 80 % of these patients can suffer from nociceptive pain (coming from destroyed non-neuronal tissue) and/or neuropathic pain (from damaged neuronal tissue) (Hagen & Rekand, 2015). Also, several infections might occur in these people. For example, pressure ulcers can form due to the lack of mobility and sensory perception of SCI patients, which further prolongs their immobility time and may progress into a larger infection (Kruger *et al*, 2013). Additionally, SCI patients are also affected at a social level. For instance, almost 65 % of adults with SCI are unemployed (Ottomanelli & Lind, 2009). Also,

misconceptions, negative attitudes, and lack of infrastructures that facilitate the motility of SCI patients contribute to the exclusion of these people from society. Adding to this, their high degree of dependence may lead to anxiety and depression, which further plays a negative role in patient recovery and general health (Müller *et al.*, 2017).

Overall, all of these comorbidities combined lead to higher chances of premature death when compared with people without SCI (Savic *et al.*, 2017; Shao *et al.*, 2011; Soden *et al.*, 2000).

### 1.3.1 SCI pathophysiology

SCI has a complex pathophysiology with a high degree of heterogeneity between lesions. However, it can be separated into different overlapping phases: primary and secondary injury. The primary injury occurs as a consequence of the initial insult, resulting in the disruption of the spinal cord cellular and tissue architecture. This leads to a cascade of events termed secondary injury, responsible for the majority of the damage (Silva *et al.*, 2014).

In a first instance, along with cellular disruption, the BSCB is breached, resulting in increased permeability to peripheral components like immune cells and cytokines (Alizadeh *et al.*, 2019). Neutrophils are the first immune cells to arrive and infiltrate the lesion site through damaged blood vessels, being followed by macrophages some days later (Alizadeh *et al.*, 2019; Donnelly & Popovich, 2008). Together with microglia, these cells mainly exert phagocytic activity, necessary for debris cleaning. Additionally, T and B-cells activated against CNS antigens infiltrate the spinal cord, releasing inflammatory molecules, stimulating macrophages/microglia, and promoting cell death (Jones, 2014). Although beneficial in a first instance, the nefarious environment at the lesion maintains the phenotype of these immune cells in a pro-inflammatory state (Monteiro *et al.*, 2018). This activation profile promotes the release of more inflammatory, growth-inhibitory, and cytotoxic molecules, exacerbating the harm to the spinal cord and impairing a regenerative response. Furthermore, as lymphocytes become autoreactive, i.e, react against own body antigens, the normal tissue that is initially spared become the target of these cells (Donnelly & Popovich, 2008; Jones, 2014). Moreover, immune cells increase their numbers at the injury site throughout time (Alizadeh *et al.*, 2019). The combination of the increased number of immune cells present at the injury site with their exacerbated pro-inflammatory state contributes to a dysfunctional immune response intensifying the secondary injury.

Several other processes add to the lesion complexity. For instance, after SCI, glutamate concentration increases in the extracellular space, resulting in overactivation of glutamate receptors and, consequently, excitotoxicity and cell death (Alizadeh *et al.*, 2019; Silva *et al.*, 2014). Under

physiological conditions, glutamate is able to trigger the influx of $Ca^{2+}$ into neurons, glia, and endothelial cells. However, during glutamate excitotoxicity, an aberrant cytosolic and mitochondrial increase of $Ca^{2+}$ occurs, activating several cell death pathways (Alizadeh *et al.*, 2019). Additionally, mitochondrial dysfunction leads to ATPase failure and ionic imbalance of $Na^{+}$ and $K^{+}$, which, in turn, leads to cell membrane depolarization and a higher degree of ATPase failure. Altogether, these events, coupled with the immune cells reactivity, induce an increase in free radicals which leads to glycolysis failure, ATP depletion, and lipid peroxidation (Alizadeh *et al.*, 2019; Silva *et al.*, 2014). Lipid peroxidation leads to cytotoxic byproducts, such as 4-hydroxinonenal and 2-propenal, and destabilizes cellular membranes increasingly contributing to ionic imbalance (Silva *et al.*, 2014).

All these processes increase cell death at the injury site, at a neuronal and non-neuronal level. Moreover, cell death releases molecules that exacerbate the secondary injury, either by contributing to a pro-inflammatory state or by inhibiting a possible regenerative response (Alizadeh *et al.*, 2019; Silva *et al.*, 2014). In fact, when oligodendrocytes die, myelin is fragmented into debris that is highly inhibitory for axonal regeneration (Hutson & Di Giovanni, 2019; Silva *et al.*, 2014). It was also shown that this debris can exacerbate the pro-inflammatory state of macrophages, deepening the inflammatory imbalance (X. Wang *et al.*, 2015). These processes continue on the following days, with an increase in demyelination and cell death.

To contain the damage spreading, there is the formation of a physical barrier around the lesioned site, known as glial scar, composed by activated astrocytes, macrophages, microglia, fibroblasts, and extracellular matrix (ECM) molecules (Alizadeh *et al.*, 2019; Cregg *et al.*, 2014). After the injury, astrocytes become hypertrophic, swelling in size and increasing the expression of intermediate filament proteins, forming a physical barrier around the injury (Alizadeh *et al.*, 2019; Cregg *et al.*, 2014). While astrocytes form this barrier, microglia and macrophages occupy the innermost portion of the scar. Along with this, fibroblasts secrete ECM molecules like fibronectin, collagen, and laminin and, also, axon-repulsing molecules, thus forming a fibrotic scar (Cregg *et al.*, 2014). Moreover, the production of chondroitin sulfate proteoglycans, a sugar that highly inhibits axonal regeneration, is increased (Alizadeh *et al.*, 2019; Silva *et al.*, 2014). Taking this into account, although, in an acute phase, the glial scar functions as a barrier to contain immune cells and prevent the spreading of tissue damage, in a chronic phase, it functions as a chemical and physical barrier to axon regrowth. Additionally, there is the possibility of the formation of a cystic cavity, aggravating the chances of possible recovery (Silva *et al.*, 2014).

Although several processes contribute to the inhospitable environment found at the injury site, special attention should be given to the vascular changes that occur following SCI. Besides the relevance of blood flow alterations after the lesion from a clinical point of view, endothelial cells also participate in almost every secondary process of the injury. Accordingly, special importance will be given in this thesis to the endothelial role after SCI.

### 1.3.2 Vascular alterations after SCI

Throughout time, several reports demonstrated that the vascular and nervous systems are not independent, being in constant communication from development to disease, meaning that phenotypic alterations in each system lead to reciprocal alterations in the other (Carmeliet, 2003; Paredes *et al.*, 2018; Tam & Watts, 2010; Wälchli *et al.*, 2015). One of the earliest findings of this interaction comes from Andreas Vesalius, in the 16th century, where he described the similarities between the vascular and the neural patterning, stating the beginning of a neurovascular link (Wälchli *et al.*, 2015). However, only almost half a millennium later, evidence from the importance of this interaction started to appear. Indeed, the first description of a barrier between CNS and peripheral tissue only appeared in the early 20th century by the experiments of Goldman (Tam & Watts, 2010).

Years later, the work of Stewart and Wiley, in 1981, showed that CNS cells could provide the appropriate cues to induce the unique features of nervous system endothelial cells to non-CNS endothelial cells. In addition to this, the authors showed that CNS parenchyma could provide signals that induce endothelial sprouting towards the CNS (Stewart & Wiley, 1981). Since then, several reports have elucidated the mechanisms behind these interactions. For instance, it was demonstrated that, during development, endothelial cells and nerves share several common signals and pathways, with almost simultaneous growth and maturation (Carmeliet, 2003; Paredes *et al.*, 2018). Additionally, the growth cone of a nerve is often compared to the tip cell of a sprouting vessel, since both exhibit filopodia and lamellipodia structures and are influenced by common guidance molecules (Tam & Watts, 2010; Wälchli *et al.*, 2015). Beyond these shared molecular and cellular mechanisms, neuronal activity also influences cerebrovascular patterning during development as well as cerebral blood flow, in adulthood (Paredes *et al.*, 2018). Furthermore, conditions that stimulate neurogenesis also seem to trigger angiogenesis (Carmeliet, 2003).

Consequently, endothelial cells are also able to influence neural development and growth. For instance, blood vessels secrete factors capable of influencing neural stem cells (NSCs) behavior in adulthood (Paredes *et al.*, 2018). Supporting this fact, endothelial cells and NSCs are found in the

same CNS niches, where NSCs proliferate in small clusters around dividing capillaries (Carmeliet, 2003). However, the impact of endothelial cells on development neurogenesis is still to be totally elucidated (Paredes *et al.*, 2018). Interestingly, endothelial cells can also act as guides to newborn neurons and axon projections (Dray *et al.*, 2009; Grasman & Kaplan, 2017). Furthermore, these cells can also act paracrinally in order to enhance axonal growth (Grasman & Kaplan, 2017). Besides these intrinsic roles of endothelial cells in neuronal homeostasis, blood vessels also function as transporters of oxygen, nutrients, growth factors and other molecular signals that impact normal neural function both in the developing and adult brain (Tam & Watts, 2010).

As already stated, the interdependence between the nervous and vascular systems means that damage to either one disrupts the other. Therefore, in SCI, the vascular changes that occur should not be underestimated given the importance of this system to normal neuronal function. Actually, the idea that vascular disruption occurs after SCI came from the early work of Allen in dogs with contusive SCI (Allen, 1914). Following SCI and as a consequence of the primary injury, several vascular networks are disrupted, resulting in hemorrhage at the epicenter (Tran & Yao, 2018). Depending on the extent of blood loss, hypovolemia can occur, which is a state of decreased intravascular volume (Alizadeh *et al.*, 2019). This can be aggravated into a hypovolemic shock, a life-threatening condition, in which the amount of blood inside the human body is insufficient to let the heart pump, resulting in hypotension with tachycardia (Mataliotakis & Tsirikos, 2016; Popa *et al.*, 2010). Besides this, the hemorrhage induces vasospasms and allows fluid accumulation which in turn increases tissue pressure, enhancing the damage (Alizadeh *et al.*, 2019; Mataliotakis & Tsirikos, 2016). This disruption of vascular supply leads to hypoperfusion, in which an insufficient blood flow reaches the spinal cord and results in tissue ischemia (Alizadeh *et al.*, 2019; Tran & Yao, 2018). As neurons are highly dependent on nutrients derived from the blood like glucose, even small amounts of tissue ischemia can lead to neuronal death (Tran & Yao, 2018). Moreover, endothelial cells around the lesion may also be affected by prolonged ischemia and other secondary injury events increasing vascular damage. It should be also noted that since gray matter houses several neuronal cell bodies, corresponding to a higher blood vessel density, it is more prone to ischemic damage and, consequently, cell death (Alizadeh *et al.*, 2019). Additionally, it was observed that hemorrhage extension is directly correlated with the area occupied by the cystic cavity and with lesion severity (Noble & Wrathall, 1989a, 1989b).

As the vascular tone is highly regulated by nerve inputs that are damaged after SCI, several systemic vascular changes occur after the lesion, persisting even during the chronic phase (Mataliotakis & Tsirikos, 2016; Popa *et al.*, 2010). The disruption of the autonomic pathway with loss of sympathetic

input and sustained parasympathetic stimulation may lead to neurogenic shock (Mataliotakis & Tsirikos, 2016). This shock is characterized by hypotension and bradycardia derived from uncontrolled vasodilation. This reduces tissue perfusion leading to circulatory collapse (Mataliotakis & Tsirikos, 2016).

In addition to this, patients may suffer from additional peripheral vascular complications, involving low cardiac output, low blood pressure, vasodilation, and hypothermia (Popa *et al.*, 2010). Works in mice demonstrated that after SCI, endothelial permeability is augmented in several organs like the spleen, the bladder, and the kidneys, leading to tissue edema and dysfunctions in several organs (Yuan *et al.*, 2019). Actually, in injuries above T4, blood pressure tends to drop and is associated with diminished spinal cord perfusion, ischemia, and worse clinical outcome in patients (Fassbender *et al.*, 2011). In more advanced phases, several SCI patients tend to suffer from constant arterial hypotension (Popa *et al.*, 2010). Orthostatic hypotension is also observed in SCI patients, especially those with cervical and high thoracic SCI, being manifested by dizziness, headache, nausea, fatigue, and loss of consciousness when they try to alter their position (Popa *et al.*, 2010). Although the exact mechanism behind orthostatic hypotension remains to be discovered, it is mainly attributed to sympathetic nervous system dysfunction (Popa *et al.*, 2010). Altogether, this reduced blood flow results in an increase in ischemia, which leads to the loss of initially spared tissue (Tran & Yao, 2018).

During the first days after SCI, reduced blood flow may also lead to deep vein thrombosis, muscle paralysis, venodilation, and hypercoagulability. The thrombi that are consequently formed can dislodge and go to the lungs, forming a pulmonary embolism, which can be fatal (Popa *et al.*, 2010).

Loss of control of sympathetic spinal cord neurons can also lead to autonomic dysreflexia which is characterized by peaks of uncontrolled hypertension (Mataliotakis & Tsirikos, 2016; Popa *et al.*, 2010). Although several mechanisms contribute to this, it is mainly characterized by aberrant impulses from afferent neurons that, due to the injury, no longer connect with the brain, hyper-stimulating the sympathetic neurons present at the spinal cord (Popa *et al.*, 2010). This leads to the release of norepinephrine and dopamine, increasing vasoconstriction and, consequently, hypertension (Popa *et al.*, 2010). When the brain perceives this crisis, it releases inhibitory impulses that cannot be transmitted below injury level (Popa *et al.*, 2010). If this condition is left untreated it may cause seizures, hemorrhages and even death (Mataliotakis & Tsirikos, 2016; Popa *et al.*, 2010).

Besides triggering a cascade of events that leads to additional tissue damage and systemic dysfunctions by altering body homeostasis, vascular disruption following SCI also leads to local molecular and cellular adverse effects involving other mechanisms, namely endothelial cell death and

barrier dysfunction. Indeed, endothelial cell death derived from the primary insult occurs in the first 24 hours with further cell death occurring due to ischemia and ionic imbalance (Casella *et al.*, 2002, 2006; Ng *et al.*, 2011). Furthermore, endothelial cells detach from the ECM after SCI, which decreases their survival and leads to a drastic decrease in blood vessel density 24 hours after SCI (**Figure 3**) (Benton & Hagg, 2011; Cao *et al.*, 2017; Casella *et al.*, 2002, 2006; Fassbender *et al.*, 2011; Figley *et al.*, 2014; Whetstone *et al.*, 2003). As a reparative mechanism, the human body tries to reestablish the normal vasculature. In fact, 3 days after SCI, new vessels start to be formed by angiogenesis, with increased vascular density observed up to 7 days after injury (**Figure 3**) (Cao *et al.*, 2017; Casella *et al.*, 2002; Dray *et al.*, 2009; Figley *et al.*, 2014; Whetstone *et al.*, 2003). While some authors claim baseline revascularization, others claim that vessel density is increased in comparison to normal spinal cord tissue (**Figure 3**). It should be noted that these differences may be due to different analysis methods as well as different injury models. Also, in an SCI mouse model, endothelial progenitor cells were increased in the blood, suggesting vasculogenesis as a potential recovery mechanism after SCI, and not angiogenesis exclusively (Yuan *et al.*, 2019).

However, these newly formed vessels are highly dysfunctional, do not express certain barrier and nutrient transporter proteins, and do not associate with other cells. For these reasons, a functional NVU is never assembled (**Figure 3**) (Benton & Hagg, 2011; Casella *et al.*, 2002). In a rat SCI clip-compression model, although white matter perfusion is almost reestablished, the same does not occur in grey matter, especially at lesion epicenter (Figley *et al.*, 2014). These factors lead to a lack of nutrient and oxygen supply to the cells, hindering the chances of survival and regeneration (Benton & Hagg, 2011; Tran & Yao, 2018). Some authors also claim that these vessels retract along with the formation of the cystic cavity (**Figure 3**) (Casella *et al.*, 2002; Tran & Yao, 2018; Z. Zhang & Guth, 1997).

Coupled with these endothelial changes, in the first 24 hours, the BSCB is breached and its permeability is increased (**Figure 3**) (Figley *et al.*, 2014; Whetstone *et al.*, 2003). This originates disruption of the NVU, contributing to cell dysfunction and death (Benton & Hagg, 2011). As the new vessels do not associate with neurons, astrocytes, and pericytes, this cooperative unit is not effectively restored. This plays a major role in endothelial cell degeneration since, in addition to the disruption of barrier function, their deficient interaction with astrocytes influences endothelial cell protein expression (Whetstone *et al.*, 2003). For instance, after SCI, only vessels close to astrocytes expressed Glut-1, the major glucose transporter in the CNS (Whetstone *et al.*, 2003). As Glut-1 is the major glucose importer present in the CNS cells, its absence may lead to neuronal metabolic stress after SCI.

After this, between the third and seventh days after SCI, an increase in permeability is seen, correlated with the angiogenic process where destabilization of existing vessels occurs (**Figure 3**) (Benton & Hagg, 2011). Nevertheless, these new vessels still exhibit abnormal permeability (Benton & Hagg, 2011; Ng *et al.*, 2011). Although most studies focus on the acute and subacute effects of BSCB permeability, some studies show that BSCB remains compromised two months after injury (Cohen *et al.*, 2009). This permeability allows the entrance of inflammatory cells that play a major role in contributing to the secondary events following SCI. Endothelial cells can also contribute to unbalance the immune response by activating microglia, leading to more cellular damage, acting in conjugation with factors secreted by dead cells that activate the immune response (J. Y. Lee *et al.*, 2015). Controversially, newly formed endothelial cells can also modulate myeloid cell activity towards a reparative phenotype (Cohen *et al.*, 2009; He *et al.*, 2012). It seems that different contradictory stimuli are produced by these cells, being the balance between the different pro-inflammatory and pro-regenerative molecules as well the timing of each molecule essential to dictate the observed response. Nonetheless, in SCI, the predominant immune phenotype is a more pro-inflammatory one (Donnelly & Popovich, 2008).

Endothelial cells can also be influenced by the immune response. For instance, tumor necrosis factor-alpha (TNF-α) and interleukin (IL) 1β, two pro-inflammatory cytokines, are upregulated after SCI, enhancing vascular permeability (Donnelly & Popovich, 2008). Immune cells can also release enzymes such as elastase and matrix metalloproteinase-9 that enhance vascular permeability (Donnelly & Popovich, 2008). Endothelial cells may also be targeted by the exacerbated immune response, resulting in endothelial cell death (Lentsch & Ward, 2000). Furthermore, activated macrophages/microglia were detected within the same area of newly formed vessels after SCI (Casella *et al.*, 2002). Therefore, it seems that immune cells can enter the injury site either by damaged vessels or by the new vessels that are being formed. In contrast, immune cells are able to participate in the angiogenic process. For instance, macrophages, in a pro-inflammatory state, are responsible for the initiation of vessel sprouting, while macrophages in a more pro-regenerative phenotype, are responsible for pericyte attraction and vessel maturation (Maldonado-Lasunción *et al.*, 2018; Spiller *et al.*, 2014). However, in SCI, the pro-regenerative phenotype is transient, being a possible reason for the ineffective revascularization process (Monteiro *et al.*, 2018).

Adding to this, hemorrhage and ischemia can lead to ionic imbalance, free radical formation, oxygen deprivation, and metabolic alterations, contributing to the secondary injury and leading to more cell death (Alizadeh *et al.*, 2019). Endothelial cells also interact with myelin debris. Nogo-A, a major

myelin protein, acts not only as an inhibitory molecule of axonal regeneration but also as a negative regulator of CNS angiogenesis (Wälchli *et al.*, 2013). Moreover, endothelial cells can engulf myelin debris, which in turn upregulate genes associated with inflammation and matrix deposition and downregulate genes associated with cell adhesion and junction (T. Zhou *et al.*, 2019).

As endothelial cells play a major role in homeostasis and on SCI events, the regulation of endothelial function should be carefully addressed. Indeed, SCI has a complex pathophysiology with several interconnected mechanisms. This may explain why no effective treatment is yet available.

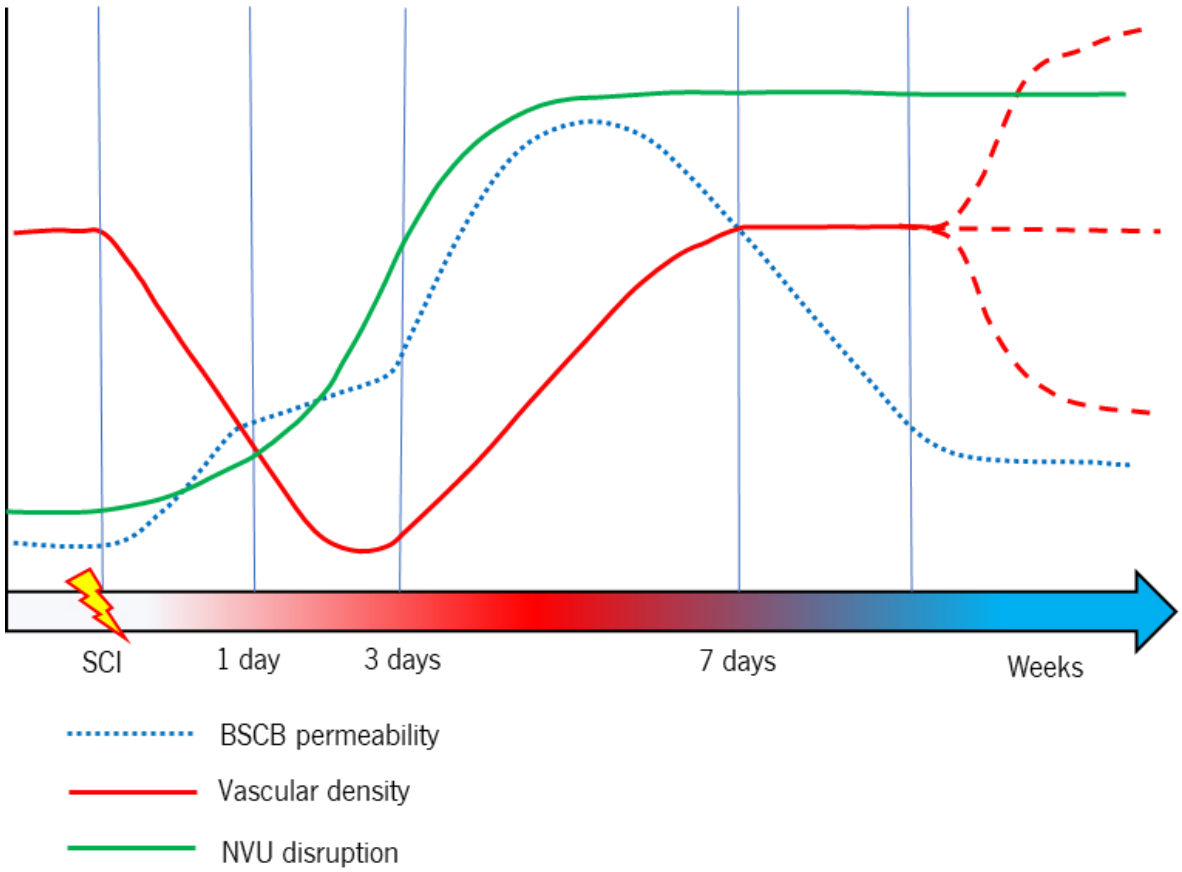


**Figure 3: Temporal course of blood vessel alterations after spinal cord injury (SCI).** With the decreased vascular density in the first hours, neurovascular unit (NVU) disruption and blood-spinal cord barrier (BSCB) permeability increases. From day 3 to day 7, there is strong angiogenic response which increases BSCS permeability. However, these new vessels are not cell-associated and therefore, NVU is not reestablished. In the coming weeks and in the chronic phase, these events are yet not well characterized, with the highest timepoint for BSCS dysfunction being two months. Furthermore, higher, lower and equal levels of vascular density prior to SCI have been reported, highlighted by the red dotted line. Either way, NVU remains disrupted, hindering the recovery chances.

## 1.4 SCI therapies

Although there is not an effective treatment for SCI patients yet, the increase of knowledge on SCI pathophysiology, the technological evolution and the creation of protocols with guidelines to conveniently handle SCI patients is allowing a faster diagnosis, better rehabilitation protocols, and consequently, better outcomes. The measures that are taken with SCI patients rely mainly on tissue

protection and preventing the spreading of damage. Typical clinical handling, following diagnosis, involves performing patient stabilization and decompression of the spinal cord (Badhiwala *et al.*, 2019; Silva *et al.*, 2014). The optimal time interval for decompression surgery remains controversial, but the best evidence suggests that better outcomes are obtained when this procedure is performed in the first 24 hours following lesion (Badhiwala *et al.*, 2019). A fundamental neuroprotective measure is to avoid hypotension in SCI patients (Hawryluk *et al.*, 2015). After that, a high dosage of methylprednisolone might be given to patients. This corticosteroid inhibits lipid peroxidation, maintains the BSCB integrity and limits the inflammatory response (Silva *et al.*, 2014). However, several adverse effects were reported, including increased risk of infection, gastrointestinal bleeding, sepsis, pulmonary embolism, and eventually death (Evaniew *et al.*, 2016; Silva *et al.*, 2014). Furthermore, its long-term benefit is controversial which made the standard guidelines to be against routine use of methylprednisolone (Evaniew *et al.*, 2016).

Despite these preventive procedures, no measures are being taken to stimulate tissue regeneration. After patient stabilization, the interventions rely mostly on palliative care and how to adapt a daily life routine to the effects of this condition (Silva *et al.*, 2014). As no effective treatment is yet available, several approaches to change it have been tested in this field. SCI therapy research can be divided mainly into two areas: neuroprotection and neuroregeneration (Ashammakhi *et al.*, 2019; Kabu *et al.*, 2015). On one hand, it is necessary to find novel strategies to protect the tissue from further damage, hampering secondary injury progression. On the other hand, it is also necessary to regenerate the damaged tissue in order to achieve normal function (Kabu *et al.*, 2015). The consensus across this field states that neuroprotective measures should be applied in early timepoints while regenerative approaches should be employed after (Kabu *et al.*, 2015). Nonetheless, several approaches that are being studied tackle both issues.

The reasons behind the lack of effective treatments for SCI lie on the complex pathophysiology associated to the condition (as already discussed) and in the intricate association between neuronal and non-neuronal cells in the spinal cord tissue. Because of this, therapies that only target neuronal cells, either neuroprotective or neuroregenerative, may be insufficient to produce clinically effective treatments. Beyond neuronal populations, SCI therapies must tackle the non-neuronal part of the injury, with some approaches being made in this direction. For instance, some researchers are trying to develop immunomodulatory therapies that shift the environment towards regeneration, while hampering the pro-inflammatory state. Unfortunately, up until today, none has shown a substantial impact on the course of the disease or in clinical outcomes (Hutson & Di Giovanni, 2019; Kabu *et al.*, 2015). Another

approach is to tackle the vascular changes that occur after injury. As a major component of the spinal cord milieu and its association to several events after SCI, diverse advantages can be gained by tackling the vascular network in SCI research. In fact, regrowth of the vascular network has been correlated with functional recovery after SCI (L. Wang *et al.*, 2017). Indeed, protection of spared vessels may allow normal nutrient and oxygen supply, decreasing ischemia and cell death (Benton & Hagg, 2011). Moreover, by protecting the vasculature, immune cell infiltration will be decreased, resulting in less tissue damage. Also, by targeting vasculature in an early phase, some comorbidities such as chronic hypotension and organ permeability may be attenuated in more advanced phases of SCI.

Still in this line of thought, due to the biphasic peaks of BSCB permeability in the acute phase (24h and 3-7 days), some authors argue that these timepoints should be used as time windows for drug delivery to the injury site (Benton & Hagg, 2011). Contrarily, it should be noted that the natural angiogenic response only occurs 3 days after injury and this period without proper nutrients and oxygen might be responsible for irreversible damage to the spinal cord. Therefore, strategies to induce vascularization should occur at earlier timepoints.

Despite this, there are some problems with revascularization strategies. One of them is the stabilization of these new vessels. As new vessels formed in the lesion epicenter tend to degrade, maintenance and protection of these newly formed structures remain a challenge (Tran & Yao, 2018). Furthermore, research should also consider that vessels formed after SCI do not associate with neuronal cells, and consequently, are not properly functional.

With this in mind, the development of a successful SCI therapy should tackle the recovery of neural cells and circuits as well as the vascular network in order to form a properly functional NVU to ensure the proper regulation of oxygen, nutrient supply and vascular tone by neuronal tissue (Tran & Yao, 2018).

### 1.4.1 Novel strategies for SCI treatment

As stated before, current research is mostly focused on neuroprotection and neuroregeneration, although some groups are trying to address other SCI issues. However, as a complex injury, interfering with one aspect of the pathophysiology may affect other related aspects of SCI. For example, by promoting regain of vascular function, one may fulfill the neural metabolic demand and, consequently, improve regeneration and functional recovery.

Neuroprotective research has been focusing on blocking glutamate excitotoxicity, hypothermia therapy, modulation of cell death pathways, and immunomodulation (Ulndreaj *et al.*, 2017). On the

other side, neuroregeneration has been focusing on increasing neuronal intrinsic signaling to regrow, altering the neuronal extrinsic inhibitory environment, bridging the injured severed spinal cord and/or modulating neuronal activity (Hutson & Di Giovanni, 2019). All of this is being explored using different therapeutic strategies. Some authors employ molecular approaches by administering different classes of molecules acting on diverse SCI pathophysiological events (Silva *et al.*, 2014). Others address the problem with tissue engineering by producing biomaterials to act as scaffolds, delivery agents or instruct cells and tissue to a more regenerative phenotype (Assunção-Silva *et al.*, 2015; Rocha *et al.*, 2020b). Still in the field of engineering, electrical stimulation in the CNS has demonstrated promising results (Courtine & Sofroniew, 2019).

Despite the majority of these strategies tend to focus on the neuronal part, some authors made some attempts in the regeneration of a vascular network. Regarding molecular approaches, the main focus has been the administration of classical pro-angiogenic molecules like VEGF and Ang-1 or anti-inflammatory drugs (Kumar *et al.*, 2017; Tran & Yao, 2018). Others have proposed biomaterials as angiogenic modulators of SCI, either by acting as a scaffold for vascular and neural regeneration or to act as a delivery vehicle of other angiogenic mediators (Haggerty *et al.*, 2018; Rocha *et al.*, 2018). Regarding electrical stimulation, a contusion SCI rat model showed improved muscle capillary distribution after epidural stimulation combined with locomotor training (Kissane *et al.*, 2019). Additionally, some authors suggest that moderate hypothermia contributes to vascular and neural network preservation after SCI (Kao *et al.*, 2011).

A widely explored therapeutic approach in SCI research, with promising results, is cellular therapy. Several cell types have been used in pre-clinical and clinical studies ranging from Schwann cells to induced pluripotent stem cells. As a matter of fact, the majority of studies regarding cell therapy for SCI have been focused on different types of stem cells, either by their differentiation potential or their support function in a regenerative response (Gomes *et al.*, 2020; Kabu *et al.*, 2015; Mothe & Tator, 2012; Silva *et al.*, 2014; Vismara *et al.*, 2017).

#### 1.4.1.1 Cell therapy

Cell therapy consists in the transplantation of cells either from the own individual (autologous) or from another person (allogeneic) to treat some disorder. The first successful cell therapy occurred in 1931 with the work of Paul Niehans and involved the transplantation of small pieces of steer parathyroid gland into a patient (Fundukian, 2011). In the mid-1950s, the work of Edward Donnall Thomas on bone marrow transplantation boosted the research on this direction (Thomas, 2000).

Regarding SCI application, the first experiments came in 1980 by the Aguayo lab where it was shown that peripheral nerve grafts promoted regeneration of CNS severed axons (Richardson *et al.*, 1980).

In the last forty years, several different cell types have been investigated and some demonstrated promising therapeutic effects (reviewed elsewhere) (Gomes *et al.*, 2020; Kabu *et al.*, 2015; Mothe & Tator, 2012; Silva *et al.*, 2014; Vismara *et al.*, 2017))

One of the most promising cell types for SCI therapy are mesenchymal stem/stromal cells (MSCs). These adult stem cells are appealing due to their high accessibility and possibility to be expanded without major ethical concerns (Cofano *et al.*, 2019). They were first described by Friedenstein, where it was shown the osteogenic potential of MSCs (Friedenstein *et al.*, 1974). In fact, these cells can differentiate into osteoblasts, adipocytes, and chondrocytes. Moreover, to be termed MSCs, the cells should be plastic-adherent and have a very defined cell surface antigen profile, namely the expression of cluster of differentiation (CD) 105, CD73, CD90 and lacking the expression of CD45, CD34, CD14 or CD11b, CD79α or CD19 and HLA-DR isotype (Dominici *et al.*, 2006). With this, several tissues were identified as possible sources of MSCs namely, the bone marrow, adipose tissue, and umbilical cord. As these new sources came to literature, questions about the stem-like properties of these cells emerged. Because of that, in 2005, the International Society for Cellular Therapy defined these cells as mesenchymal stromal cells unless a given population meet stem cell criteria (Horwitz *et al.*, 2005).

Regardless of the term, MSCs have demonstrated potential for SCI therapy by modulating inflammation, secrete neuroprotective factors, stimulate angiogenesis and axonal growth (Assunção-Silva *et al.*, 2015; Badhiwala *et al.*, 2019; Kabu *et al.*, 2015; Mothe & Tator, 2012; Ulndreaj *et al.*, 2017). These cells have a good homing capacity, being able to sense an injury and migrate towards it (Chamberlain *et al.*, 2007). However, no natural MSCs homing to the damaged spinal cord has been reported.

The first experiments involving MSCs were made thinking that these cells could differentiate into neurons and glial cells, and that their transplantation would allow replacing the lost ones due to the injury (Gomes *et al.*, 2020). However, this characteristic was not fully confirmed by other groups and it seems that the beneficial effects of MSCs come from their intrinsic capacity to shape the environment through paracrine activities and not from their differentiation potential (Arboleda *et al.*, 2011; H.-T. Zhang *et al.*, 2009).

Although their neuroprotective and neuroregenerative potential is attractive, their role in other secondary aspects of SCI might be crucial for their therapeutic efficacy. In fact, MSCs can modulate the immune response interacting with different immune cell types and promoting a normal immune

response (Bernardo & Fibbe, 2013). Indeed, transplantation of these cells into the injury site of a rat SCI model decreased macrophage infiltration, with improved functional recovery (Z. Zhou *et al.*, 2013).

Furthermore, these cells have gained a lot of clinical interest due to their ability to induce blood vessel formation (Gu *et al.*, 2017; Melchiorri *et al.*, 2014; Watt *et al.*, 2013). This led to the development of some clinical trials for cardiovascular dysfunctions with functional improvements in some of them (Watt *et al.*, 2013). Although some studies report that some MSCs can differentiate into endothelial cells, this remains controversial (Cano *et al.*, 2017; Gu *et al.*, 2017; Maacha *et al.*, 2020). Therefore, another possible mechanism for this pro-vascularization activity is MSCs paracrine activity, due to the fact that MSCs secrete several proteins and extracellular vesicles that have been associated with the vascularization process (Gu *et al.*, 2017; Maacha *et al.*, 2020). Another interesting feature of these cells is their ability to induce differentiation of endothelial progenitor cells, in a transwell system, revealing another possible paracrine mechanism for the favorable pro-vascularization response elicited by MSCs (Ge *et al.*, 2017). Moreover, MSCs are also able to remodel the ECM creating a more favorable environment for vessel formation to occur (Song *et al.*, 2016).

As these cells tend to be found in close contact with blood vessels, it is theorized that cell contact improves vessel stability, with some authors suggesting that this physical interaction is essential for tubule formation and maintenance (Pill *et al.*, 2015; Rohringer *et al.*, 2014; Watt *et al.*, 2013). Indeed, Rohringer *et al* showed that although MSCs supernatants induce endothelial cells to form some degree of tubule formation on fibrin gels, the close contact between MSCs and endothelial cells enhanced the degree of interconnection and was necessary for the stability and maturation of these vessels (Rohringer *et al.*, 2014). This is supported by the fact that MSCs have been found in close association with blood vessels in several tissues (Melchiorri *et al.*, 2014).

Bone marrow MSCs (BM-MSCs) are the most studied MSCs. Their administration to human patients seemed to improve their quality of life while maintaining a safe profile, in diverse clinical trials (Gomes *et al.*, 2020). Currently, a phase II/III clinical trial with autologous BM-MSCs transplant is being performed (NCT01676441). Nonetheless, BM-MSCs isolation still represents an invasive procedure (Gomes *et al.*, 2020). For that reason, alternative sources are being explored.

One of those sources lies in adipose tissue. Adipose tissue-derived stem/stromal cells (ASCs) were first described in 2002 and rapidly became an attractive cell source of MSCs because of their non-invasive accessibility and higher yield (Seo *et al.*, 2019). Furthermore, ASCs and BM-MSCs do not seem to differ on their angiogenic potential, and some studies even show a higher network density with the use of ASCs instead of BM-MSCs (Pill *et al.*, 2015, 2018). However, only a few studies investigated

endothelial response to both types of MSCs in the same context. Nevertheless, both types seem to stimulate the formation and maturation of vessel-like structures (Pill *et al.*, 2015).

Pre-clinical data has shown promising results also in different rodent models. While some authors reported improvements by injecting cells up to 7 days after the lesion, demonstrating their regenerative and immunomodulatory profile, others used treatments immediately after the lesion, highlighting their protective role (Gomes *et al.*, 2020; Vismara *et al.*, 2017). One interesting work from Zhou and colleagues reported that MSCs increased angiogenesis and axon preservation while reducing macrophage infiltration and lesion cavity, after a thoracic SCI. These effects were increased in ASCs when comparing to BM-MSCs (Z. Zhou *et al.*, 2013).

Adding to this, SCI dog models also have been tested for ASCs infusion with improved functional recovery, without adverse effects (Gomes *et al.*, 2020; Vismara *et al.*, 2017). This exciting data led to two phases I clinical trials with published results. Intrathecal and intravenously autologous transplants of ASCs were performed without major complications and even with some functional improvements (Hur *et al.*, 2016; Ra *et al.*, 2011). These helped in the development of new clinical trials, highlighting one that compared BM-MSCs with ASCs and one evaluating intrathecal single dose injections of ASCs (NCT03308565; NCT02981576). Taking into consideration the regenerative and protective phenotype that ASCs have shown in pre-clinical and clinical trials and their less invasive and higher yield extraction method, it seems that ASCs hold promise for a future SCI therapy.

Besides the recent advances in cell therapy, some challenges remain when using this approach. The first is to obtain a sufficient number of cells in a feasible way and at an affordable cost (Kabu *et al.*, 2015; Mothe & Tator, 2012). For instance, for the clinical trial of R-Bio (NCT01274975), 400 million cells were used in each patient (Ra *et al.*, 2011). Although ASCs are possible to obtain with high yields and expansion rates, the exact number of cells needed for human therapy is still unknown (Kern *et al.*, 2006). Also, how the SCI environment affects the regenerative potential and survival of these cells must be further studied (Cofano *et al.*, 2019; Kabu *et al.*, 2015). Additionally, the administration route is a crucial step (Cofano *et al.*, 2019; Kabu *et al.*, 2015). While intravenous injections are less invasive than intrathecal injections and MSCs have a homing ability to the injury, some authors described that MSCs administered by this route are often "trapped" in highly vascularized tissues like the lung (Chamberlain *et al.*, 2007). Therefore, a larger number of cells is required and the safety of the inclusion of MSCs in these tissues needs to be carefully assessed. Given that MSCs have a regenerative potential mainly due to their paracrine activity, a new field for SCI therapy has emerged. Some authors are now collecting the

secreted molecules (secretome) of these cells and evaluating their therapeutic potential for several CNS pathologies (Mendes-Pinheiro *et al.*, 2020; Pinho *et al.*, 2020).

#### 1.4.1.2 Secretome-based therapies

Secretome is defined as the set of factors/molecules cells secreted to the extracellular space (Vizoso *et al.*, 2017). The first works began in 2000, with Tjalsma and colleagues, who studied the pathways for protein transport and secretion of *Bacillus Subtilis* (Tjalsma *et al.*, 2000). Five years later, the work of Gnecchi and collaborators introduced the idea of using the secretome as a possible therapeutic agent (Gnecchi *et al.*, 2005). In this work, the authors demonstrated that the secretome of rat BM-MSCs could protect cardiomyocytes from hypoxic-associated damage, reduce cellular apoptosis and the infarct size of the heart in a coronary occlusion rat experimental model (Gnecchi *et al.*, 2005, 2006).

Since then, several works detailed the potential of the secretome for regenerative medicine applications and helped to develop this field (Salgado *et al.*, 2010b; Vizoso *et al.*, 2017). The use of secretome is appellative in comparison to cell-based therapies for several reasons. Firstly, its application overcomes the issue of cell survival and phenotype alteration after transplantation (Teixeira & Salgado, 2020). Additionally, secretome can be treated as a conventional pharmacological agent with safety, dosage, potency, and the possible creation of an off-the-shelf product with immediate availability for the desired treatment (Teixeira & Salgado, 2020; Vizoso *et al.*, 2017). Additionally, work from our group has shown that, *in vitro*, the secretome of ASCs collected from passage (P) 3 to P12 was able to maintain its capacity to promote neurodifferentiation and axonal growth (Serra *et al.*, 2018). As the secretome stability is maintained throughout passages, it is possible to obtain a large amount of secretome extracted from an initial cell collection, making its use more economical (Serra *et al.*, 2018). However, the same has to be confirmed for other applications and other cell types. Furthermore, mass-production, standardization and biological modifications to enhance some desired phenotype are possible (Teixeira & Salgado, 2020; Vizoso *et al.*, 2017).

The secretome is composed of two fractions: the proteic and the vesicular fraction (Pinho *et al.*, 2020; Teixeira *et al.*, 2013). The protein fraction is mainly constituted by growth factors and cytokines while the vesicular fraction comprehends vesicles containing intracellular proteins and/or RNA that act on different biological processes (Pinho *et al.*, 2020). Both fractions contain molecules involved in immunomodulation, cell survival, neuroregeneration, neurodifferentiation, axon guidance, remyelination, angiogenesis, and vasculogenesis (Cofano *et al.*, 2019; Pinho *et al.*, 2020; Salgado *et al.*, 2010b;

Teixeira *et al.*, 2013; Vizoso *et al.*, 2017). However, some authors argue that only some of the molecules present in the secretome are beneficial for these processes and it led scientists to analyze the contribution of each fraction for their therapeutic goal. Data from our lab indicates that, in a compression SCI mice model, each fraction of the secretome of ASCs by itself could not elicit the same recovery as the secretome as a whole (Pinho, 2019). It seems that the interaction between the different molecules works synergistically to produce a therapeutic effect. It should be also noted that, even though several proteins and vesicles are being characterized, the exact mechanisms in which the secretome acts are not yet described.

One attractive feature of MSCs secretome is its ability to modulate different neural and non-neural populations present in SCI. For instance, in a DRG explant, ASCs secretome induced neurite growth (Assunção-Silva *et al.*, 2018; Gomes *et al.*, 2018). Furthermore, this population of MSCs induced a higher degree of axonal growth in comparison to BM-MSCs or umbilical cord MSCs (UM-MSCs) (Assunção-Silva *et al.*, 2018). Also, in a microfluidic chamber, it was demonstrated that the secretome of UM-MSCs induces axonal regeneration in a cell body-independent way (Martins *et al.*, 2017). Moreover, the aforementioned types of MSCs could induce the same extent of neurodifferentiation (Assunção-Silva *et al.*, 2018). Additionally, secretome is also able to influence neural metabolic viability, survival, and proliferation (Fraga *et al.*, 2013; Ribeiro *et al.*, 2012; Salgado *et al.*, 2010a; Teixeira *et al.*, 2015a)

Regarding influencing non-neural cells that take part in SCI, MSCs secretome can also act in immune cells. Indeed, it reduces the inflammatory action of macrophages and T-cells, polarizing these cells from an inflammatory state to a more pro-regenerative one (Bernardo & Fibbe, 2013; Maldonado-Lasunción *et al.*, 2018). Additionally, endothelial cells are also influenced by the molecules released by MSCs. Since the first works by Gnecchi and coworkers, which demonstrated the potential of secretome for vascular regeneration, several others have tried to deepen the knowledge regarding this application. Several molecules secreted by these cells are related to the vascularization process, such as VEGF, basic fibroblast growth factor (bFGF), transforming growth factor β, platelet-derived growth factor, hepatocyte growth factor, and angiopoietins (Maacha *et al.*, 2020). Additionally, besides the diversity of angiogenic proteins present in the secretome, several angiogenic microRNAs, such as miR-31 and miR-125a, have been found in MSCs extracellular vesicles (Maacha *et al.*, 2020).

Human umbilical vein endothelial cells (HUVECs) are one of the most used cell types to study endothelial cells and the vascularization process (Staton *et al.*, 2009). Indeed, the secretome of ASCs was able to have a positive effect both on the outgrowth of HUVECs and on their vascular organization

in fibrin spheroids (Verseijden *et al.*, 2010). Moreover, the secretome of BM-MSCs could also induce these endothelial cells to form vessels in matrigel, both *in vitro* and *in vivo* (Estrada *et al.*, 2009). Furthermore, in a transwell assay, BM-MSCs could induce the differentiation of endothelial progenitor cells into mature endothelial cells through paracrine mechanisms, supporting a possible vasculogenesis approach to enhance vascularization (Ge *et al.*, 2017).

Paradoxically, different authors claim different MSCs sources as having the biggest angiogenic potential (Maacha *et al.*, 2020). As this may depend on the technical details of each research, these observations are still debatable. However, independently of the source, all seem to point to the fact that MSCs indeed support vessel formation (Maacha *et al.*, 2020). For this reason, they hold great promise in several applications ranging from ischemia to vascularization of biomaterials in tissue engineering.

Regarding the use of the secretome of MSCs to treat SCI, reports are only from pre-clinical models. Cantinieaux and colleagues used the secretome of rat BM-MSCs and injected it intrathecally for 7 days in a thoracic contusion injury model. This leads to better functional recovery, reduced cystic cavity and increased blood vessel diameter (Cantinieaux *et al.*, 2013). These results were further validated by Cizkova and coworkers in a compression injury rat model (Cizkova *et al.*, 2018). More recently, Tsai *et al* showed similar results by administering BM-MSCs secretome intravenously for 3 days in thoracic contusive injury (Tsai *et al.*, 2018). However, caution should be taken before taking the next step. Although the use of MSCs secretome as a therapy for SCI shows promising results in distinct SCI models, several challenges need to be addressed before translating it to the clinic. MSCs comprise cells from different tissue sources with variations among them (Vizoso *et al.*, 2017). Indeed, work from our lab showed that the secretome of MSCs from different tissue sources present different compositions, which may lead to differences regarding their therapeutic potential (Pires *et al.*, 2016). For instance, BM-MSCs seem to secrete more molecules related with anti-oxidant properties than ASCs or UM-MSCs, while the latter cells secreted more molecules associated with excitotoxicity protection (Pires *et al.*, 2016). Even so, it is not yet known if this different secretory profile translates into different functional outcomes. Additionally, several aspects can influence the MSCs secretome within the same tissue, namely cell density in culture flasks, medium, temperature, oxygen levels, and even gender, age and health status of the donor (Teixeira & Salgado, 2020). For instance, the collection time of the secretome has shown to differently impact mature neurons and glial cells (Ribeiro *et al.*, 2012). Moreover, 3D cultures can also modulate the secretome of these cells when comparing to 2D cultures (Teixeira *et al.*, 2016a). Lastly, the delivery strategy also influences the observed therapeutic outcomes (Veneruso *et al.*, 2019). As the mechanisms behind the therapeutic recovery are not yet understood, adding to the

mentioned factors that differently influence cell behavior and, consequently, the secretome, no optimal conditions for its application are yet established.

To fully understand the therapeutic potential of the secretome, interlaboratory standardized protocols for the use of these cells and secreted molecules should be created. Although some work has been done to address this issue, more research needs to be done to identify the optimal characteristics and procedures for the use of MSCs and their secretome in a reproducible therapeutic approach (Jung *et al.*, 2012; Teixeira *et al.*, 2016b). Even if a standardized protocol for optimal recovery, for example, in SCI, is created, it should be revised and modified when tackling other pathological conditions.

Furthermore, regarding SCI, the use of either cells or their secretome alone did not elicit the total functional recovery of the animals. This can be due to the application of non-optimal procedures to these cells that do not stimulate their highest therapeutic response. Currently, several authors are trying to modulate the behavior of MSCs with different stimuli to enhance cell and secretome therapeutic responses (Mendes-Pinheiro *et al.*, 2020; Pinho *et al.*, 2020; Vizoso *et al.*, 2017). Some of these approaches will be addressed in the next section.

#### 1.4.1.3 Improving cell and secretome based therapies

MSCs are highly plastic cells with the ability to change their profile according to the surrounding environment. Aiming to explore this characteristic, several authors tried to modulate different factors to enhance the therapeutic response of MSCs (Mendes-Pinheiro *et al.*, 2020).

##### 1.4.1.3.1 Three-dimensional cultures

Since, in physiological conditions, cells live in a three-dimensional (3D) environment, some authors are starting to question whether this type of culture should not be the standard type of cell culture in the future (Jensen & Teng, 2020). 3D cell culture can be divided into scaffold-based and scaffold-free techniques (Jensen & Teng, 2020).

The former consists in the conjugation of biomaterials with cells to modulate cell behavior, enhance cell survival in a transplantation strategy or even serve as secretome release systems (Assunção-Silva *et al.*, 2015; Rocha *et al.*, 2020b). Several biomaterials have been used ranging from natural-based ones to synthetic polymers (Rocha *et al.*, 2020b). Indeed, Grotenhuis and coworkers showed that synthetic polypropylene and polyethylene terephthalate-based materials could alter the paracrine crosstalk between macrophages and ASCs (Grotenhuis *et al.*, 2016). Moreover, Oliveira *et al* demonstrated that different natural hydrogels differently impact the behavior of ASCs, even at a

functional level (Oliveira *et al.*, 2017). Another work from Silva and collaborators demonstrated that by altering a gellan gum hydrogel with a fibronectin-based peptide, the secretome of BM-MSCs cultured in this hydrogel showed to better support the survival and differentiation of hippocampal neurons (Silva *et al.*, 2013).

The same hydrogel mentioned above, with ASCs encapsulated within its structure, led to extensive neurite growth in a DRG model and significant motor improvements in rats with lumbar SCI (Gomes *et al.*, 2016). Additionally, ASCs within this hydrogel potentiated vascular recruitment in a chick chorioallantoic membrane assay and HUVECs were also able to form vascular-like structures within the hydrogel in the presence of ASCs (Rocha *et al.*, 2020a).

Regarding scaffold-free 3D environments for SCI applications, one possible strategy might be to culture MSCs as spheroids. Spheroids are cell clusters that grow in suspension, in an attempt to mimic cell interactions in a 3D environment (Haycock, 2011; Jensen & Teng, 2020). Moreover, MSCs cultured in spheroids have enhanced anti-inflammatory and angiogenic properties (J. H. Lee *et al.*, 2016; Murphy *et al.*, 2017). Another promising scaffold-free strategy is the use of bioreactors. Bioreactors are systems that provide an interactive 3D environment where biological and biochemical processes occur in controlled conditions (Haycock, 2011; Kaasi & Jardini, 2016). This allows the expansion of MSCs at a clinically relevant scale with consequent scale-up of secretome production (Jung *et al.*, 2012; Vizoso *et al.*, 2017). Usually, cells are cultured in microcarriers to form spheroids or within hydrogels (Kaasi & Jardini, 2016). Bioreactors can overcome some disadvantages of MSCs donor variability, producing more homogenous cell populations from different donors (Hupfeld *et al.*, 2014). Also, bioreactors can modulate gene expression and paracrine signaling of MSCs (Hupfeld *et al.*, 2014; Teixeira *et al.*, 2016a). Indeed, Teixeira and colleagues showed that computer-controlled bioreactors enhanced the neuroregulatory profile of the secretome of MSCs (Teixeira *et al.*, 2016a). Furthermore, it was observed that bioreactors with mechanical loading stimulation enhanced the angiogenic profile of the secretome of MSCs, influencing blood vessel formation and endothelial proliferation (Kasper *et al.*, 2007). However, 3D cell culturing still faces some challenges, namely cost and imaging analysis (Jensen & Teng, 2020). Also, the best type of 3D culture that maximizes the therapeutic effect is still unknown. For that reason, several authors are trying other approaches to improve MSCs and their secretome.

#### 1.4.1.3.2 Hypoxia

One of the alternative approaches to enhance the properties of cells and the secretome is the use of hypoxia. Although in pathological conditions hypoxia may lead to cell death, in cell culture it can

increase the proliferation of MSCs as well as change their transcription profile, with the potential to enhance the angiogenic and neurotrophic action of these cells (Teixeira *et al.*, 2015b; Wobma *et al.*, 2018; Zhilai *et al.*, 2016). Indeed, when MSCs were exposed to hypoxic conditions and then transplanted to SCI rat models, enhanced functional and histological improvements were observed when comparing to MSCs cultured in normoxia conditions (W. Wang *et al.*, 2018; Zhilai *et al.*, 2016). Furthermore, MSCs pre-conditioned with hypoxia showed higher survival rates in the injured spinal cord than normoxia MSCs (W. Wang *et al.*, 2018; Zhilai *et al.*, 2016). However, the best oxygen concentration and timing of hypoxic stimulus for the desired application remains unclear. For instance, the secretome of UM-MSCs cultured in 5 % $O_2$ or 21 % $O_2$ did not have a different impact on neuronal differentiation *in vitro*, although showing different secretome profiles (Teixeira *et al.*, 2015b). Furthermore, Buizer and colleagues showed that BM-MSCs proliferation, metabolic rate, and angiogenic profile varied in different $O_2$ concentrations (Buizer *et al.*, 2018).

#### 1.4.1.3.3 Genetic engineering

An alternative strategy to modulate cell behavior is using genetic engineering. The first works regarding the application of the secretome by Gnecchi showed that overexpressing the survival gene *Akt1* on BM-MSCs increased the capacity of the secretome of these cells to protect hypoxic cardiomyocytes and augmented the restoration of ventricular function (Gnecchi *et al.*, 2005, 2006). From there, genes mainly related with survival, migration and immunomodulatory properties, like superoxide dismutase 2, C-X-C chemokine receptor 4, *IL-10*, and *IL-4* were the principal targets of genetically modified MSCs (Seo *et al.*, 2019). However, for SCI, genes associated with neuronal function have also been studied, including brain-derived neurotrophic factor (BDNF), stromal-derived factor-1, and glial-derived neurotrophic factor, with overall positive effects in functional recovery (Gransee *et al.*, 2015; Khan *et al.*, 2018; Rooney *et al.*, 2009; Shahrezaie *et al.*, 2017; A. N. Stewart *et al.*, 2017). Also, suppression of apoptosis-related genes seems to promote better functional recovery (Edalat *et al.*, 2013). However, there are still some limitations on the clinical translation of genetically engineered MSCs. These include the safety and efficacy of gene integration strategies and elucidation of the most relevant genes to be targeted in MSCs to produce better results in SCI (Seo *et al.*, 2019).

#### 1.4.1.3.4 Molecular pre-conditioning

Another strategy to improve cell and secretome function is to pre-condition MSCs with molecular cues. In comparison to the previously mentioned alterations, this type of strategy has the advantage of

not needing special equipment and methodology for cell culture. Additionally, pre-conditioned MSCs can be combined with previous techniques to enhance their therapeutic efficacy.

Within this research topic, the scientific community is divided into two branches: pre-conditioning with pharmacological or bioactive molecules and pre-conditioning with inflammatory stimuli (Seo *et al.*, 2019). The first strategy comprises a wide range of factors that act on survival, differentiation, regenerative ability, and migration of MSCs. For instance, curcumin pre-treated MSCs have increased survival, angiogenic potential, and improved locomotor performance in a rat compression SCI model (Liu *et al.*, 2015; Ruzicka *et al.*, 2018). Furthermore, Nagashima and coworkers used human dental pulp MSCs pre-conditioned with bFGF in a complete transection rat SCI model. The results showed that pre-treated cells promoted enhanced axonal regeneration and locomotor recovery (Nagashima *et al.*, 2017). Another study used an already approved drug for the treatment of iron poisoning: deferoxamine. This chelating agent augmented the levels of angiogenic, neuroprotective and anti-inflammatory molecules in ASCs secretome (Oses *et al.*, 2017). Furthermore, ASCs pre-treated with $H_2O_2$ are currently under a phase I/II trial, to treat patients with SCI (NCT02917291).

Despite this, the major focus of molecular stimulation is the pre-conditioning with inflammatory molecules to enhance MSCs immunomodulatory properties (Saparov *et al.*, 2016; Seo *et al.*, 2019). Indeed, MSCs are able to closely interact with immune cells and their factors, being able to modulate and be modulated by these interactions (Bernardo & Fibbe, 2013; Li & Hua, 2017; Shi *et al.*, 2012). Besides that, some authors also explored other functions of immune-stimulated MSCs. For instance, it was observed that TNF-α enhanced the angiogenic paracrine function of ASCs (Heo *et al.*, 2011; Kwon *et al.*, 2013; M. Wang *et al.*, 2007). Another pro-inflammatory molecule that gained attention in this field is interferon-gamma (IFN-γ). Krampera and coworkers showed that this pro-inflammatory cytokine enhanced the immunosuppressive properties of MSCs (Krampera *et al.*, 2006). Additionally, Sivanathan *et al* suggested that pre-activation of MSCs with IFN-γ could improve their therapeutic efficacy by enhancing the reparative properties of these cells as well as their homing and immunomodulatory capacity (Sivanathan *et al.*, 2014). As a matter of fact, this strategy has been tested in pre-clinical trials in several inflammatory disease models (Sivanathan *et al.*, 2014).

An alternative class of inflammatory molecules being tested are toll-like receptor (TLR) agonists. This class of receptors contributes to the host defense mechanism by recognizing molecular patterns associated with pathogens or cellular damage to activate a proper inflammatory response (Seo *et al.*, 2019). Although these receptors have been mainly associated with immune cells, MSCs have been described to also express some TLRs (Bernardo & Fibbe, 2013; Hwa Cho *et al.*, 2006).

Lipopolysaccharides (LPS) are a major component of the outer membrane of Gram-negative bacteria contributing to their integrity and function (G. Zhang *et al.*, 2013). LPS activate TLR4, being a widely used molecule for the induction of an inflammatory state in laboratory settings. Indeed, a 12-hour period of LPS stimulation altered the secretome composition of bovine MSCs, namely in proteins associated with angiogenesis, tissue remodeling, and antioxidative functions (de Moraes *et al.*, 2017). This was confirmed at a functional level with human and porcine ASCs, where the secretome of MSCs previously stimulated with LPS enhanced angiogenesis (Bernardini *et al.*, 2019; S. C. Lee *et al.*, 2015). Moreover, stimulated human ASCs were also able to promote hepatocyte survival and liver regeneration (S. C. Lee *et al.*, 2015).

On the other side of the inflammatory spectrum, pre-conditioning with classical anti-inflammatory cytokines is not well explored. Still, Saldaña *et al.* showed that IL-10 secreted by macrophages is able to potentiate the immunomodulatory potential of MSCs (Saldaña *et al.*, 2019). Moreover, co-cultures of MSCs with anti-inflammatory macrophages enhanced their immunomodulatory role (Cho *et al.*, 2014; Saldaña *et al.*, 2019). Also, anti-inflammatory cytokines like IL-10 and TGF-β supported the growth of MSCs (Freytes *et al.*, 2013). However, how these anti-inflammatory molecules are able to influence the regenerative potential of MSCs is now known.

Even though some promising results were obtained, cell and secretome therapy still face some challenges before being effectively translated to the clinical setting. One of these challenges is the insufficient therapeutic potency of MSCs in SCI. Thus, functional enhancement of these cells is needed. However, the conditions that enhance this therapeutic potential are still unknown and more research needs to be developed in this direction.

# 2. Research objectives

MSCs, and within these, ASCs, have shown promising results in the development of SCI therapies, either with cells or with secretome, in part due to their ability to induce neuronal and vascular regeneration. However, there is a need to enhance the therapeutic potential of these cells. One possible strategy is by conditioning ASCs with inflammatory molecules as it has been reported that these cells have a strong relationship with immune cells being able to modulate and be modulated by them and their molecules. Although these inflammatory stimuli seem to promote a more immunomodulatory profile in ASCs, few reports show the effects of this stimulation at a neuronal and vascular level within the same setting. Therefore, the objectives of the present work were:

1. Understand the impact of pre-conditioning ASCs with pro and anti-inflammatory mediators on their ability to induce vessel formation, at a paracrine and non-paracrine level.
2. Understand the impact of pre-conditioning ASCs with pro and anti-inflammatory mediators on neurite outgrowth, at a paracrine and non-paracrine level.
3. Evaluate how the different inflammatory molecules could alter the genetic expression of ASCs.

# 3. Materials and Methods

## 3.1 ASC culture

Professor Jeffrey Gimble (LaCell LLC) kindly provided ASCs collected from human lipoaspirates of consenting donors, according to a protocol previously described (Dubois *et al.*, 2008).

Cells were cryopreserved at -196 °C, with 90 % (v/v) Fetal Bovine Serum (FBS) (Sigma) and 10 % (v/v) dimethyl sulfoxide (DMSO) (Sigma) and thawed when needed. All experiments were done with, at least, one passage after thawing and ranging from P5 to P8. ASCs were expanded in ASCs culture medium composed by Minimum Essential Medium – alpha (α-MEM) (Thermo Fisher Scientific) supplemented with 10 % (v/v) FBS and 1 % (v/v) Penicillin/Streptomycin (PenStrep) (Gibco), at 37 °C and 5 % $CO_2$ (v/v).

When 80 to 90 % confluence was reached, cells were detached using trypsin-ethylenediaminetetraacetic acid (trypsin-EDTA) 0.05 % (v/v) (Gibco), for 5 minutes, at 37 °C and 5 % $CO_2$ (v/v). Then, enzymatic activity inhibition was performed by diluting with media followed by a centrifugation step (249 g, 5 minutes), in which the supernatant was discarded (Procedure termed trypsinization from here onwards). Cells were counted with trypan blue and a Neubauer chamber. ASCs were plated at 4000 cells/$cm^2$ unless stated otherwise. Medium was changed every 2 to 3 days.

### 3.1.1 ASCs stimulation

In order to study the impact of inflammatory mediators on ASCs regenerative capacity, several different molecules were used. For the pro-inflammatory stimulus, 20 ng/ml of IFN-γ (Peprotech) and 100 ng/ml of LPS (Sigma) were used. For the anti-inflammatory stimulus, 200 ng/ml of IL-10 (Peprotech) was used. A group without any stimulation was also employed in all experiments.

ASCs were plated for 72 hours before being stimulated for 24 hours with the inflammatory mediators diluted in ASCs culture medium.

#### 3.1.1.1 ASCs morphology assessment

To observe if the inflammatory stimulus altered the ASCs morphology, 24 hours after stimulation, ASCs were fixed with 4 % paraformaldehyde (PFA) for 20 minutes. Also, a group in which the stimulus was removed and switched for ASCs regular culture medium for 3 days before fixation was performed.

After this, cells were submitted to a 30-minute staining with phalloidin (0.1 µg/ml) (Sigma) and 4′,6-Diamidino-2-phenylindole dihydrochloride (DAPI) (1 µg/ml) (Invitrogen), in phosphate-buffered

saline (PBS) 1x, to mark actin and cell nuclei, respectively. Next, each well was washed 3 times with PBS 1x. All images were taken on Olympus Widefield Inverted Microscope IX81.

### 3.1.2 Secretome collection

All secretome collections were done in serum-free conditions. After reaching P6, ASCs were maintained in culture medium for 72 hours. Then, ASCs were stimulated as described previously (**Section 3.1.1**). Afterward, the medium was removed and cells were washed 4 times with PBS without $Ca^{2+}$ and $Mg^{2+}$ (Invitrogen) to remove any excess proteins adsorbed to tissue culture plastic. As the vascular morphogenesis and the neurite outgrowth are performed in different media, the secretome of each experiment was also collected in different media. Therefore, for the vascular morphogenesis assay, endothelial growth medium (EGM) (R&D Systems) with 1 % (v/v) PenStrep was used, while for the neurite outgrowth assays, Neurobasal medium (Thermo Fisher Scientific) with 1 % (v/v) PenStrep was added to cells. After 24 hours, these media were collected and centrifuged (249 g, 5 minutes) to pellet cell debris. The supernatant was frozen on liquid nitrogen and stored at -80 °C for further use. This final solution was termed secretome. The same procedure was made with an empty flask (without cells) to obtain a control group.

## 3.2 HUVECs isolation and culture

Human endothelial cells from the umbilical vein were used for the studies of vascular morphogenesis. To achieve an endothelial cell bank, umbilical cords of healthy consenting donors from "Hospital de Braga", under an approved protocol by the review board of the Ethical Commission for Health of "Hospital de Braga", were used. After cleaning the umbilical cord with PBS 1x, a cannula was placed in the umbilical vein, held by a zip tie. Then, the vein was washed with PBS 1x to remove any blood clots and excesses of blood. Afterward, the umbilical cord was closed on the other end, and the vein rinsed with α-MEM containing 0.2 % (w/v); (210 U/ml) Type I Collagenase (Gibco) and 1 % (v/v) PenStrep. This procedure took 15 minutes with the umbilical cord submerged on PBS 1x, at 37 °C and 5 % $CO_2$ (v/v). After this, to guarantee homogenous digestion, the cord was massaged and the digestion product was transferred to a 50 ml Falcon, with subsequent washes of α-MEM (with 10 % (v/v) FBS and 1 % (v/v) PenStrep), PBS 1x, and air. Then, the solution was centrifuged (249 g, 10 minutes), with supernatant removal. The pellet was resuspended in EGM supplemented with 2 % (v/v) of endothelial growth supplement (EGS) (R&D Systems), and 1% (v/v) PenStrep (complete EGM). Meanwhile, 6-well plates were coated with 1 % (w/v) Type B bovine gelatin (Sigma) for 30 minutes, at 37 °C and 5 % $CO_2$

(v/v). After the coating, the cell suspension was plated and left overnight, at 37 °C and 5 % $CO_2$ (v/v), to let cells attach. The following day, non-adherent cells were removed and culture medium was changed every two days. When cells reached confluence, they were trypsinized and then frozen for further experiments, following the same protocol applied to ASCs. When needed, HUVECs were thawed using the same procedures as for ASCs, and grown on a coating of 1 % gelatin in complete EGM changed every two days.

### 3.2.1 HUVECs purity assessment

HUVECs in P2 were fixed with PFA 4 %, for 20 minutes, to be stained for Von Willebrand Factor (VWF) (endothelial cytoplasm protein), to estimate the efficacy of the established protocol. The next step consisted on permeabilization (with PBS with 0.3 % Triton (PBS-T) for 5 minutes) to allow an easier antibody entry, followed by the addition of a blocking solution (PBS 1x with 10 % Newborn Calf Serum (NBCS) (Gibco) for 1 hour), to reduce unspecific binding. Rabbit anti-VWF (1:500) (Abcam) diluted in blocking solution was added for another hour. Then, donkey anti-rabbit Alexa Fluor 594 (1:1000) (Invitrogen) secondary antibody was added for another hour, also diluted in blocking solution. Finally, counterstain with DAPI was done for 20 minutes as previously described. Between each solution, cells were washed 3 times with PBS 1x. Between primary and secondary antibodies, cells were washed with PBS with 0.5 % NBCS. All images were taken on Olympus Widefield Inverted Microscope IX53. The efficacy of the isolation was determined by counting the number of VWF positive cells among the total number of cells determined by DAPI.

## 3.3 Vascular morphogenesis assay

Endothelial cells have the capacity to form vessel-like structures (vascular morphogenesis) when plated on an ECM.

In order to implement this model, several optimization steps were needed. For that, HUVECs in complete EGM were combined with rat tail collagen type I (BD Bioscience), an ECM. In a series of experiments, different cell densities ranging from 10 000 cells/$cm^2$ to 60 000 cells/$cm^2$, combined with different gel concentrations (2.5 - 3.15 mg/ml) were done. Also, the presence of angiogenic factors (VEGF (Peprotech) and fibroblast growth factor 2 (FGF-2) (Peprotech) was tested. Furthermore, a 3D environment where HUVECs were encapsulated into collagen was also assessed. Despite all these variable changes, none were able to elicit a robust formation of vessel like-structures, even when spanning the experiment for 7 days.

Therefore, the next step involved switching from collagen to matrigel (BioCell, Inc), a richer ECM. With this matrix, HUVECs plated on top of it, at a cell density of 20 000 cells/cm$^2$ were able to form vessel-like structures within 16 hours. After this, cells were fixed with 4 % PFA for 45 minutes. All experimental assays were done in α-MEM 10 % FBS 1 % PenStrep unless stated otherwise. Therefore, this experimental setup was used for the different vascular morphogenesis assays. Moreover, a positive control in complete EGM was used to assess experiment quality.

### 3.3.1 Indirect co-culture system to study vascular morphogenesis

In order to assess how ASCs influence the vascularization process through paracrine mechanisms, a 24-well transwell system with a polyester membrane with 0.4 µm pores (Corning) was used. The experimental setup was designed as in **Figure 4**.

Prior to this, ASCs were passaged as detailed formerly and plated on the bottom of the transwells for 72 hours, with the insert kept apart in order to keep it dry. There, ASCs were stimulated as described in **Section 3.1.1** for 24 hours. In the co-culture day, a drop of 40 µl of matrigel was placed in the upper half of the insert and kept for 1 hour at 37 °C and 5 % $CO_2$ (v/v) to let it gel. Then, HUVECs were plated on top of matrigel (20 000 cells/cm$^2$) within 100 µl of medium. After ASCs stimuli removal, the insert was placed back in the plate with ASCs for 16 hours.

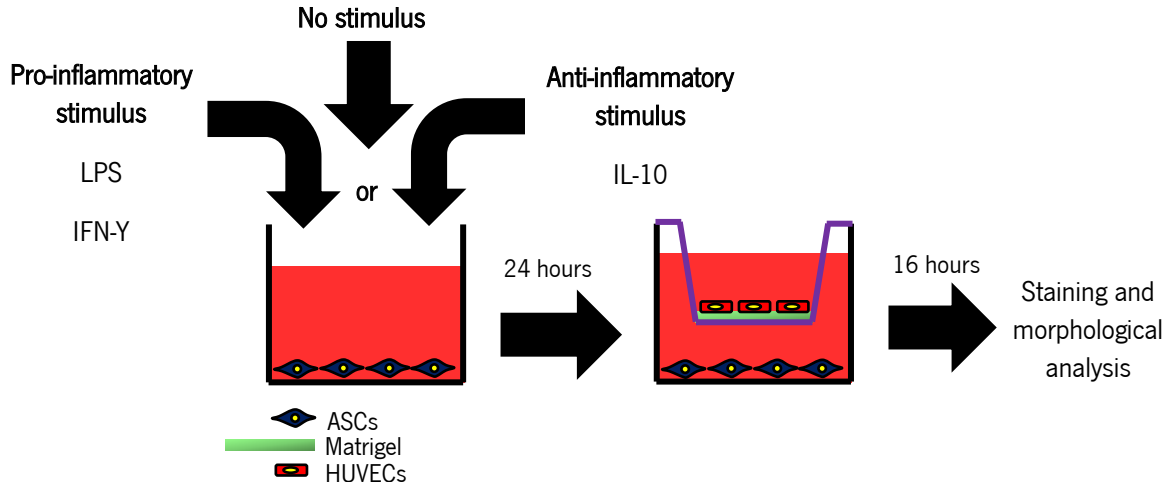


**Figure 4: Scheme of the indirect co-culture system for the study of vascular morphogenesis.** ASCs were stimulated for 24 hours with pro or anti-inflammatory stimulus (or without stimulus). After, HUVECs were plated on the matrigel droplet in the upper chamber of the transwell system. 16 hours later, cells were fixed and stained for analysis.

### 3.3.2 System to study the impact of ASCs secretome on vascular morphogenesis

To assess if the molecules secreted by ASCs could elicit the same response as the paracrine crosstalk on the vascular morphogenesis, the setup described in **Figure 5** was used.

Briefly, after matrigel gelling on a 96-well plate (SPL), HUVECs were resuspended in the ASCs secretome and plated on top of this gel, for 16 hours.

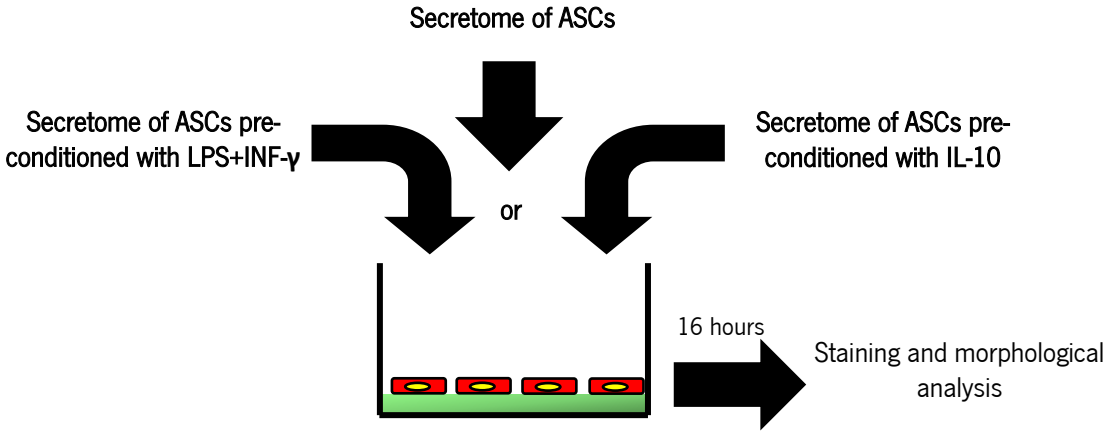


**Figure 5: Scheme of the system to evaluate the effect of the different secretomes on vascular morphogenesis.** HUVECs were resuspended in ASCs secretome collected previously and plated on top of matrigel for 16 hours before being fixed and stained for morphological analysis.

### 3.3.3 Direct co-culture system to study vascular morphogenesis

To assess the impact of the direct contact of ASCs on HUVECs vascular organization, there was a need to adapt the model developed in order to decrease the distance between ASCs and HUVECs, as illustrated in **Figure 6**. For that, 24 hours before the co-culture ASCs were encapsulated in matrigel on cell density of 30 000 cells/ 40 ul of matrigel, by resuspending in the appropriate volume of matrigel and then plating on a 96-well plate. After gelling, α-MEM with 10 % FBS and 1 % PenStrep and the appropriate stimulus was added to the encapsulated cells. 24 hours later, the stimulus was removed and HUVECs were plated on top of the gel, for 16 hours, as described for other experiments.

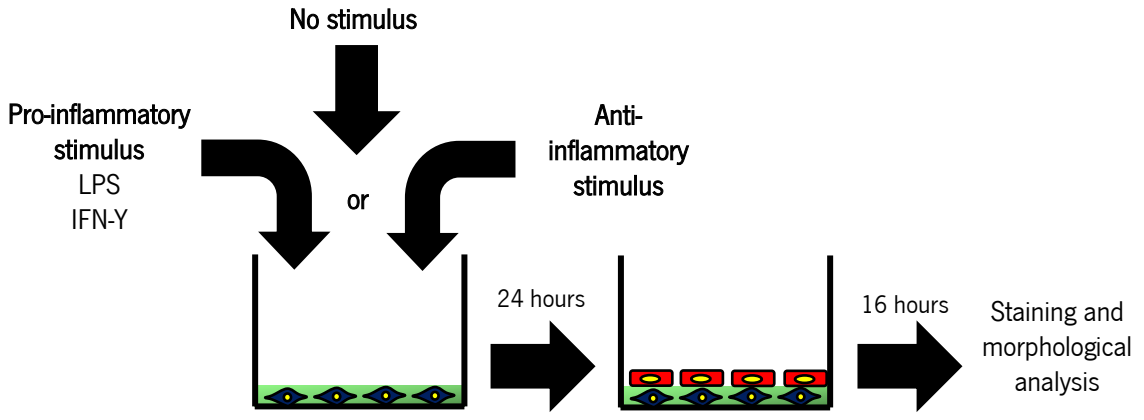


**Figure 6: Scheme of the system used to study vascular morphogenesis on closed contact environment between ASCs and HUVECs.** ASCs were encapsulated on matrigel in a density of 30 000 cells/40 µl of gel, and incubated with the stimulus for 24 hours. Then, HUVECs were placed directly on top of ASCs and fixed 16 hours later for the morphological analysis.

### 3.3.4 HUVECs on matrigel immunocytochemistry

To visualize the vessels formed by HUVECs, VWF antibody was used to mark endothelial cells in the non-paracrine assay. All experiments were counterstained with phalloidin and DAPI.

In the indirect assays, prior to the beginning of the ICC, the insert membrane containing the matrigel was cut and place on a 24-well plate. After this, the procedure was similar to all three types of vascular morphogenesis assays.

The initial step consisted in the permeabilization with PBS-T 0.3 % (w/v) for 10 minutes followed by 3 washes with PBS 1x. Blocking solution of PBS 1x 10% (v/v) NBCS was added for 90 minutes, followed by the addition of VWF antibody. After overnight incubation at 4°C, the gel containing the cells was washed 3 times with PBS with 0.5% NBCS. Alexa Fluor 488 Goat anti-rabbit secondary antibody was added for 3 hours before washing. The final step consisted on staining the cells with DAPI and phalloidin for 45 minutes, followed by 3 washes with PBS 1x. All images were taken in Olympus Widefield Inverted Microscope IX81, using the Stage Navigator tool of the CellSens software (Olympus), to do a mosaic of the vessel-like structures obtained.

### 3.3.5 Vascular morphogenesis analysis

To evaluate the degree of vascularization, AngioTool64 Version 0.6a Software was used. After opening the resulting image and defining the scale and the fluorescence threshold, the software allows for background and small particle removal. After this correction, the software automatically forms a skeleton overlaying the original picture giving quantitative data about different parameters related to vascular organization (**Table 1** and **Figure 7**). In particular, the software first quantified the explant area that is the area occupied by the convex hull containing the vessels. Then, it quantifies the total area of the vessels as well as the number of junctions between each vessel, depicted in blue dots in **Figure 7.** Both of these parameters were normalized to explant area giving the percentage of the vessel area and junction density. Also, the total length of the vessels of the image is obtained and a calculation of the mean length of the vessels is performed. Finally, the number of endpoints (White arrows **Figure 7**) is calculated. In the present work, the total vessel length and the number of endpoints were also normalized to the explant area.

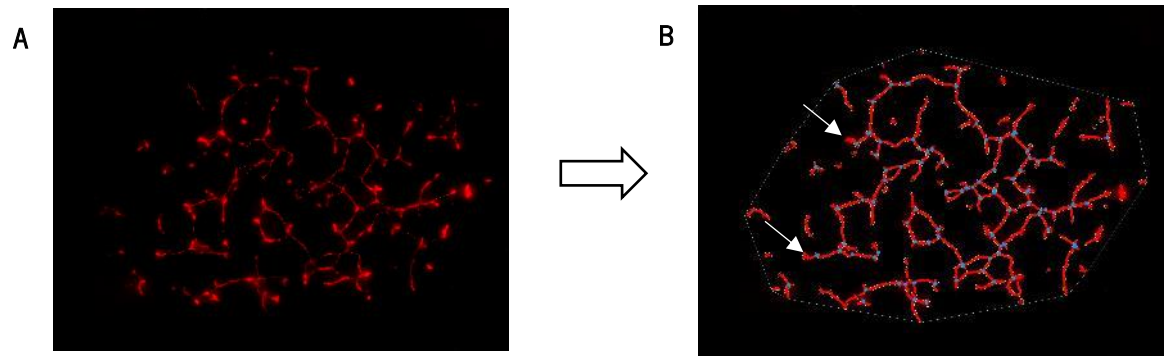


**Figure 7: Representative image of the vascular morphogenesis analysis run by AngioTool software. (A)** After using drawing tools to highlight some staining, the image is run on the software resulting in the image on the right. **(B)** Software image after analysis showing all vessels in red, with the blue dots being considered branching points. White arrows depict endpoints. The dashed line around is the explant area.

**Table 1: Morphological parameters assessed on the vascular morphogenesis assay.**

| Parameter | Description |
|---|---|
| Explant area | The area occupied by the convex hull containing the vessels in the image |
| Vessel area | The area of the segmented vessels |
| Junction density | The number of vessel junctions normalized per unit area |
| Total vessel length | The sum of Euclidean distances between the pixels of all the vessels in the image |
| Average vessel length | Mean length of all the vessels in the image |
| Number of endpoints | The number of open-ended segments |

## 3.4 Dorsal Root Ganglia explants

To study the potential of ASCs and their secretome on neurite outgrowth, a DRG explant was used. DRG explants are a useful model as they are able to produce neurites after extraction, under appropriate conditions (Gomes *et al.*, 2016). To achieve this, DRG were dissected from the thoracic regions of Wistar-Han rat pups ranging from postnatal day 5 to 7. Then, any residue of peripheral nerves was removed. These assays were conducted on sterile conditions and by keeping DRG on cold Hank's Balanced Salt Solution buffer (HBSS) (Gibco, pH=7.2) during extraction and cleaning to maintain cell viability. All experiments had a group where DRGs were grown on Neurobasal medium supplemented with 6 mg/ml D-Glucose (Sigma) B27, 2mM L-glutamine (Invitrogen), 2% B27 (Invitrogen), 1% PenStrep (complete Neurobasal) and 50 ng/ml of recombinant human β-Nerve Growth Factor (Peprotech) to assess DRGs quality. All DRG were kept at a humified atmosphere with 5% (v/v) $CO_2$ and 37 °C.

### 3.4.1 Indirect co-culture between ASCs and DRGs

Previous work from our group with this model showed that placing DRG on an ECM like collagen could promote its adhesion as well as neurite outgrowth. Therefore, to study the paracrine influence of ASCs on DRG, collagen hydrogel droplets were used to separate these two cell types. (**Figure 8**)

Prior to this, ASCs were passaged, as described formerly, and plated on 24-well plates (SPL) for 72 hours, before being stimulated for 24 hours as already described. On DRG extraction day, rat tail collagen type I was mixed with Dulbecco Modified Eagle Medium (DMEM) (Gibco) 10x concentrated on a proportion of 89.6 % (v/v) collagen to 10 % (v/v) of DMEM. Then, 0.4 % (v/v) of sodium bicarbonate (7.5 % (w/v)) (Sigma) was added and droplets of 30 µL were made on a cell culture plate. To gel these droplets, a period of 90 minutes of incubation, at 37 °C and 5 % (v/v) $CO_2$, was applied. After this, cell medium of ASCs was removed and the collagen droplet was transferred to the top of ASCs. Then, the cleaned DRG were placed on the top of the collagen gel and incubated with complete Neurobasal medium. Also, a control group without ASCs was performed. The experiment was maintained for 4 days before being fixed with PFA during 45 minutes, with medium change two days after the beginning of the experiment.

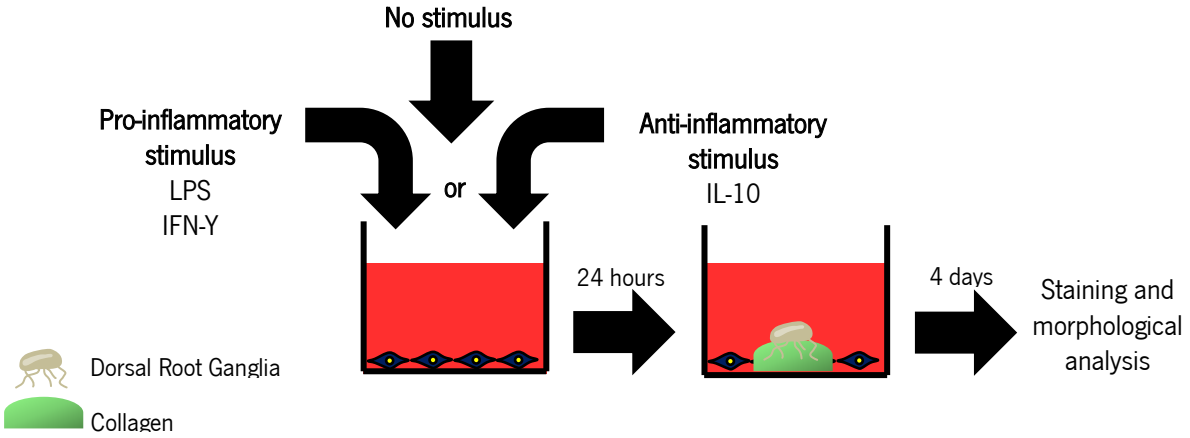


**Figure 8: Scheme of the setup used to study neurite outgrowth at a paracrine level.** ASCs were stimulated for 24 hours with the pro-inflammatory stimulus or anti-inflammatory stimulus (or no stimulus) before a collagen droplet with the DRG on top was placed on top of them. After 4 days, cells were fixed and stained for morphological analysis.

### 3.4.2 DRG assay with secretome

Using a similar setup from the previous section, the effect of ASCs secretome was studied as shown in **Figure 9**. After DRG cleaning and formation of collagen gels, DRG were placed on top of the gels with the respective secretome collected in Neurobasal medium. Experiments were extended for 7 days with medium change every 2 days, before the cells being fixed for 45 minutes.

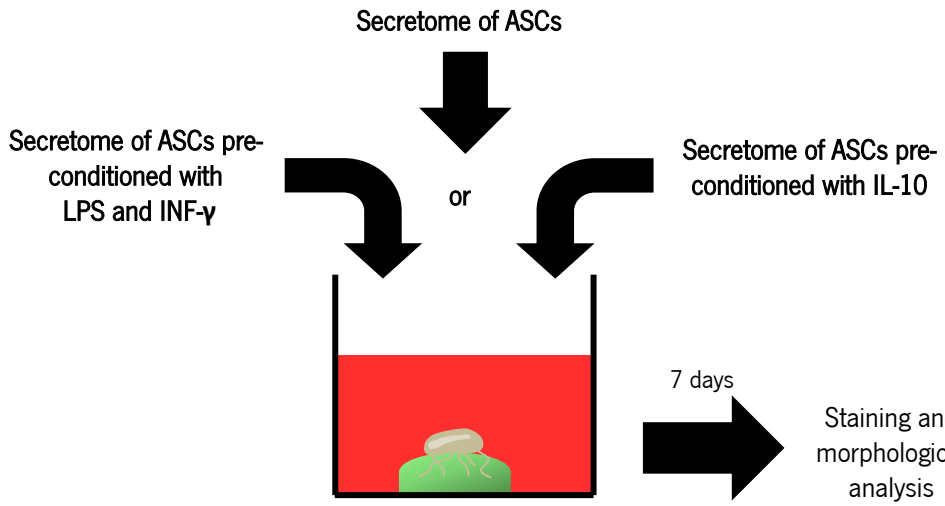


**Figure 9: Scheme of the setup used to study neurite outgrowth induced by ASCs secretome.** After putting the DRG on the collagen droplet, previously collected secretome was added to the culture and changed every two days until day 7 where cells were fixed for further morphological analysis.

### 3.4.3 Direct co-culture between ASCs and DRG

In order to achieve a conceivable way of studying the relationship on a direct contact level between ASCs and DRG, the experiment was done under the same conditions of the indirect co-culture but without the collagen gel (**Figure 10**). Therefore, the DRG were put directly on top of cells and maintained there for 4 days with medium change on the second day. A group without ASCs was used as control.

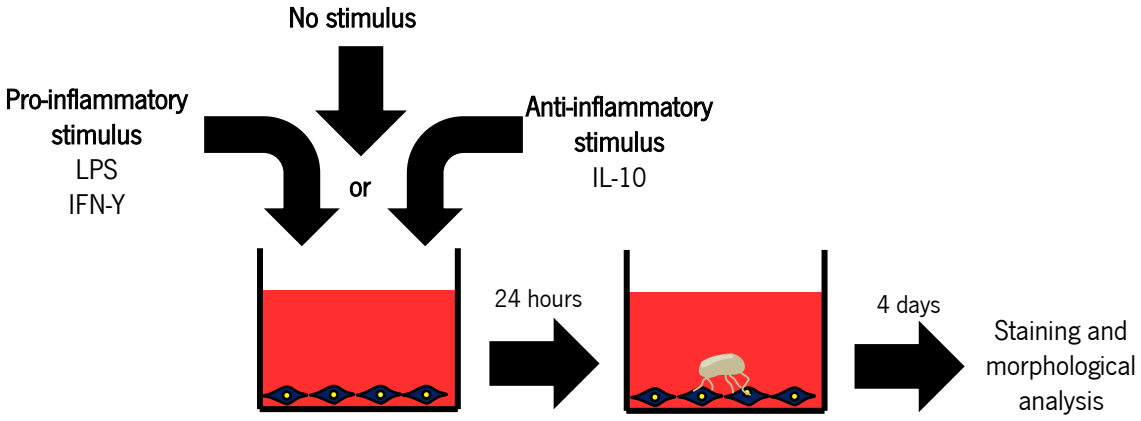


**Figure 10: Scheme used to study how direct contact between ASCs and DRG affect neurite outgrowth.** ASCs were stimulated for 24 hours with the pro-inflammatory stimulus or anti-inflammatory stimulus (or no stimulus). Then, the DRG was placed directly on top of ASCs. After 4 days, cells were fixed and stained for morphological analysis.

### 3.4.4 DRG immunocytochemistry

To achieve a way of visualizing the neurites produced by the DRG, cells were stained with anti-neurofilament antibody, a major component of neural cytoskeleton, and counterstained with DAPI. Also, phalloidin was used in the direct contact assay to visualize ASCs.

For the assays done on collagen (indirect contact and secretome), a permeabilization step of 10 minutes with PBS-T 0.3% (w/v) was first done followed by 3 washes with PBS 1x. Then a blocking step with PBS 1x supplemented with 10% (v/v) NBCS was done for 90 minutes, followed by the addition of mouse anti-neurofilament (1:200) (Millipore), for 24 hours, on blocking solution. After this time, each well was washed 3 times with PBS 1x with 0.5% NBCS before adding goat anti-mouse Alexa Fluor 488 (1:1000) (Invitrogen) secondary antibody. After 3 hours, cells were washed with PBS 1x before being counterstained with DAPI, for 30 minutes. All images of DRGs into collagen gels were taken on Olympus LPS Confocal FV1000 using the Multi Area Time Lapse tool to acquire the entire DRG and its neurites.

For the direct contact, the same steps were taken but with 5 minutes of permeabilization, 1 hour of blocking, 1 hour of primary antibody, and 1 hour of secondary antibody. Finally, these cells were counterstained with phalloidin and DAPI for 30 minutes. These images were taken on Olympus Widefield Inverted Microscope IX81, using the Stage Navigator tool of the CellSens software (Olympus)

### 3.4.5 DRG analysis

After image retrieval, its analysis was performed using ImageJ software with the plugin Neurite-J. After defining the scale, and defining the cell body with the help of drawing tools and threshold selection, a new threshold is applied to define the neurites. After noise cleaning, the software forms concentric rings around the cell bodies and counts the number of intersections on each ring. The longest neurite was defined as the last ring with at least 1 intersection or an area higher than 1. Also, the total neurites area was obtained.

## 3.5 Gene expression analysis by qPCR

After 6 hours of stimulation of ASCs with the different factors, the expression levels of several genes were analyzed using glyceraldehyde 3-phosphate dehydrogenase *(GADPH)* and peptidylprolyl isomerase A *(PPIA)* as reference genes, by quantitative polymerase chain reaction (qPCR). The genes analyzed were: *VEGF*, angiogenin, nerve growth factor *(NGF)*, *BDNF*, *FGF-2*, *IL-6*, chemokine (C-X-C motif) ligand *(CXCL)* 1 and *CXCL2*. Also, a group in which ASCs did not receive any stimulus was performed. To achieve this, three steps were needed. The first consisted on the RNA extraction from

cells, followed by transformation of this RNA on complementary DNA (cDNA). Then, with specific primers, the genes of interest were amplified and quantified using a double-strand DNA binding fluorescent dye. Furthermore, to have a good yield of RNA, the ASCs on this experiment were plated on a 6-well plate with 100 000 cells/well (around 10 000 cells/$cm^2$) for 72 hours before being stimulated.

### 3.5.1 RNA extraction

After 6 hours of incubation with the inflammatory molecules, ASCs were treated with TripleXTractor (Grisp) (100 µL/$cm^2$) in each well to lyse the cells and extract their intracellular contents. After 5 minutes with TripleXtractor at room temperature, the samples were frozen at -80°C for later use. ASCs culture without stimulation was used as control.

Following manufacturer guidelines, after thawing the extracts, 200 µL/ml of chloroform (Carlo Erba) was added followed by fast mixing with incubation of 2-3 minutes before centrifuging. This allows for phase separation with the RNA being bound on the upper aqueous phase. After careful removal of this upper phase, in order to promote RNA precipitation, isopropanol (Sigma) (same volume as TripleXtractor) was added and kept for 10 minutes at room temperature before being centrifugated again for 10 minutes. Then, the supernatant was removed and the pellet was washed with ethanol 70% (v/v) to remove any impurities. After another centrifugation step, the RNA pellet was obtained and resuspended in 10 ul of GRS PCR Grade Water (Grisp). RNA was conserved at -80° for further use.

### 3.5.2 cDNA synthesis

On the day of cDNA synthesis, RNA was thawed and quantified using NanoDrop 1000 spectrophotometer (Thermofisher Scientific). Then, 500 ng of each sample was used to obtain the respective cDNA. This step was carried using Xpert cDNA synthesis Supermix (with gDNA eraser) (Grisp), according to manufacturer instructions. With this mix, any remains of DNA in the sample are eliminated before the reverse transcription step. The heating program advised by the manufacturer was carried out in the T100 Thermal Cycler (Biorad). After the protocol, the samples were diluted in 1:1 to increase the amount of cDNA available for qPCR.

### 3.5.3 qPCR

In order to amplify the cDNA and quantify it in real-time, Xpert Fast SYBR blue mastermix (Grisp), with ROX reference dye, was used. After blending this mastermix with the respective primers and adequate amount of PCR Grade Water, 19 µL were pipetted into each well of the PCR plate (Nerbe

Plus), followed by the addition of 1 µL of the corresponding cDNA. The amplification was done by heating to 95°C for 2 minutes (to activate the enzyme and denature the cDNA), succeeded by 40 cycles of 95°C during 5 seconds and 30 seconds at 60°C for annealing/extension and DNA detection.

The expression levels of the target genes were normalized against the reference genes (GADPH and PPIA). Data was presented as fold-change in comparison to unstimulated ASCs, calculated using the $2^{-\Delta\Delta_{ct}}$ method. Primers were designed using the Primer-BLAST tool from NCBI website, getting the sequences described in **Table 2**.

**Table 2: Primer sequences of the genes analyzed by qPCR.**

| Gene | Forward sequence (5'→3') | Reverse sequence (5'→3') |
|---|---|---|
| *GADPH* | ACATCAAGAAGGTGGTGAAGCAGG | AGCTTGACAAAGTGGTCGTTGAGG |
| *PPIA* | GTCAACCCCACCGTGTTCTT | CTGCTGTCTTTGGGACCTTGT |
| *VEGF* | TGTGTGCCCCTGATGCGATG | CTTGCTCTATCTTTCTTTGGTCTGC |
| *Angiogenin* | CGACCAGTGTCAAGACCAAGT | GAGAGCAGATGGCGGGAAA |
| *NGF* | GGCATACAGGCGGAACCACA | CGAAGGGCAGTGTCAAGGGA |
| *BDNF* | ACAGCACACTACTGACACTGAT | GGTGGAACTGTAGGGAGAAAGCA |
| *FGF-2* | CAAGCAGAAGAGAGAGGAGTTGT | CTCATCCGTAACACATTTAGAAGC |
| *IL-6* | CCACACAGACAGACAGCCACTCACCT | TTTCACCAGGCAAGTCTCCTCAT |
| *CXCL-1* | CCCAAACCGAAGTCATAGCCA | CAGGAACAGCCACCAGTGAG |
| *CXCL-2* | ATGTGACGGCAGGGAAATGT | GCTCTAACACAGAGGGAAACAC |

## 3.6 Statistical analysis

All statistical analysis was done with SPSS version 25 (IBM). Before applying any test, normal distribution was evaluated through histogram visualization, skewness and kurtosis analysis, and Shapiro-Wilk test for normality distribution. If the samples followed a normal distribution, Levene's test was used to test homogeneity of variances. Two-way ANOVA was used to analyze the number of neurite intersections, but only comparisons between groups for each distance were presented. One-way ANOVA was used in all other experiments, with the correction of Welch when Levene's test null hypothesis was rejected. For post-hoc tests, Tukey test was considered for normal data with homogeneity of variances and Games-Howell test when there was no variance homogeneity. For non-parametric data, Kruskal-Wallis test was used with Dunn pairwise tests with Bonferroni correction.

Appropriate effect sizes for each test were calculated (ANOVA and Kruskal-Wallis: eta-square ($\eta^2$); Welch's ANOVA: omega-square ($\omega^2$); Tukey and Games-Howell post-hoc: Cohen's d (d) and Dunn post-hoc: r).

All samples were expressed as mean + standard deviation (SD) unless stated otherwise. Statistical significance was considered if p-value (p) $\leq 0.05$. All tests were performed with 95 % confidence interval.

# 4. Results

## 4.1 HUVECs extraction

As the first objective of the present work was to develop a model to study the vascular morphogenesis process and how ASCs could influence this process, there was a need to implement a culture of endothelial cells. For that, HUVECs were chosen. After following the protocol described in **Section 3.2**, cells were photographed 1 day, 4 days and 7 days after the extraction. It was possible to observe that these cells proliferated well, acquiring a cobblestone shape, reaching confluence within a week (**Figures 11A-C**). Moreover, they survived the trypsinization protocol and were able to proliferate and reach confluency (**Figures 11D-E**).

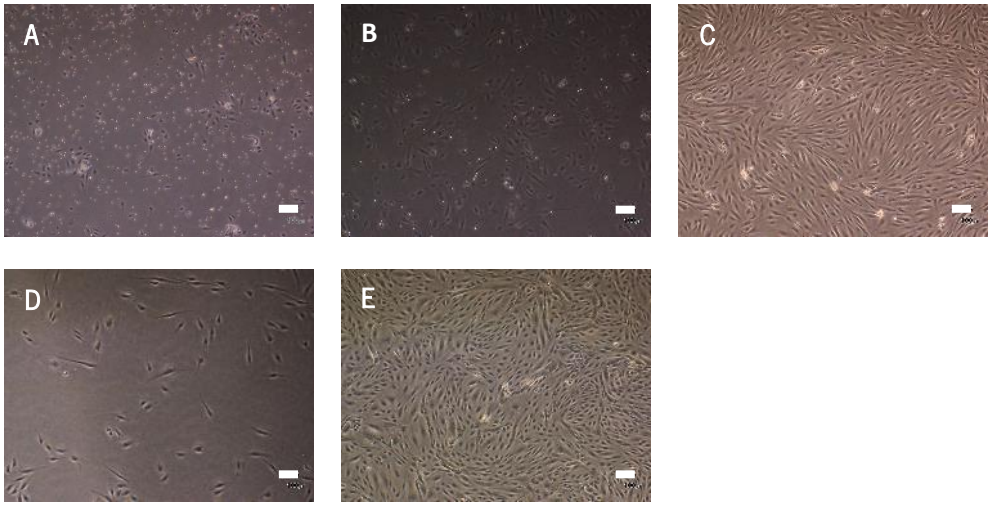


In **Figure 11: HUVECs culture. (A-C)** Morphology of HUVECs 1 day, 4 days and 7 days after the extraction, respectively.**(D-E)** Morphology of HUVECs 1 day and 5 days after trypsinization protocol. Scale bar: 100 µm.

To test the purity of the extraction protocol, these were stained for an endothelial cell marker, VWF, in which 95.20 % (SD=0.04) of total cells (counted by DAPI) were VWF positive (**Figure 12**).

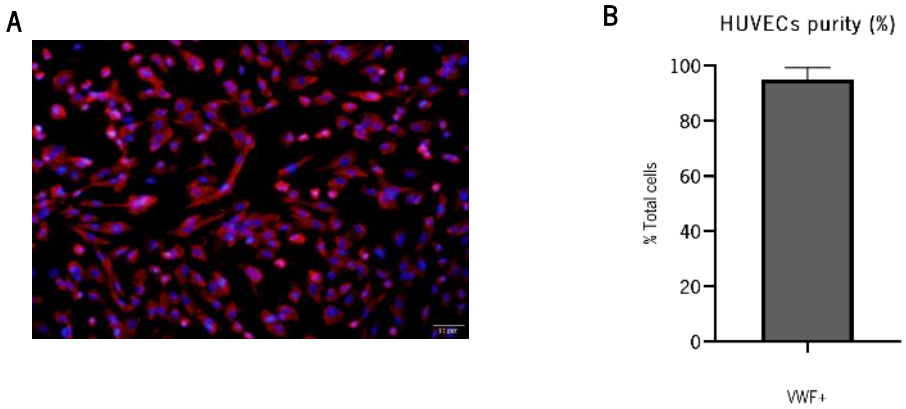


**Figure 12: Immunocytochemistry assay for HUVECs culture at P2. (A)** HUVECs were stained for VWF (red) and DAPI (Blue). Scale bar: 50 µm. **(B)** Quantification of VWF+ among DAPI+ cells, indicating high purity of VWF+ cells (95.20 ± 0.04 %). Mean + SD. N=4.

## 4.2 Co-culture medium testing

The next step was to understand in which cell culture medium the co-cultures would occur. For that, ASCs were cultured on their normal medium (**Figure 13A**) and also in complete EGM (**Figure 13B**). Also, HUVECs were cultured with the same media (**Figures 13C** and **13D**, respectively) plus one more group in which EGS was added to ASCs media (**Figure 13E**). Both experiments were done for 7 days, after which, phalloidin and DAPI staining was performed. It was observed that ASCs growth and morphology was not affected by cell culture media. Moreover, HUVECs could also grow in both cell culture medium that has EGS present.

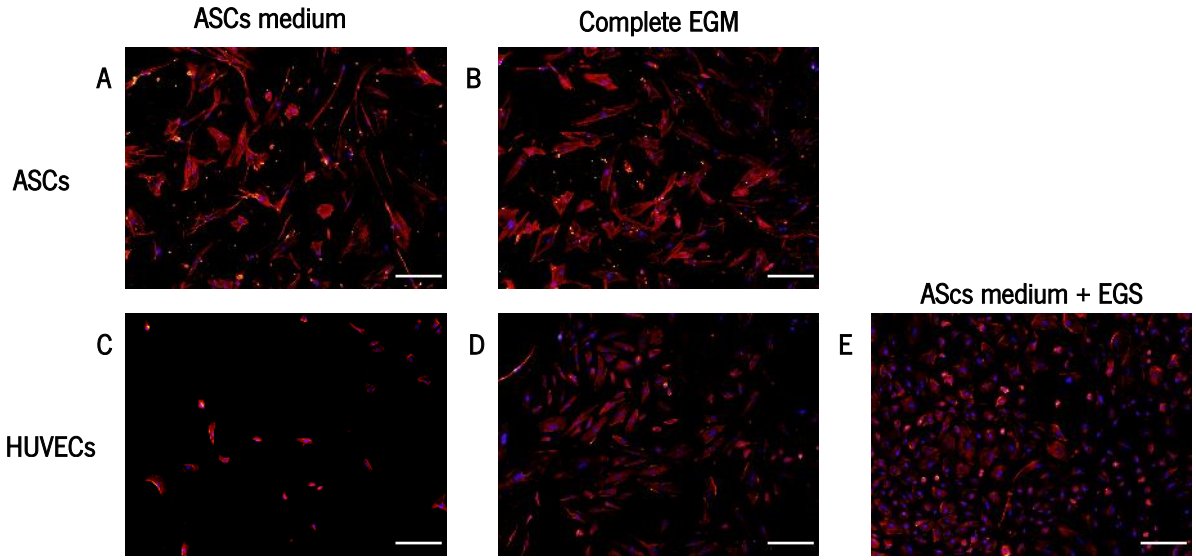


**Figure 13: Co-culture medium testing. (A, B)** ASCs were cultured in their medium and also in complete EGM, for 7 days, and then stained with phalloidin (red) and DAPI (blue). **(C-E)** HUVECs were cultured in the same conditions and then in ASCs medium with the endothelial growth supplement (EGS). Scale bar: 200 µm.

## 4.3 Effect of inflammatory mediators on ASCs

ASCs were stimulated with different inflammatory mediators to understand how these molecules could influence the regenerative potential of ASCs. However, it was necessary to understand if these molecules could elicit cytotoxicity. For that, ASCs were stimulated with pro-inflammatory mediators (LPS+IFN-γ) or with an anti-inflammatory mediator (IL-10) for 24 hours on concentrations that have previously demonstrated to be able to modulate immune cells phenotype, namely macrophages (Kigerl *et al.*, 2009; Makita *et al.*, 2015; Mantovani *et al.*, 2004). After phalloidin and DAPI staining, no visible differences were observed in ASCs morphology between treated and untreated ASCs at 24 hours (**Figures 14A-C**). Moreover, even after removing the stimulus and let cells grow for 3 days, no differences were found and cells seem to proliferate well (**Figures 14D-F**).

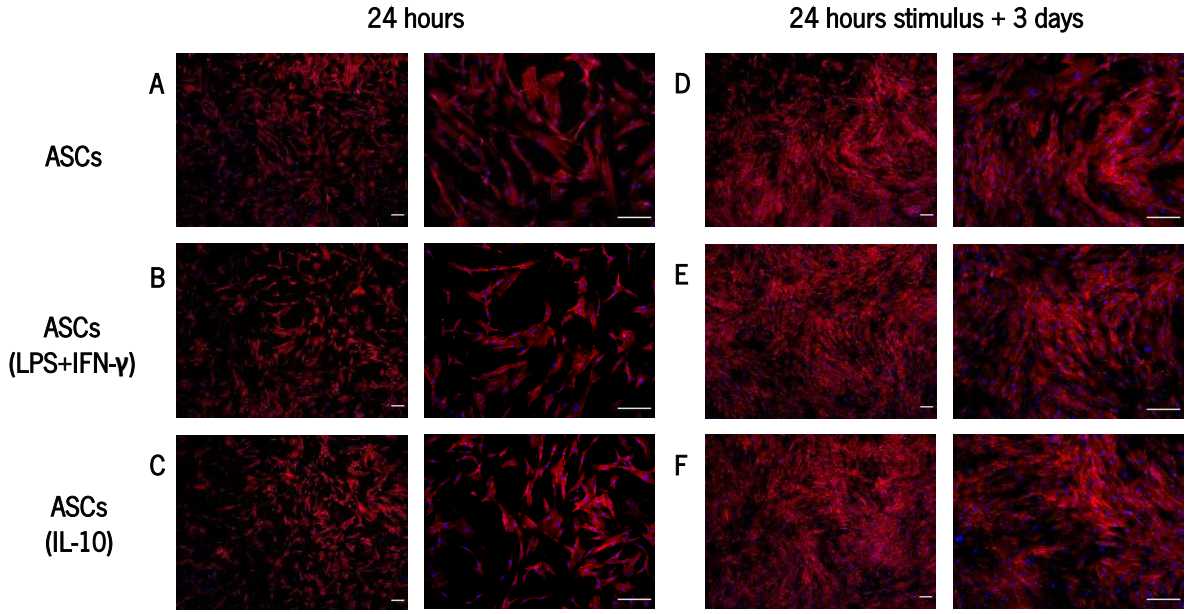


**Figure 14: Effect of inflammatory mediators on ASCs morphology. (A-C)** ASCs were stimulated with pro-inflammatory (LPS+IFN-γ) or anti-inflammatory (IL-10) molecules for 24 hours and then stained for phalloidin (red) and DAPI (blue). **(D-F)** Also, after stimulus removal, cells were let to grow for 3 days before being fixed and stained with the same markers. Scale bar: 200 μm.

## 4.4 Vascular morphogenesis assay

To study the vascularization process, namely vascular morphogenesis, it was necessary to implement a model that was suitable for this purpose, while simultaneously being able to be used within the paracrine and non-paracrine mechanisms pursued in the scope of this thesis. It is described that HUVECs assemble into vessel-like structures when plated on a gel that mimics the ECM (Goodwin, 2007; Staton *et al.*, 2009). With this in mind, several optimization steps were undertaken to achieve a model that fulfilled these criteria. The initial idea consisted in using collagen type I as a matrix. Several

different parameters were tested namely cell density, gel concentration, the presence of angiogenic factors, and encapsulation or not of HUVECs. However, none could elicit a robust formation of vessel-like structures, even when spanning the experiment to 7 days. Therefore, the ECM gel was switched from collagen to matrigel. With this matrix, using a cell density of 20 000 cells/cm$^2$, vessels-like structures were observed after 16 hours. After staining, several parameters were analyzed. All parameters were normalized to the explant area except for average vessel length. This was done to correct the degree of cell spreading as well as cut parts of the borders of the image due to technical limitations.

### 4.4.1 Indirect co-culture of HUVECs and ASCs

To understand how the paracrine crosstalk between ASCs and HUVECs could influence HUVECs ability to form vessels, the setup described in **Section 3.3.1** was used. It was possible to observe the formation of vessel like-structures at 16 hours (**Figure 15**). No statistical differences were found in the percentage of vessel area, junction density, and average vessel length (**Figure 16**) (**Table 1A**). Regarding explant area, ASCs (LPS+IFN-γ) presented higher values when compared to control ($p=0.033$, $r=0.693$). However, when analyzing total vessel length and number of endpoints, unstimulated ASCs have statistically higher values than the control group. ($p=0.028$, $d=2.043$ and $p=0.010$, $d=2.371$); but this effect was not seen with inflammatory stimulation (**Figure 16**) (**Tables 1A** and **2A**). This data indicates that, under paracrine crosstalk, ASCs without any stimulation seem to induce more vessel like-structures but without any major alterations on average vessel length and interconnectivity.

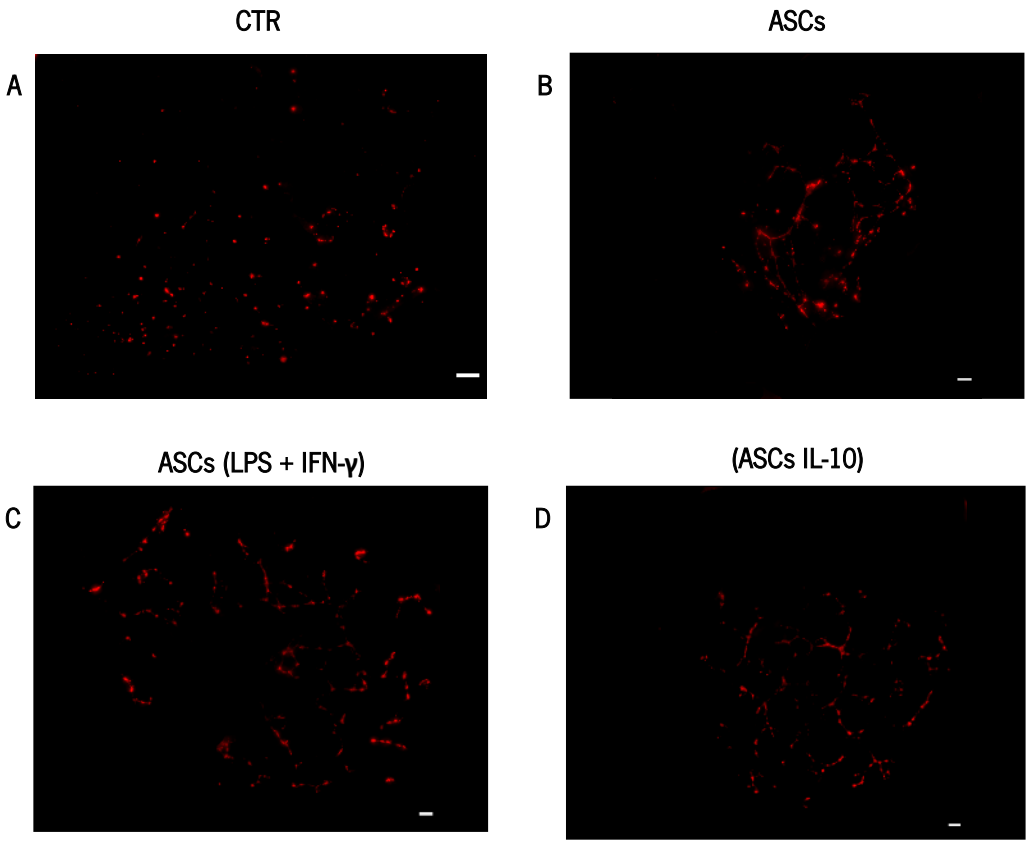


**Figure 15: Indirect contact impact on vascular morphogenesis. (A-D)** Representative images of the vessel-like structures formed by HUVECs when in indirect contact with no cells, with unstimulated ASCs, ASCs preconditioned with LPS+IFN-γ or with ASCs preconditioned with IL-10, respectively. HUVECs were stained with phalloidin (red). Scale bar: 200 µm.

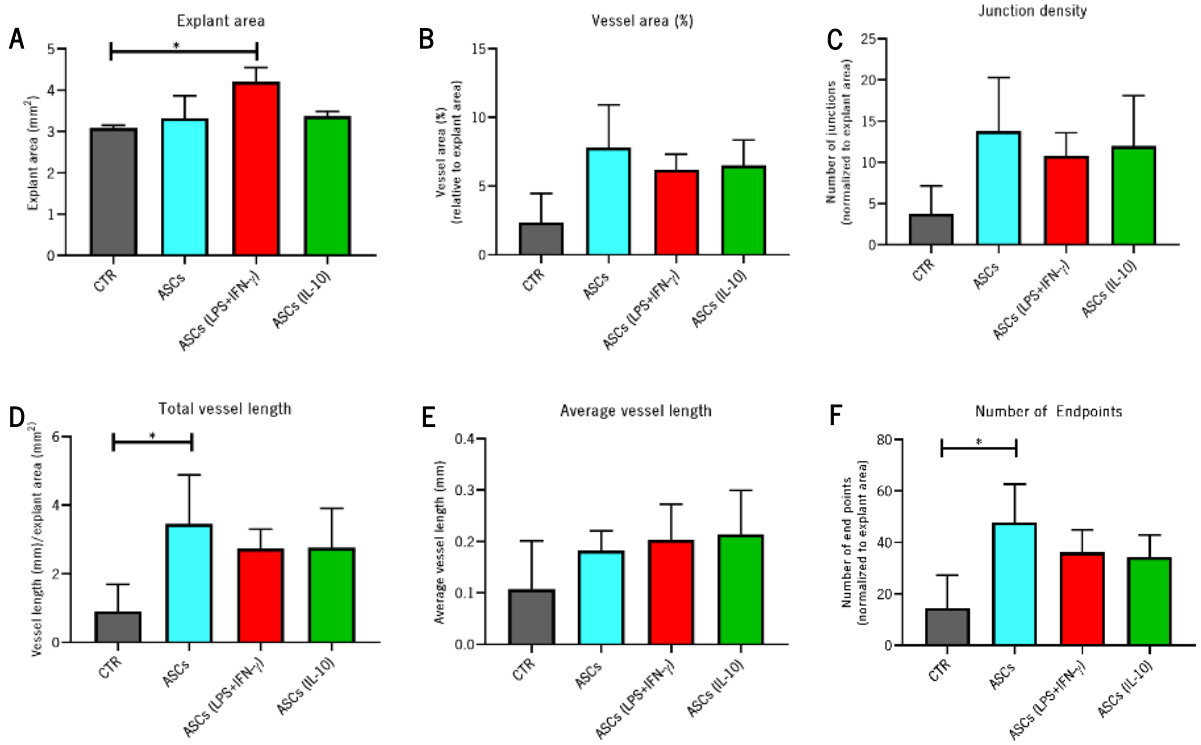


**Figure 16: Vascular morphogenesis parameters on indirect co-cultures.** After the staining of HUVECs, several parameters related to the vascular organization were analyzed on AngioTool Software. All data except average vessel length was normalized to explant area. Data presented as mean + SD except for explant area which is represented as median + interquartile range. N=3-4 per group. **(A)** Kruskal-Wallis

with Dunn pairwise test with Bonferroni correction. **(B)** Welch's ANOVA. **(C, E)** One-way ANOVA. **(D, F)** One-way ANOVA with Tukey post-hoc test *p≤0.05.

### 4.4.2 Secretome effect on vascular morphogenesis

Regarding the secretome impact on vascular morphogenesis, it was also possible to observe the formation of blood vessels (**Figure 17**). However, it should be noticed that secretome without EGS added did not elicit vessel-like structures formation. No statistical differences were found between groups on explant area (**Figure 18, Table 3A**). In contrast to the indirect co-culture, the secretome of ASCs (LPS+IFN-γ) presented higher total vessel length (compared to ASCs (IL-10) (p=0.049, d=2.338) as well as higher average vessel length (compared to unstimulated ASCs (p=0.013, d=2.822) and ASCs (IL-10) (p=0.006, d=3.110)) (**Table 4A**). This was accompanied by a higher degree of interconnection observed by the increased junction density in this group (compared to ASCs (IL-10) (p=0.033, d=2.733). It should be noted that although no statistical differences were found between the secretome of unstimulated ASCs and ASCs (LPS+IFN-γ) regarding junction density these p-values are near the limit the statistical significance, with a high effect size similar to the groups where statistically significant differences were found (p=0.053, d=2.737). The same was observed for average vessel length when comparing ASCs (LPS+IFN-γ) and control (p=0.053, d=2.016). This data reinforces the idea that the secretome of ASCs stimulated with the pro-inflammatory mediators could promote a higher degree of vascular morphogenesis either at length and complexity.

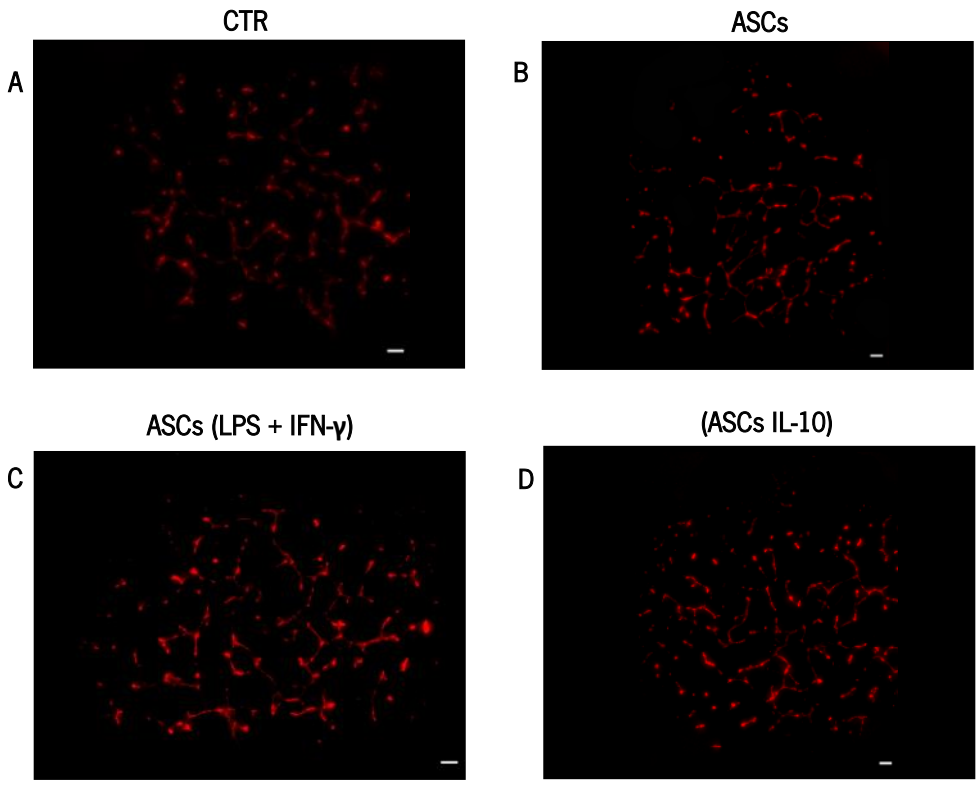


**Figure 17: Secretome impact on vascular morphogenesis. (A-D)** Representative images of the vessel-like structures formed by HUVECs when cultured with medium used for secretome collection, with Secretome of ASCs, with the secretome of ASCs preconditioned with LPS+IFN-γ or with the secretome of ASCs preconditioned with IL-10, respectively. HUVECs were stained with phalloidin (red). Scale bar: 200 µm.

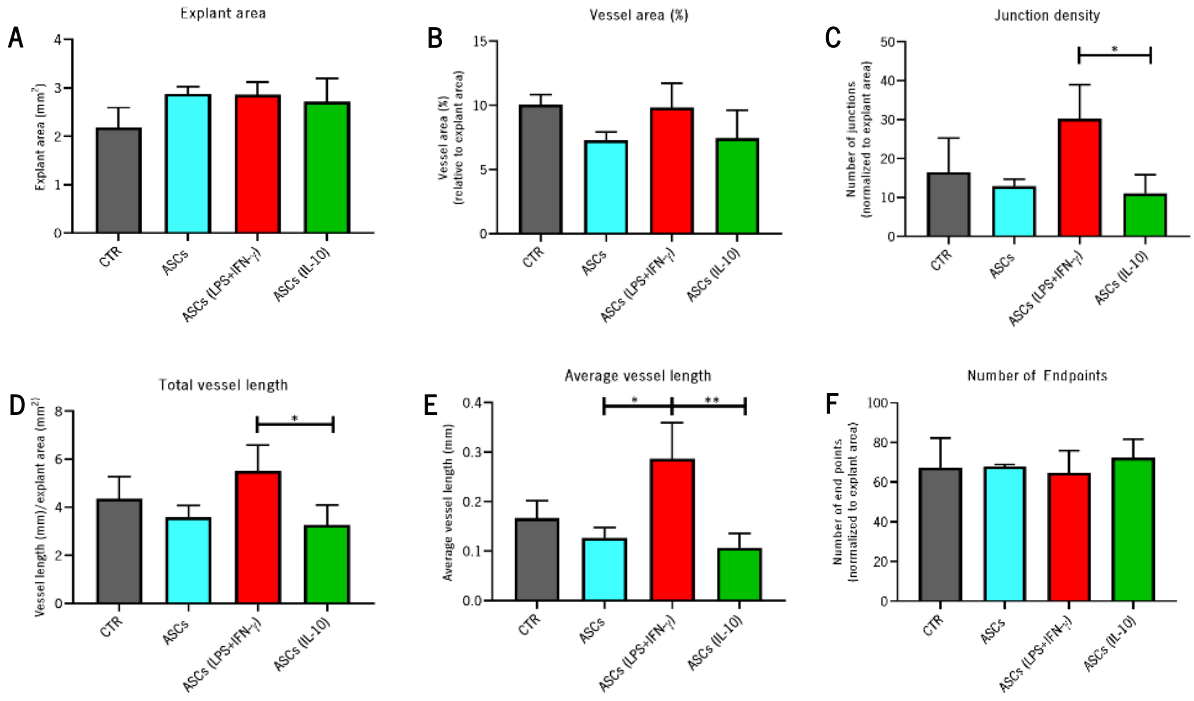


**Figure 18: Vascular morphogenesis parameters in secretome cultures.** After the staining of HUVECs, several parameters related to the vascular organization were analyzed on AngioTool Software. All data except average vessel length were normalized to explant area. Data presented as mean + SD. N=3 per group. One-way ANOVA with Tukey post-hoc test. *p<0.05.**p<0.01.

### 4.4.3 Cell contact co-culture of ASCs and HUVECs

Concerning the experimental setup used to study how ASCs could modulate the vascularization process in a close contact approach, it was not possible to observe a robust blood vessel formation with the majority of cells acquiring a round appearance and not elongating (**Figure 19**). Nonetheless, analysis of the different parameters revealed that ASCs (IL-10) presented significant higher vessel area and junction density (compared to control (p=0.030, d=2.922 and p=0.022, d=5.974) and to unstimulated ASCs (p=0.037, d=2.523 and p=0.002, d=5.768) (**Figure 20**) (**Tables 5A** and **6A**). This effect was also observed in the number of endpoints where this group presented more endpoints than the control group (p=0.009, d=4.694). In contrast, all group with cells have less average vessel length than the group without cells (Ctr vs ASCs: p=0.011, d=3.958; Ctr vs. ASCs (LPS+IFN-γ): p=0.019, d=2.646; Ctr vs ASCs (IL-10): p=0.024, d=2.839) (**Figure 20**) (**Tables 5A** and **6A**). However, these results should be looked at with caution when taking conclusions as no robust vessel formation was observed in all groups.

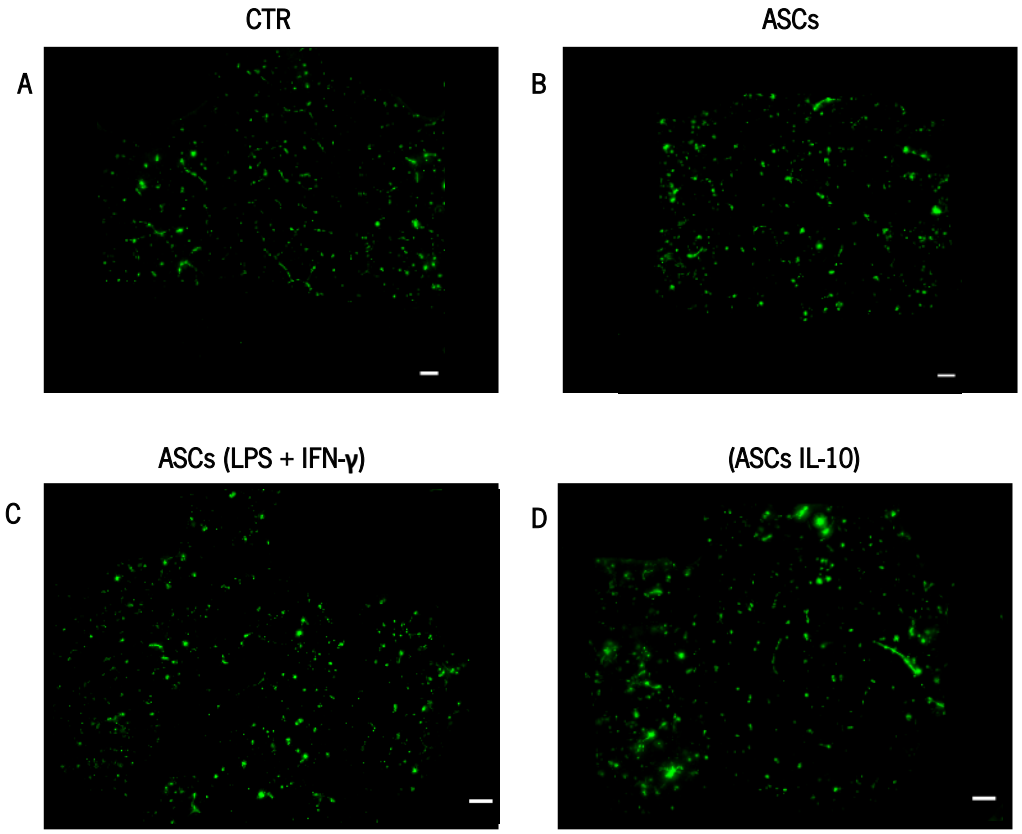


**Figure 19: Direct contact impact on vascular morphogenesis. (A-D)** Representative images of the vessel-like structures formed by HUVECs when in direct contact with no cells, with unstimulated ASCs, ASCs preconditioned with LPS+IFN-γ or with ASCs preconditioned with IL-10, respectively. HUVECs were stained with VWF (green). Scale bar: 200 µm.

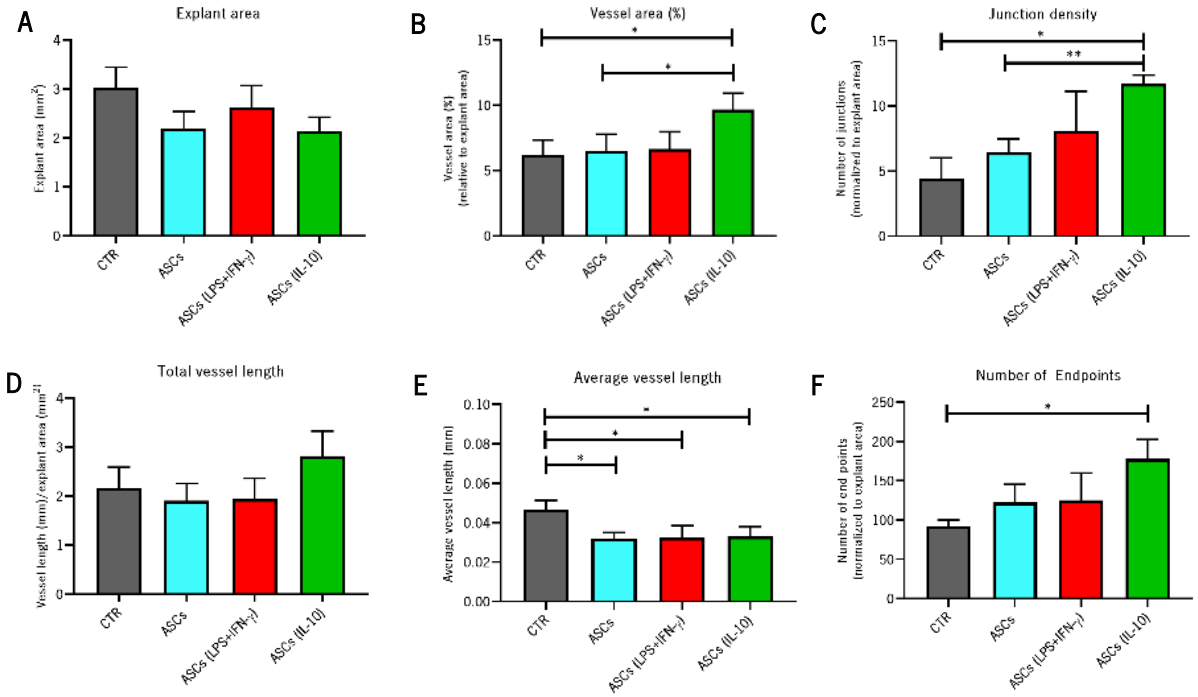


**Figure 20: Vascular morphogenesis parameters on direct contact co-cultures.** After the staining of HUVECs, several parameters related to the vascular organization were analyzed on AngioTool Software. All data except average vessel length was normalized to explant area. Data presented as mean + SD. N=3-4 per group. **(A, B, D, E, F)** One-way ANOVA with Tukey post-hoc test. **(C)** Welch's ANOVA with Games-Howell post-hoc. *p<0.05. **p<0.01.

## 4.5 Neurite Outgrowth assay

To study how the ability of ASCs to promote neurite growth was influenced by the different inflammatory factors, a DRG model was used as DRG produce neurites under specific conditions that can be compared between different treatments. In all groups, the neurite area, the longest neurite and the arborization pattern were evaluated.

### 4.5.1 Paracrine crosstalk impact on neurite outgrowth

To understand how the different inflammatory molecules used could influence ASCs ability to induce neurite outgrowth, a droplet of collagen with the DRG was put on top of ASCs that were previously stimulated. Although it was possible to observe neurite outgrowth with this setup, no differences were found in any parameter evaluated (**Figures 21, 22** and **23**) (**Tables 7A** and **8A**).

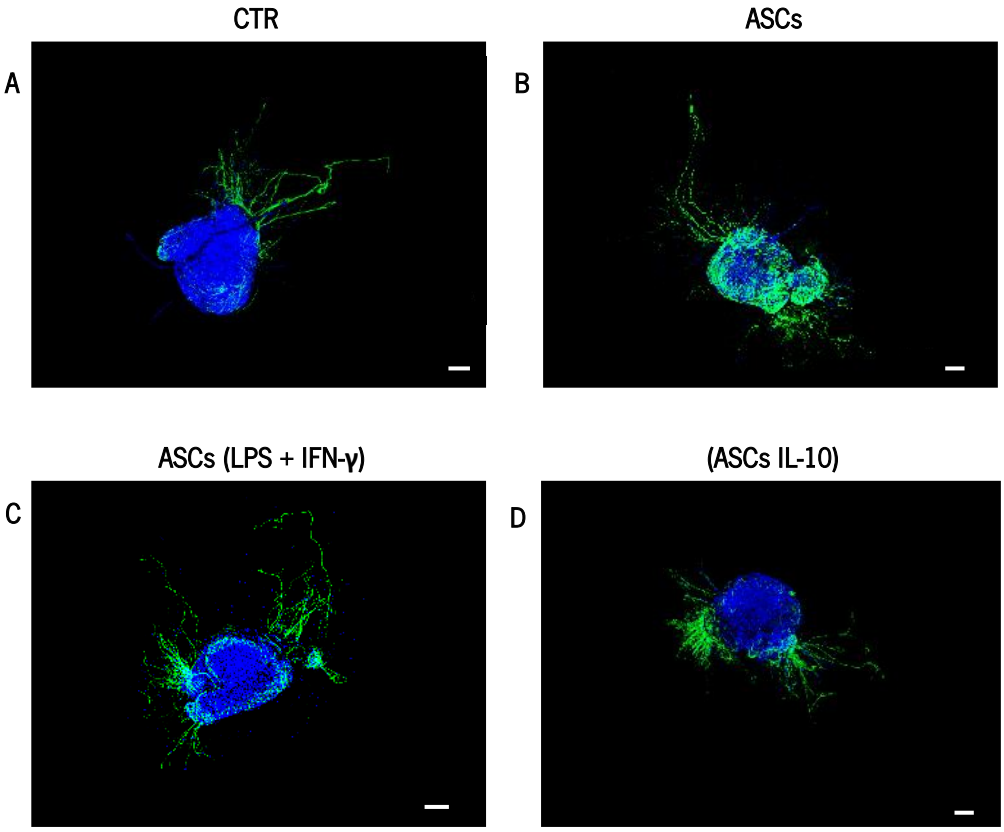


**Figure 21: Indirect contact impact on neurite outgrowth. DRG explants were used as a model to assess neurite outgrowth. (A-D)** Representative images of the DRG stained with neurofilament (green) and DAPI (blue) when in indirect co-cultures with no cells, with unstimulated ASCs, ASCs preconditioned with LPS+IFN-γ or with ASCs preconditioned with IL-10, respectively. Scale bar: 200 µm.

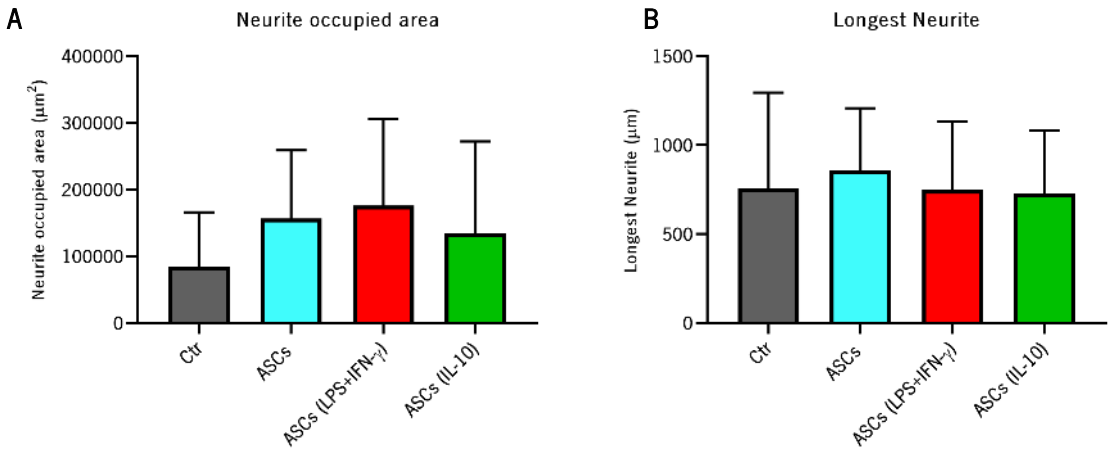


**Figure 22: Neurite outgrowth analysis after indirect co-culture. (A-B)** Neurite area and longest neurite quantified using the NeuriteJ plugin of ImageJ. Data represented from two independent experiments with N=8-9 from each group/experiment. Mean + SD. One-way ANOVA.

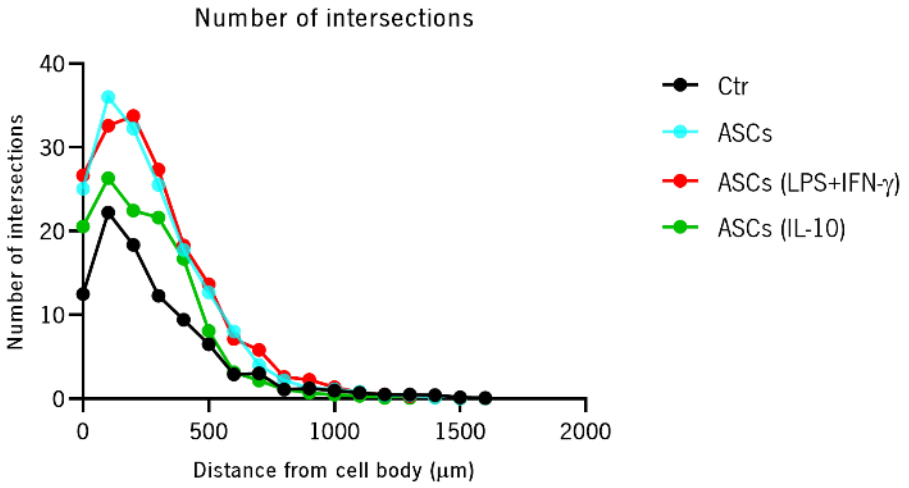


**Figure 23: DRG neurite complexity in indirect co-culture.** Using the NeuriteJ plugin, concentric rings were created around the cell body and the number of neurite intersections at each 100 µm was acquired. Data presented as means values from two independent experiments with N=8-9 from each group/experiment. Two-way ANOVA.

### 4.5.2 Secretome effect on neurite outgrowth

Using the same model as previously described, the effect of ASCs secretome on neurite outgrowth was assessed (**Figure 24**). No DRG from the control group was able to grow. Due to this, no statistical test was able to be performed taking this group into account. Therefore, it is possible to observe that the secretome of ASCs could promote neurite growth, in contrast to control. However, this growth was less than in indirect contact (**Figures 25** and **26, Tables 9A** and **10A**).

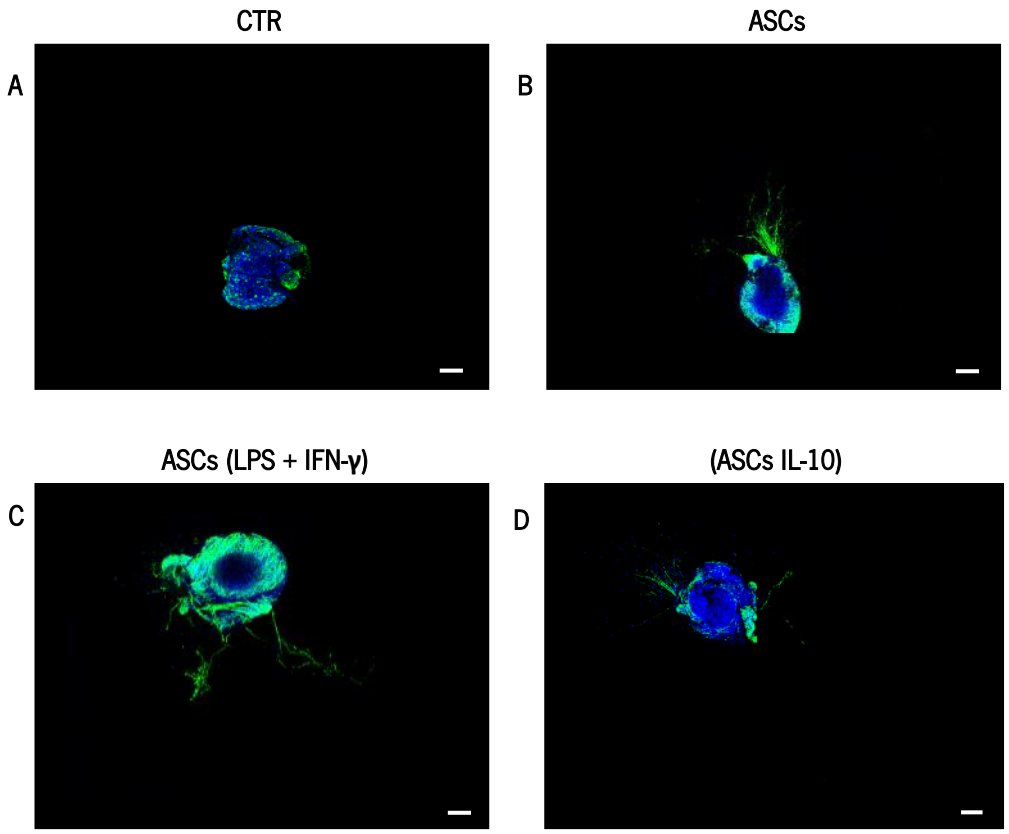


**Figure 24: Secretome impact on neurite outgrowth. (A-D)** Representative images of the DRG stained with neurofilament (green) and DAPI (blue) when cultured with medium used for secretome collection, with secretome of ASCs, with the secretome of ASCs preconditioned with LPS+IFN-γ or with the secretome of ASCs preconditioned with IL-10, respectively. Scale bar: 200 µm.

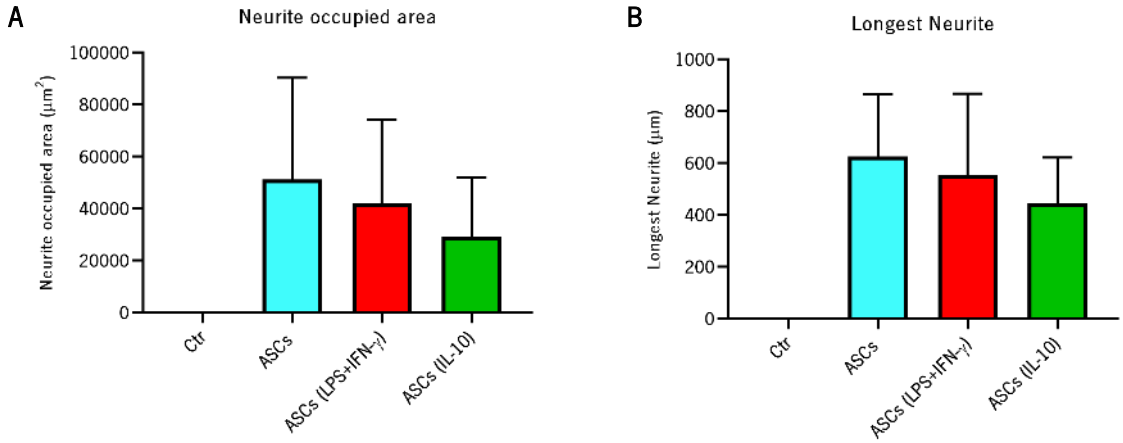


**Figure 25: Neurite outgrowth analysis after secretome cultures. (A-B)** Neurite area and longest neurite quantified using the NeuriteJ plugin of ImageJ. Data represented from two independent experiments with N=3-5 from each group/experiment. Mean + SD. One-way ANOVA.

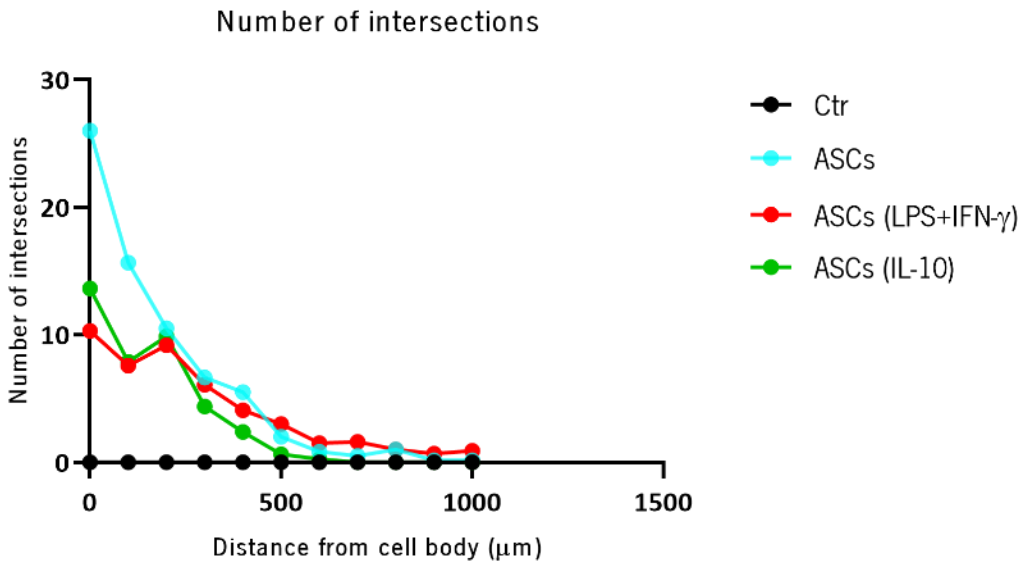


**Figure 26: DRG neurite complexity in secretome cultures.** Using the NeuriteJ plugin, concentric rings were created around the cell body and the number of neurite intersections at each 100 µm was acquired. Data presented as means values from two independent experiments with N=3-5 from each group/experiment.

### 4.5.3 Direct contact between DRG and ASCs

The final parameter to be evaluated on DRGs was if the direct contact could elicit the same type of response when compared to the paracrine experiments. It was observed that the control group did not elicit any growth and therefore all values were considered zero and no statistical test was performed considering this group. Furthermore, no differences were found between groups on the two parameters evaluated. However, this setup presented the higher mean values of neurite growth when compared to the paracrine experiments (**Figures 27, 28** and **29 Tables 11A** and **12A**).

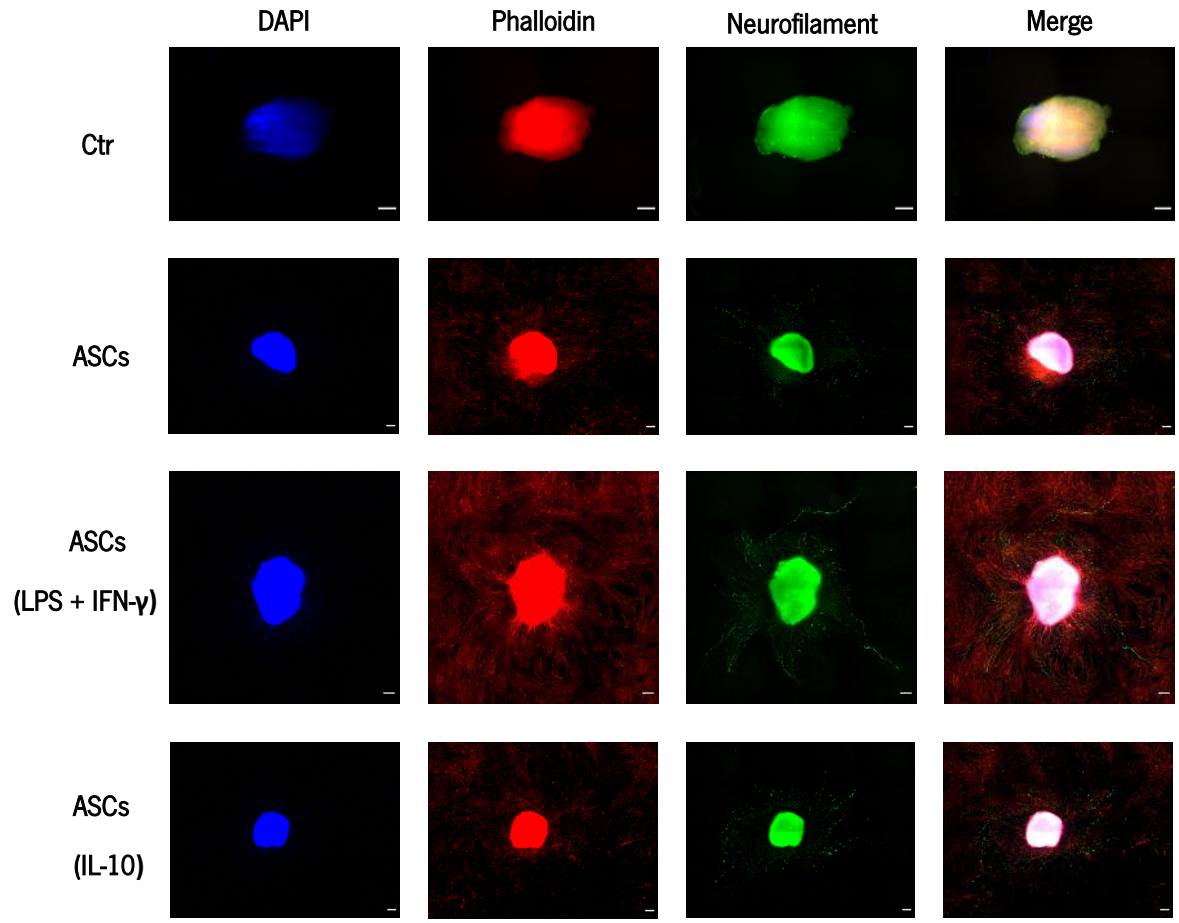


**Figure 27: Direct co-culture impact on neurite outgrowth. (A-D)** Representative images of the DRG stained with neurofilament (green), phalloidin (red) and DAPI (blue) when cultured in direct co-cultures with no cells, with unstimulated ASCs, ASCs preconditioned with LPS+IFN-γ or with ASCs preconditioned with IL-10, respectively. Scale bar: 200 µm.

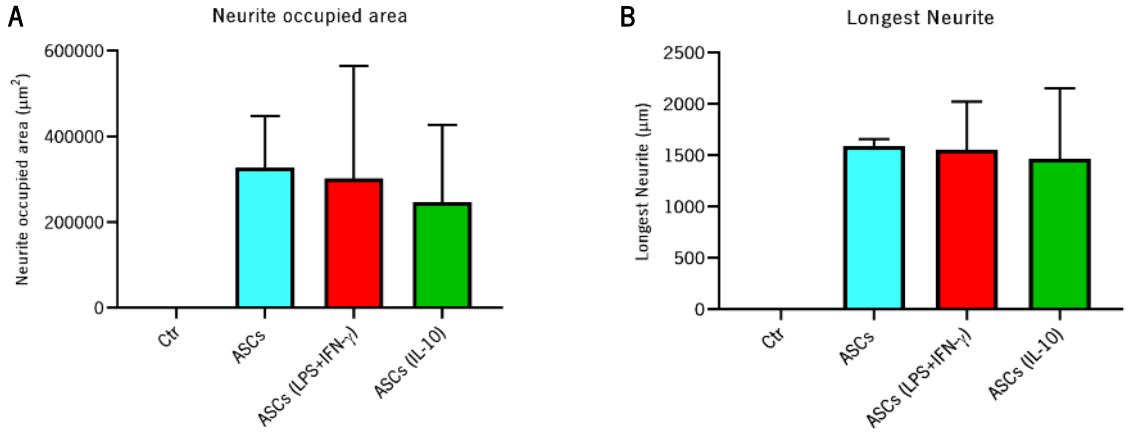


**Figure 28: Neurite outgrowth analysis after direct co-culture. (A-B)** Neurite area and longest neurite were quantified using the NeuriteJ plugin of ImageJ. N=4 for the control group and N=6-9 for other groups. Mean + SD. Welch's ANOVA.

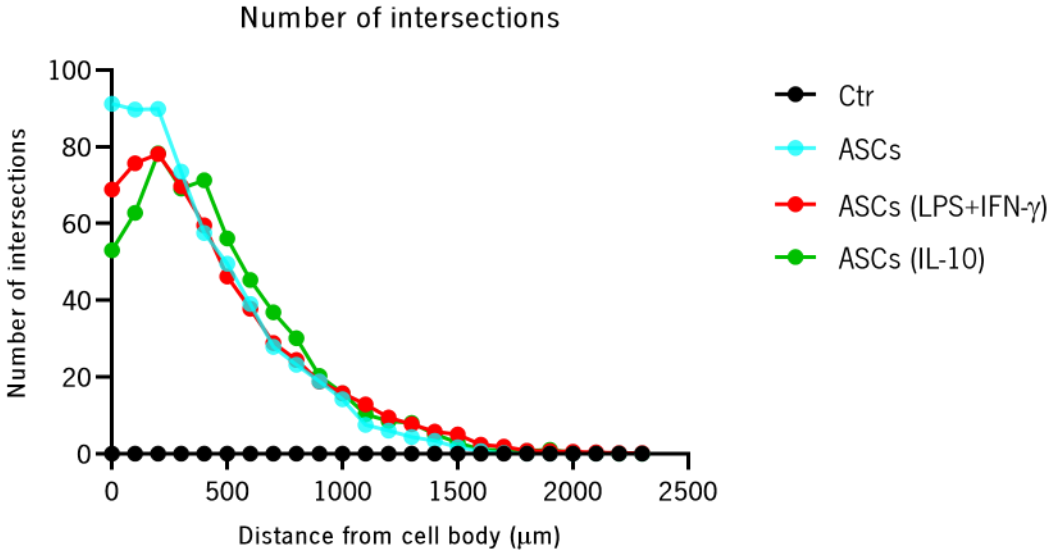


**Figure 29: DRG neurite complexity in direct co-culture.** Using the NeuriteJ plugin, concentric rings were created around the cell body and the number of neurite intersections at each 100 µm was acquired. Data presented as means values. N=4 for the control group and N=6-9 for other groups. Two-way ANOVA.

## 4.6 Gene expression analysis after inflammatory stimulation

To further explore some possible mechanisms behind the biological responses observed, the expression levels of several genes were assessed by qPCR. 6 hours after stimulating the ASCs with LPS+IFN-γ or IL-10, mRNA levels were measured to different genes associated with vascularization, neurite growth, and immune response (**Table 2**). The reference genes were similar across groups as no differences between the cycle of quantification were observed.

Taking this account, the fold difference normalized to the reference genes and to control groups was plotted for the different genes (**Figure 30**). No differences were found between groups on BDNF, FGF-2, CXCL1, and CXCL2 expression levels. On the other side, VEGF was significantly augmented in the ASCs (LPS+IFN-γ) comparing to the unstimulated group (p=0.047, d=3.250) (**Tables 13A** and **14A**). However, angiogenin expression was significantly decreased compared to ASCs (IL-10) (p=0.044, d=2.144) (and with a near significant p-value and high effect size against the unstimulated group (p=0.054, d=3.412). Moreover, NGF expression was significantly diminished in ASCs (LPS+IFN-γ) compared to the unstimulated ASCs (p=0.022, d=0.303) and ASCs (IL-10) (p=0.010, d=0.206), albeit with small effect sizes. Finally, IL-6 expression was augmented in this group compared to unstimulated ASCs (p=.008, d=6.519) and ASCs (IL-10) (p=0.005, d=3.106). Overall, pre-conditioning with the different inflammatory mediators led to specific alterations in gene expression related to processes studied, with the group ASCs (LPS+IFN-γ) being the most affected.

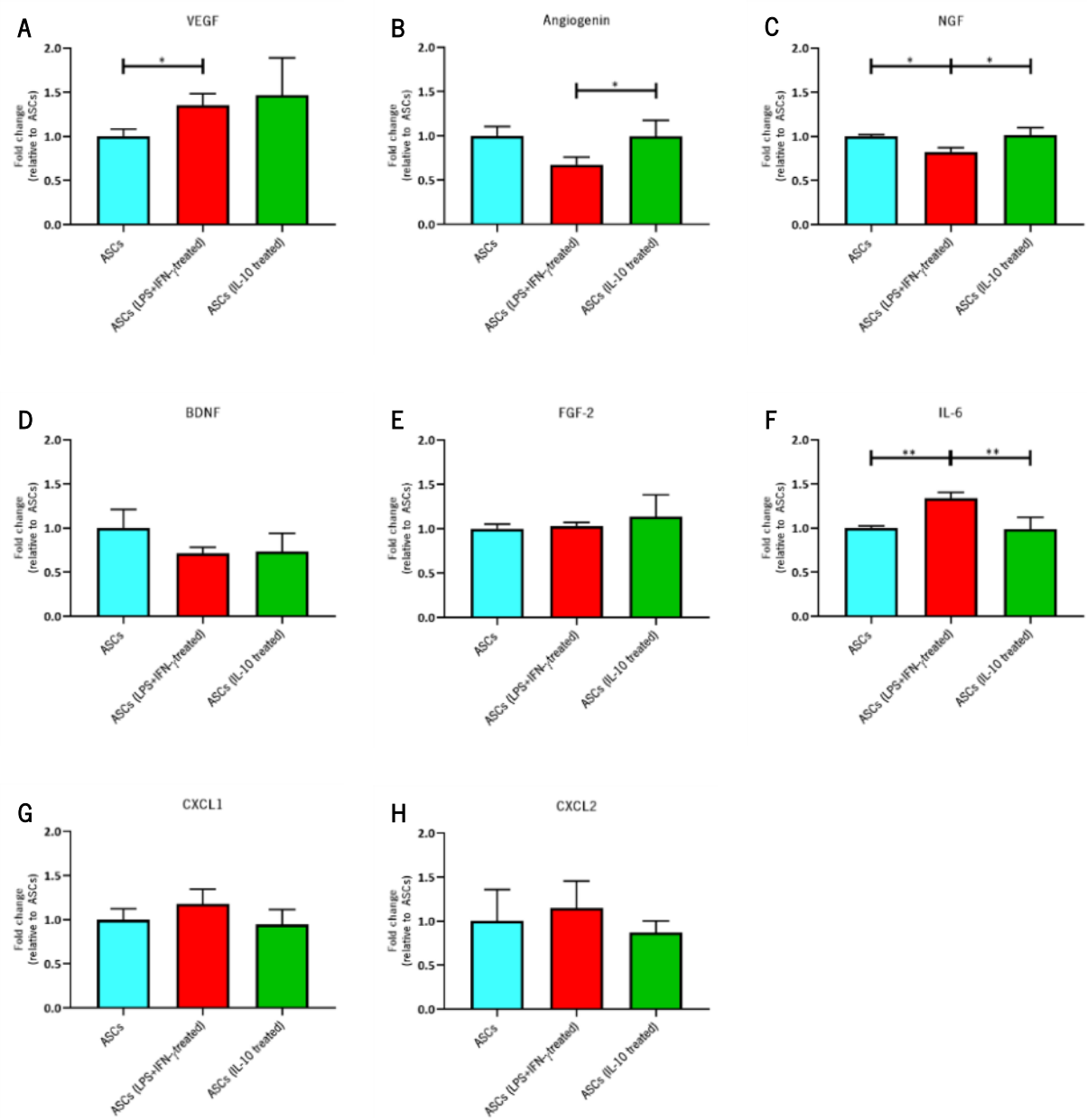


**Figure 30: Gene expression analysis.** After 6 hours of incubation with the inflammatory molecules, RNA from ASCs was collected and gene expression analysis was performed by qPCR, for several different genes. All data is normalized to two reference genes and presented as fold difference expression related to unstimulated ASCs and presented as mean + SD. n=3-4 per group **(A)** Welch's ANOVA with Games-Howell post-hoc test. **(B, C, F)** One-way ANOVA with Tukey post-hoc test. (D, E, G, H) One-way ANOVA.

# 5. Discussion

SCI is a devastating condition, with several biochemical processes contributing negatively to the progression of the injury, to which there is not an effective treatment available. One major aspect of the injury pathophysiology that has not been fully addressed is the vascular dysfunction that occurs after injury. Indeed, some reports showed the contribution of endothelial cells to the limited recovery observed after SCI either at a major vascular level or by alterations at a cellular and molecular level (Benton & Hagg, 2011; Figley *et al.*, 2014; Mataliotakis & Tsirikos, 2016; Popa *et al.*, 2010).

The damage of neuronal cells plays a key role on the loss of function seen after SCI, and for that reason, has been the focus of research for novel therapies. However, in order to accomplish a successful treatment, research should also take into consideration the complexity of SCI and tackle other issues that may hinder the outcome observed, such as endothelial cells and the biological processes where they participate.

Several therapeutic approaches are being developed in order to treat the injured spinal cord, being one of the most promising the use of either stem cells or the molecules secreted by them (Gomes *et al.*, 2020; Kabu *et al.*, 2015; Mothe & Tator, 2012; Silva *et al.*, 2014; Vismara *et al.*, 2017). In our group, ASCs and their secretome have shown promising results in SCI and have been positively associated with processes associated with vascularization, immunomodulation, neurodifferentiation, and nerve repair. (Assunção-Silva *et al.*, 2018; Gomes *et al.*, 2016, 2018; Pinho, 2019; Pires *et al.*, 2016; Rocha *et al.*, 2020a; Serra *et al.*, 2018).

However, a fully effective response was not yet developed and this may be due to non-optimal procedures applied to these cells. Despite that our group and others are already searching for new ways to improve their therapeutic potential, such as the use of bioreactors or genetic engineering, further work needs to be performed to achieve a satisfactory response (Mendes-Pinheiro *et al.*, 2020; Teixeira *et al.*, 2016a; Teixeira & Salgado, 2020; Vizoso *et al.*, 2017). One possible strategy to improve cell and secretome therapies is by pre-conditioning stem cells with molecular stimuli. Within these, inflammatory factors are particularly interesting as these cells are known to respond to inflammation, and modulate its behavior according to it (Bernardo & Fibbe, 2013; Li & Hua, 2017; Shi *et al.*, 2012). However, the major focus of inflammatory preconditioning has been on improving the immunomodulatory profile of stem cells. Therefore, there was a need to understand what these stimuli would do to the ASCs regenerative capacities at the neural and vascular levels. Moreover, as the most effective strategy for SCI between cells or secretome is not yet defined, it is also important to understand if the inflammatory molecules affect in the same way the paracrine and non-paracrine mechanisms of ASCs.

For these reasons, in this work, we aimed to understand how pro and anti-inflammatory stimuli influenced ASCs ability to induce vascularization and neurite outgrowth, as these two parameters are essential for a successful SCI therapy.

To achieve these aims we first set out to establish an *in vitro* system that could be used as a means to evaluate the vascularization process. The first step on that was to have a culture of endothelial cells. Although many endothelial cells are now available for research use, HUVECs are still one of the most used when assessing vascularization due to their easy extraction, maintenance, and available know-how. Therefore, we aimed to establish a culture of HUVECs in our group. For that, umbilical cords from consenting donors from Hospital de Braga were used for the extraction of these cells. It was observed that within a week these cells acquired confluence and cobblestone morphology. Moreover, they could survive and proliferate well after the trypsinization protocol (**Figure 11**). However, these cells should not be used in high passages as their ability to perform vessel-like structures is diminished (Xie *et al.*, 2016). For this reason, HUVECs were only used until P4. Using VWF, a protein important for the adhesion of platelets to the blood vessels, as a marker to characterize our culture, it was observed an HUVECs purity of around 95 % (**Figure 12**). Although this represents almost 100 %, there are about 5 % of cells that do not express this marker. This small impurity could be explained using two reasons. The first one is that there is a contamination of other cells in this culture and therefore it would be interesting to understand if this percentage is maintained along passages as well as to do other stainings for possible contaminant cells. The second reason goes with the know-how acquired through the development of single-cell sequencing where it has been shown that within a given population, the expression of a given gene may be heterogeneous. Thus, it is possible that some endothelial cells may not express this marker and other markers are needed to be assessed as well as other techniques (e.g flow cytometry) to give a more robust characterization of this population.

After this culture was established, the next step consisted of the development of an assay that allowed the study of the paracrine and non-paracrine interaction of primed ASCs on vascularization. The formation of new vessels comprises a complex process that can occur in mainly two ways: vasculogenesis and angiogenesis. The first, mainly present during embryonic development, consists in the differentiation of angioblasts into endothelial cells, followed by their aggregation and generation of a vascular structure (Kolte *et al.*, 2016; Naito *et al.*, 2020). On the other hand, angiogenesis is the formation of new blood vessels from pre-existing ones, being the most common process of vascularization in the adult. It has several stages that can be divided into matrix degradation, migration, proliferation, sprouting, morphogenesis, and vessel maturation, with several techniques already

described to study these functions. (Goodwin, 2007; Kolte *et al.*, 2016). One of the most common is the use of endothelial cells on top of an ECM like collagen or matrigel (Arnaoutova & Kleinman, 2010; Staton *et al.*, 2009). With this setup, endothelial cells are able to form vessel-like structures within a short period of time, allowing for the study of vascular morphogenesis. As in SCI, an angiogenic response is observed in the first week, it is important to understand how ASCs could influence the vessel organization of these cells. As collagen gels were already established in the group, the first experiments consisted on using these gels. Several different variables were tested, namely: cell density, gel concentration, presence of angiogenic factors, and encapsulation of HUVECs, but none could elicit a robust formation of vessel-like structures even in longer experiments. Several factors may have contributed to this. For instance, the collagen gels that were used derive from rat and this may cause some incompatibility with human cells. Additionally, in these experiments type I collagen was used, where it has been described that type IV and V collagens induce more vessel formation since they are present in the basement membrane while type I collagen is more interstitial (Staton *et al.*, 2009). To overcome this technical problem collagen gels were subsequently changed to matrigel. The latter is obtained by using the secreted molecules of mouse sarcoma cells being mainly constituted by laminin, collagen type IV, plasminogen activator and other growth factors secreted by these tumor cells. With this matrix, HUVECs formed vessels within 16 hours. Although no studies longer than 16 hours were performed in the present work, some reports indicate that vessels start to degrade after 18-24 hours (DeCicco-Skinner *et al.*, 2014). This is indicative that the vascularization process is indeed complex and a branching and organization stimulus is not sufficient to maintain vessels. In fact, some authors demonstrated that ASCs promoted longer periods of vessel maintenance (Pill *et al.*, 2018).

As the main goal was to conduct co-culture experiments with ASCs, it was necessary to understand which cell culture medium could be applied as ASCs and HUVECs grow in different media. For this reason, each cell type was tested in both media in the same conditions, with an additional group for HUVECs with ASCs medium plus the endothelial supplement (**Figure 13**). It was observed that ASCs proliferated well in both media but HUVECs only seem well when EGS was present. However, to have the most basal medium possible, when in co-culture with ASCs, EGS was removed. It was observed that HUVECs were able to form vessels even in ASCs medium without EGS when in co-culture with ASCs. This indicates that ASCs also secrete factors that influence HUVECs proliferation and survival. However, as the control group without ASCs also shown some degree of vascularization (although small as cells tended to be more rounded shape), the matrigel alone may be also contributing to better survival of HUVECs.

After selecting the medium for the co-cultures, it was necessary to focus on the main goal, that is to understand if different inflammatory molecules influence ASCs regenerative capacity. For this purpose LPS+IFN-γ and IL-10 were used as stimuli for the pro-inflammatory and anti-inflammatory stimulus, respectively, as it has been reported that these molecules can lead to the respective phenotype alterations on immune cells (Kigerl *et al.*, 2009; Mantovani *et al.*, 2004) As shown in **Figure 14** the stimulus did not elicit any visible change in ASCs morphology and number. Even when the stimulus was removed for 3 days, no changes in cell behavior was observed. Nonetheless, it would be interesting to do a deeper characterization of these stimulations regarding cell viability, proliferation, and even differentiation.

After all these necessary preliminary experiments the objectives of this work could begin to be answered. Using a transwell system, ASCs were plated on the bottom and stimulated for 24 hours. Then, HUVECs on matrigel were placed on the insert. In this way, a porous membrane was separating HUVECs and ASCs allowing changes between secreted factors. 16 hours later, cells were fixed and it was observed that vessel-like structures had been formed (**Figure 15**). Using AngioTool Software, it was possible to analyze this interconnected system by analyzing different parameters. The explant area gave the area in which the vessels were spread and was useful to give a normalization parameter as not all the groups had the same individual values of this area. Vessel area, vessel length and average vessel length gave information regarding the number of vessels that were formed as well as their length. However, this data needed to be normalized to explant area as higher explant area tend to have higher vessel area and length which difficult the interpretation of the results. The average vessel length was maintained as it is not expected to vary drastically with higher explant areas. Regarding the system interconnectivity, the number of junctions was also analyzed, i.e., the number of connections between different vessels, that when normalized to explant area could be interpreted as junction density and a measure of interconnectivity. On the other side, it was also analyzed the number of endpoints, meaning the number of points that do not connect to other vessels, which is also useful to understand the degree of complexity of the system.

So, regarding the paracrine system developed, in the control group without ASCs, HUVECs tended to be round-shaped with few elongations In contrast, when co-cultured with ASCs, HUVECs formed vessel-like structures (**Figure 15**). This resulted in higher mean values in all the parameters analyzed compared to control but with only statistical differences in total vessel length and number of endpoints between control and unstimulated ASCs (**Figure 16**). This indicates that unstimulated ASCs are able to form more vessels but with an average size equal to other groups and also with the same degree of

connections. This may suggest that the pre-conditioning with inflammatory mediators affected the paracrine crosstalk between HUVECs and ASCs. As the molecular pathways that are altered in this crosstalk are not fully elucidated, it would be interesting to measure the levels of different angiogenic-related molecules present in the cell culture media after the assay. Additionally, gene expression levels of these molecules and their receptors could be evaluated in further experiments to dissect the crosstalk between these cells.

With this same setup, the effect of the secretome of the different stimulated and unstimulated ASCs was evaluated. Once again, it was possible to observe vessel-like structures after 16 hours (**Figure 17**). This goes along with some reports that show the angiogenic paracrine proprieties of ASCs (Bernardini *et al.*, 2019; Estrada *et al.*, 2009; Verseijden *et al.*, 2010). However, in this secretome experiments, HUVECS were not able to form vessels in the absence of EGS, showing that matrigel is not enough to promote the survival and organization of these cells. Therefore, the supplement was added to the secretome and the control group. Nonetheless, with this experiment, the ASCs stimulated with the pro-inflammatory stimulus were able to induce more vessel length, with a higher average length of each vessel (**Figure 18**). Additionally, this group was also able to induce the highest degree of interconnectivity. This goes accordingly with the few reports that evaluate pre-conditioning with pro-inflammatory stimulus effect on secreted angiogenic molecules (Bernardini *et al.*, 2019; de Moraes *et al.*, 2017; Kwon *et al.*, 2013). In fact, the secretome may be the most affected by the pre-conditioning as ASCs only respond to these stimuli and not by factors secreted by HUVECs, as in the previous assay. Several reports are showing that these cells when sensing a pro-inflammatory environment, for instance, in an injury, change their phenotype and secretory profile to help in resolving inflammation (Bernardo & Fibbe, 2013; Maldonado-Lasunción *et al.*, 2018). As the formation of new vessels is part of the repair process and ASCs have been linked to the angiogenic process, it is not surprising that the angiogenic potential of these cells is enhanced when in contact with LPS and IFN-γ. Additionally, this data indicates that the molecules secreted by these cells have a direct impact on the vascularization process and do not act through external mechanisms like the recruitment of other cells. Also, it is important to note that transplanted cells into an actual SCI will respond to the different stimuli present at the injury site and that the local inflammatory milieu is more complex than this *in vitro* setting. Still, this data suggests that ASCs are able to respond to inflammatory stimulus which can induce a higher degree of reparative functions. However, one should take in consideration that pro-inflammatory molecules also act on other cells present in the lesion and that the beneficial effects of ASCs might be diminished when compared to the deleterious effects of other cells. Moreover, it has been described

that other molecules present in the lesion site, like chondroitin sulphated proteoglycans, diminish MSC angiogenic and neuro-adhesive paracrine activity (Wood *et al.*, 2018).

The direct contact assay with ASCs and HUVECs did not lead to the formation of robust vessel-like structures (**Figure 19**). However, these results should be taken with caution as it does not necessarily mean that cell proximity inhibits vascular morphogenesis (**Figure 20**). It may be just a technical issue as a consequence of cell densities inside the matrigel. It is possible that there may be a deficient diffusion of nutrient and growth factors that may influence HUVECs migration and organization. Besides, no studies were done to understand if the encapsulated ASCs in matrigel alter their phenotype and lose some regenerative potential. One fact that corroborates this is the reports showing that the direct contact between MSCs and endothelial cells can induce vessel-like structures (Pill *et al.*, 2018). For that reason, in future experiments, this assay should be optimized, including the use of different cell densities or by plating ASCs and HUVECs directly on top of the matrigel. For this reason, the differences obtained in the different parameters on the direct contact assay should not be fully interpreted as one group promoting more vascular morphogenesis than the other, as no strong vessel-like structures were observed. In fact, the average vessel length was around 10x times shorter than other assays which imply even further that this setup was not successful to study vascular morphogenesis.

Taken into account all experiments, the data indicate that ASCs can induce vascular morphogenesis, at least in a paracrine way. Also, the different inflammatory stimuli impacted ASCs differently. By looking at the secretome data, it seems that pro-inflammatory stimulation increases the secretion of the molecules responsible for this vascular organization. On the other hand, this effect was not seen on the indirect contact assays. This led to believe that while pro-inflammatory molecules may activate some angiogenic pathways, they also may act on some pathways that affect the communication with other cells, namely, HUVECs. The specific crosstalk between HUVECs and ASCs was not assessed in this work, and in the future, it would be interesting to evaluate which are the predominant molecules and pathways involved in this crosstalk and how the inflammatory molecules impact this crosstalk, at a molecular level. Regarding IL-10, it seems that it did not alter ASCs behavior at an angiogenic level. This leads to hypothesize that an anti-inflammatory environment may not cause an impact in ASCs regenerative ability, which, in turn, makes sense as no strong angiogenic response is needed in the final stages of the repair phase. Also, the impact of endothelial cells on ASCs was not evaluated. For instance, Bidarra *et al.* showed that HUVECS were able to increase the proliferation rate and metabolic activity of BM-MSCs as well as increase their osteogenic differentiation, when in co-culture (Bidarra *et al.*, 2011). It would be interesting to know if the same conclusion can be drawn with

the experimental setups here described. On top of that, it is a possibility that HUVECs are also able to influence ASCs secretory profile altering the regenerative potential of these cells. On the other hand, endothelial cells are also able to influence the environment present in SCI, for instance, in promoting inflammation (T. Zhou *et al.*, 2019). It would be interesting to see if ASCs could modulate this behavior. Our data goes accordingly with what others have reported, however, all the vascularization assays were done *in vitro* with a defined concentration and time of stimulation. More experiments are needed to fully comprehend how the injury environment may influence the angiogenic potential of these cells or their secretome

Finally, another important aspect that needs to be elucidated is to know if ASCs can influence the barrier function of endothelial cells. It is described that although a strong vessel formation occurs in the first week after SCI, these vessels lack proper transporter and barrier function (Benton & Hagg, 2011; Casella *et al.*, 2002; Whetstone *et al.*, 2003) That could not be addressed here as HUVECs do not present the phenotype of CNS endothelium. However, there are already described different models to mimic the BBB *in vitro* either by using CNS endothelial cells or by differentiating induced pluripotent stem cells to CNS endothelial cells, that can be implemented in further experiments (Lippmann *et al.*, 2012; Watson *et al.*, 2013).

To use ASCs in a successful SCI therapy it is also necessary to understand how these cells are able to modulate the behavior of neuronal cells. For that reason, the second aim of this project was to evaluate how the ability of ASCs to induce neurite outgrowth is influenced by inflammatory stimuli. Previous work from our lab showed that both ASCs and their secretome promote neurite outgrowth (Assunção-Silva *et al.*, 2018; Gomes *et al.*, 2016; Serra *et al.*, 2018). Herein, using a DRG model, it was again observed that the secretome or the direct contact of ASCs (stimulated or not) promotes axonal growth when comparing to control. In fact, none of these controls elicited neurite outgrowth (**Figures 24** and **27**). However, the same was not observed using the transwell system where no differences between control and the other groups were found (**Figure 21**). Some important notes should be taken into account when analyzing this. The first one is that this model presents high standard deviations which is a technical limitation hard to surpass. So, other in vitro models of axonal growth could be analyzed, for instance, dissociated DRG or motor neuron cultures. Moreover, this goes accordingly with previous work from Oliveira and colleagues where it was shown that the neurite outgrowth promoted by collagen gels alone is similar to the neurite outgrowth promoted by ASCs encapsulated in these gels (Oliveira *et al.*, 2017). However, when using different matrices the neurite

outgrowth was much higher in the group with cells when compared to the gel alone (Gomes *et al.*, 2016; Oliveira *et al.*, 2017). This reveals the importance of the ECM on cell behavior.

As referred above, when using the secretome, it was observed that ASCs promoted neurite growth while the control did not elicit any type of growth. It should be taken into consideration that the control group from this assay is different from the control of the indirect co-culture. In the secretome assay, the media used is just Neurobasal with PenStrep while in the indirect co-culture it has other factors namely B27, glutamine, and glucose, which are also important for the induction of neurite outgrowth. Taking this into consideration, the observation that the secretome alone can induce some degree of neurite outgrowth is remarkable. However, the mean values of the parameters evaluated have a huge decrease when compared to the mean values of the indirect assay. Once again, this may be due to the media used in the different cell culture systems and therefore direct comparisons are hard to make. However, no differences were found between stimulated groups but as these values were low it becomes hard to detect any strong difference (**Figure 25**). It would be interesting to repeat this experiment but using the same medium as the indirect co-culture to see if the secretome can even induce more neurite outgrowth and, if so, if there is a difference between stimulations.

Finally, the last DRG experiment was done to evaluate how direct contact could affect the neurite outgrowth of these cells. For that reason, DRG were directly put on top of ASCs. The media used was the same as indirect co-culture but none of the controls had neurite growth. This happened because several DRG from the control group were not properly adhered. This indicates that ASCs are a good subtract for neurites to adhere and grow. Also, with the phalloidin staining, it was possible to observe some cells with ASCs morphology surrounding the DRG (**Figure 27**). Furthermore, the direct contact was able to promote the highest neurite outgrowth of all experimental setups, but no difference between stimuli was observed (**Figure 28**).

The data regarding neurite outgrowth obtained with this project suggest that ASCs are able to induce neurite outgrowth at different levels. Although the indirect and the secretome assays were done in different cell culture media, both assays could produce neurites, indicating that paracrine mechanisms are a factor to be considered when evaluating ASCs neurotrophic ability. Still, when in direct contact with the ASCs, higher values of neurite area, longest neurite, and number of intersections at lower distances were observed. Taking this into consideration, one may suggest that in the direct contact cultures, besides the secreted molecules by ASCs that are enough to elicit neurite outgrowth, cell-contact interactions and matrix deposition may play a role in enhancing the effect already seen in the paracrine cultures.

The DRG presented a common arborization pattern between the different assays (**Figures 23, 26 and 29**). There are a high number of intersections near the cell body that then gradually decreases. However, the intensity of the arborization was different from assay to assay, going accordingly with the data from the neurite area and longest neurite.

Unlike the vascularization assays, the inflammatory stimulation did not impact the ability of ASCs to promote neurite outgrowth. Although this data suggests that inflammatory preconditioning of ASCs do not seem a viable strategy for inducing axonal growth, some aspects must be considered. Like the vascularization process, the growth of a new axon is a complex process (Mar *et al.*, 2014; O'Donnell *et al.*, 2009). Although the axonal regeneration needed for SCI is not the same as axon elongation in development, some mechanisms are similar (Mar *et al.*, 2014). Indeed, a proper axon growth needs external stimuli to act as guides to the desired location as well as internal stimuli that provoke a reparative response. Therefore, inflammatory molecules can be modulating ASCs behavior on these aspects that are essential for axon growth, but not evaluated here. Another aspect to be taken into consideration is the fact that if inflammatory mediators really do not influence ASCs neurotrophic capacity, the use of these cells as a possible therapy for SCI has even more advantages because it may indicate that the inflammatory environment present in the lesion will not influence their ability to promote neuronal regeneration. However, it should not be forgotten that the inflammatory milieu in SCI is more complex than the one here studied.

For the final objective of this work, the aim was to evaluate the molecular changes induced by the inflammatory mediators on these cells. To do so, 6 hours after stimulation, the RNA of ASCs was collected and qPCR was performed (**Figure 30**). Results showed an increase in VEGF expression in the group stimulated with the pro-inflammatory factors which could partially explain the results from the secretome assay on vascular morphogenesis. However, angiogenin, another molecule highly associated with the vascularization process is diminished in this group. Moreover, FGF-2, an angiotrophic molecule, is not altered between groups. CXCL1 and 2, also known as angiogenic chemokines are also not altered. On the other end, NGF that has been associated with axon growth is decreased in this group, while BDNF is not altered. One interesting molecule is IL-6 that has a strong relationship with the immune system and is mainly associated with a pro-inflammatory response, which is in accordance with our data that show an increase if this cytokine on ASCs stimulated with pro-inflammatory stimulus. Also, some reports show that this molecule stimulates angiogenesis and the production of VEGF (Gopinathan *et al.*, 2015; Huang *et al.*, 2004).

Overall, it seems that these stimulations lead to different genes being differently expressed, even with them being within the same category. However, all of these gene expression alterations are subtle, as the assays of vascular morphogenesis and neurite outgrowth were. This indicates that the inflammatory stimuli are altering the molecular milieu inside ASCs but without major alterations in the outcomes analyzed. One important characteristic is that cellular pathways are really complex with several interconnected mechanisms of action. In fact, several of the molecules here analyzed have other roles than the classical for which they were initially described. For instance, VEGF besides being a major molecular player in the vascularization process, it has been linked to neuroprotective roles (Rosenstein *et al.*, 2010). On the other hand, BDNF besides its neurotrophic roles, also promotes endothelial cell survival (Kermani & Hempstead, 2007). This highlights the complexity of the molecular system inside the cell and that only expression levels of some classical angiogenic and neurotrophic genes may not be sufficient to understand what is LPS, IFN-γ, and IL-10 altering on ASCs. For that, protein levels of the genes studied could also be evaluated as well as other genes that may influence these processes. Another factor that increases the complexity is time. Here, only 6 hours after stimulation was assessed. However, molecular alterations are dynamic and it would be interesting to evaluate other timepoints to see the temporal dynamics of gene expression after inflammatory stimulation.

Overall, it seems that ASCs inflammatory pre-conditioning is leading to some specific molecular changes that then are most visible in alterations on the vascular potential of these cells, mainly on the secreted molecules. Nevertheless, ASCs seem to have a positive effect on the vascularization process as well as on the neurite outgrowth of DRG explants.

For these reasons, the data here produced contributes to the progression of a therapy based on ASCs and their secretome, despite that more research needs to be performed.

# 6. Final remarks

SCI affects several people hindering their life quality. As no effective treatment is yet available there is a need to develop one. As this injury has several interconnected pathophysiological mechanisms, therapies should aim to consider them and not just as a neurological problem.

One possible therapeutic approach is the use of ASCs as these cells are connected to several reparative processes such as angiogenesis, neuroregeneration and immunomodulation. Throughout the years, several data have shown the positive effects that these cells or their secretome could have on SCI. However, no sufficient therapeutic response was achieved, and therefore, new ways of improving these cells must be created.

With this work, the first aimed was to understand how inflammatory pre-conditioning could influence ASCs ability to influence vessel formation, at a paracrine and non-paracrine level. For that, a system to evaluate vascular morphogenesis was created. With this setup, it was shown that the stimulation with pro-inflammatory molecules enhanced the angiogenic potential of the secretome of these cells. However, it was not sufficient to elicit the same response when ASCs were in indirect contact with endothelial cells. Also, no robust vessel formation was seen in direct contact settings here established.

The second aim consisted on understanding if the same molecules could influence ASCs at a neurotrophic level. None of the stimuli could alter this potential of ASCs. Nevertheless, these stem cells were able to induce neurite outgrowth, at a paracrine and non-paracrine level.

Finally, trying to understand the molecular players that could be modulated by these inflammatory stimulations, qPCR was performed on ASCs after 6 hours of stimulation. Although some significant differences were observed in the gene expression, no clear evidence of a shifted phenotype was observed which leads to conclude that these molecules act on specific pathways that, at this timepoint, were not possible to fully understand.

Taking this into consideration, the crosstalk between ASCs, endothelial cells, inflammatory molecules, and neuronal cells needs to be further explored.

Even so, this project highlights the importance of understanding how ASCs can be modulated to enhance their regenerative potential. Additionally, it highlights the potential of these cells or their secretome to be used on a SCI therapy.

# 7. References


Alizadeh, A., Dyck, S. M., & Karimi-Abdolrezaee, S. (2019). Traumatic spinal cord injury: an overview of pathophysiology, models and acute injury mechanisms. *Frontiers in Neurology*, *10*, 1–25.

Allen, A. R. (1914). Remarks on the histopathological changes in the spinal cord due to impact: an experimental study. *The Journal of Nervous and Mental Disease*, *41*(3), 141–147.

Alvarez, J. I., Katayama, T., & Prat, A. (2013). Glial influence on the blood brain barrier. *Glia*, *61*(12), 1939–1958.

Arboleda, D., Forostyak, S., Jendelova, P., Marekova, D., Amemori, T., Pivonkova, H., Masinova, K., & Sykova, E. (2011). Transplantation of predifferentiated adipose-derived stromal cells for the treatment of spinal cord injury. *Cellular and Molecular Neurobiology*, *31*(7), 1113–1122.

Armulik, A., Genové, G., Mäe, M., Nisancioglu, M. H., Wallgard, E., Niaudet, C., He, L., Norlin, J., Lindblom, P., Strittmatter, K., Johansson, B. R., & Betsholtz, C. (2010). Pericytes regulate the blood–brain barrier. *Nature*, *468*(7323), 557–561.

Arnaoutova, I., & Kleinman, H. K. (2010). In vitro angiogenesis: endothelial cell tube formation on gelled basement membrane extract. *Nature Protocols*, *5*(4), 628–635.

Ashammakhi, N., Kim, H.-J., Ehsanipour, A., Bierman, R. D., Kaarela, O., Xue, C., Khademhosseini, A., & Seidlits, S. K. (2019). Regenerative therapies for spinal cord injury. *Tissue Engineering Part B: Reviews*, *25*(6), 471–491.

Assunção-Silva, R. C., Gomes, E. D., Sousa, N., Silva, N. A., & Salgado, A. J. (2015). Hydrogels and cell based therapies in spinal cord injury regeneration. *Stem Cells International*, *2015*, 1–24.

Assunção-Silva, R. C., Mendes-Pinheiro, B., Patrício, P., Behie, L. A., Teixeira, F. G., Pinto, L., & Salgado, A. J. (2018). Exploiting the impact of the secretome of mscs isolated from different tissue sources on neuronal differentiation and axonal growth. *Biochimie*, *155*, 83–91.

Badhiwala, J. H., Ahuja, C. S., & Fehlings, M. G. (2019). Time is spine: a review of translational advances in spinal cord injury. *Journal of Neurosurgery: Spine*, *30*(1), 1–18.

Barker, R. A., & Cicchetti, F. (2012). *Neuroanatomy and neuroscience at a glance* (4th ed.). Wiley-Blackwell.

Bartanusz, V., Jezova, D., Alajajian, B., & Digicaylioglu, M. (2011). The blood-spinal cord barrier: morphology and clinical implications. *Annals of Neurology*, *70*(2), 194–206.

Benton, R. L., & Hagg, T. (2011). Vascular pathology as a potential therapeutic target in SCI. *Translational Stroke Research*, *2*(4), 556–574.

Bernardini, C., Bertocchi, M., Zannoni, A., Salaroli, R., Tubon, I., Dothel, G., Fernandez, M., Bacci,

M. L., Calzà, L., & Forni, M. (2019). Constitutive and LPS-stimulated secretome of porcine vascular wall-mesenchymal stem cells exerts effects on in vitro endothelial angiogenesis. *BMC Veterinary Research*, *15*(1), 123.

Bernardo, M. E., & Fibbe, W. E. (2013). Mesenchymal stromal cells: sensors and switchers of inflammation. *Cell Stem Cell*, *13*(4), 392–402.

Bidarra, S. J., Barrias, C. C., Barbosa, M. A., Soares, R., Amédée, J., & Granja, P. L. (2011). Phenotypic and proliferative modulation of human mesenchymal stem cells via crosstalk with endothelial cells. *Stem Cell Research*, *7*(3), 186–197.

Buizer, A. T., Bulstra, S. K., Veldhuizen, A. G., & Kuijer, R. (2018). The balance between proliferation and transcription of angiogenic factors of mesenchymal stem cells in hypoxia. *Connective Tissue Research*, *59*(1), 12–20.

Cano, E., Gebala, V., & Gerhardt, H. (2017). Pericytes or mesenchymal stem cells : is that the question ? *Cell Stem Cell*, *20*, 296–297.

Cantinieaux, D., Quertainmont, R., Blacher, S., Rossi, L., Wanet, T., Noël, A., Brook, G., Schoenen, J., & Franzen, R. (2013). Conditioned medium from bone marrow-derived mesenchymal stem cells improves recovery after spinal cord injury in rats: an original strategy to avoid cell transplantation. *PLoS ONE*, *8*(8), e69515.

Cao, Y., Zhou, Y., Ni, S., Wu, T., Li, P., Liao, S., Hu, J., & Lu, H. (2017). Three dimensional quantification of microarchitecture and vessel regeneration by synchrotron radiation microcomputed tomography in a rat model of spinal cord injury. *Journal of Neurotrauma*, *34*(6), 1187–1199.

Carmeliet, P. (2003). Blood vessels and nerves: common signals, pathways and diseases. *Nature Reviews Genetics*, *4*(9), 710–720.

Casella, G. T. B., Bunge, M. B., & Wood, P. M. (2006). Endothelial cell loss is not a major cause of neuronal and glial cell death following contusion injury of the spinal cord. *Experimental Neurology*, *202*(1), 8–20.

Casella, G. T. B., Marcillo, A., Bunge, M. B., & Wood, P. M. (2002). New vascular tissue rapidly replaces neural parenchyma and vessels destroyed by a contusion injury to the rat spinal cord. *Experimental Neurology*, *173*(1), 63–76.

Chamberlain, G., Fox, J., Ashton, B., & Middleton, J. (2007). Concise review: mesenchymal stem cells: their phenotype, differentiation capacity, immunological features, and potential for homing. *Stem Cells*, *25*(11), 2739–2749.

Cho, D.-I., Kim, M. R., Jeong, H., Jeong, H. C., Jeong, M. H., Yoon, S. H., Kim, Y. S., & Ahn, Y.

(2014). Mesenchymal stem cells reciprocally regulate the M1/M2 balance in mouse bone marrow-derived macrophages. *Experimental & Molecular Medicine*, *46*(1), e70–e70.

Cizkova, D., Cubinkova, V., Smolek, T., Murgoci, A.-N., Danko, J., Vdoviakova, K., Humenik, F., Cizek, M., Quanico, J., Fournier, I., & Salzet, M. (2018). Localized intrathecal delivery of mesenchymal stromal cells conditioned medium improves functional recovery in a rat model of spinal cord injury. *International Journal of Molecular Sciences*, *19*(3), 870.

Cofano, F., Boido, M., Monticelli, M., Zenga, F., Ducati, A., Vercelli, A., & Garbossa, D. (2019). Mesenchymal stem cells for spinal cord injury: current options, limitations, and future of cell therapy. *International Journal of Molecular Sciences*, *20*(11), 2698.

Cohen, D. M., Patel, C. B., Ahobila-Vajjula, P., Sundberg, L. M., Chacko, T., Liu, S. J., & Narayana, P. A. (2009). Blood-spinal cord barrier permeability in experimental spinal cord injury: dynamic contrast-enhanced MRI. *NMR in Biomedicine*, *22*(3), 332–341.

Courtine, G., & Sofroniew, M. V. (2019). Spinal cord repair: advances in biology and technology. *Nature Medicine*, *25*(6), 898–908.

Cregg, J. M., DePaul, M. A., Filous, A. R., Lang, B. T., Tran, A., & Silver, J. (2014). Functional regeneration beyond the glial scar. *Experimental Neurology*, *253*, 197–207.

de Moraes, C. N., Maia, L., de Oliveira, E., de Paula Freitas Dell'Aqua, C., Chapwanya, A., da Cruz Landim-Alvarenga, F., & Oba, E. (2017). Shotgun proteomic analysis of the secretome of bovine endometrial mesenchymal progenitor/stem cells challenged or not with bacterial lipopolysaccharide. *Veterinary Immunology and Immunopathology*, *187*, 42–47.

DeCicco-Skinner, K. L., Henry, G. H., Cataisson, C., Tabib, T., Gwilliam, J. C., Watson, N. J., Bullwinkle, E. M., Falkenburg, L., O'Neill, R. C., Morin, A., & Wiest, J. S. (2014). Endothelial cell tube formation assay for the *in vitro* study of angiogenesis. *Journal of Visualized Experiments*, *10*(91), 1–8.

Dominici, M., Le Blanc, K., Mueller, I., Slaper-Cortenbach, I., Marini, F. ., Krause, D. S., Deans, R. J., Keating, A., Prockop, D. J., & Horwitz, E. M. (2006). Minimal criteria for defining multipotent mesenchymal stromal cells. the International Society for Cellular Therapy position statement. *Cytotherapy*, *8*(4), 315–317.

Donnelly, D. J., & Popovich, P. G. (2008). Inflammation and its role in neuroprotection, axonal regeneration and functional recovery after spinal cord injury. *Experimental Neurology*, *209*(2), 378–388.

Dray, C., Rougon, G., & Debarbieux, F. (2009). Quantitative analysis by in vivo imaging of the dynamics of vascular and axonal networks in injured mouse spinal cord. *Proceedings of the National*

*Academy of Sciences*, *106*(23), 9459–9464.

Dubois, S. G., Floyd, E. Z., Zvonic, S., Kilroy, G., Wu, X., Carling, S., Halvorsen, Y. D. C., Ravussin, E., & Gimble, J. M. (2008). Isolation of human adipose-derived stem cells from biopsies and liposuction specimens. In *Mesenchymal Stem Cells: Methods and Protocols, Methods in Molecular Biology* (Vol. 449, pp. 69–79). Humana Press.

Edalat, H., Hajebrahimi, Z., Pirhajati, V., Movahedin, M., Tavallaei, M., Soroush, M. R., & Mowla, S. J. (2013). Transplanting p75-suppressed bone marrow stromal cells promotes functional behavior in a rat model of spinal cord injury. *Iranian Biomedical Journal*, *17*(3), 140–145.

Estrada, R., Li, N., Sarojini, H., AN, J., Lee, M.-J., & Wang, E. (2009). Secretome from mesenchymal stem cells induces angiogenesis via Cyr61. *Journal of Cellular Physiology*, *219*(3), 563–571.

Evaniew, N., Belley-Côté, E. P., Fallah, N., Noonan, V. K., Rivers, C. S., & Dvorak, M. F. (2016). Methylprednisolone for the treatment of patients with acute spinal cord injuries: a systematic review and meta-analysis. *Journal of Neurotrauma*, *33*(5), 468–481.

Fassbender, J. M., Whittemore, S. R., & Hagg, T. (2011). Targeting microvasculature for neuroprotection after SCI. *Neurotherapeutics*, *8*(2), 240–251.

Felten, D. L., O'Banion, M. K., & Maida, M. S. (2016). Vasculature. In *Netter's Atlas of Neuroscience* (pp. 93–124). Elsevier.

Figley, S. A., Khosravi, R., Legasto, J. M., Tseng, Y.-F. F., & Fehlings, M. G. (2014). Characterization of vascular disruption and blood-spinal cord barrier permeability following traumatic spinal cord injury. *Journal of Neurotrauma*, *31*(6), 541–552.

Fraga, J. S., Silva, N. A., Lourenço, A. S., Gonçalves, V., Neves, N. M., Reis, R. L., Rodrigues, A. J., Manadas, B., Sousa, N., & Salgado, A. J. (2013). Unveiling the effects of the secretome of mesenchymal progenitors from the umbilical cord in different neuronal cell populations. *Biochimie*, *95*(12), 2297–2303.

Freytes, D. O., Kang, J. W., Marcos-Campos, I., & Vunjak-Novakovic, G. (2013). Macrophages modulate the viability and growth of human mesenchymal stem cells. *Journal of Cellular Biochemistry*, *114*(1), 220–229.

Friedenstein, A. J., Deriglasova, U. F., Kulagina, N. N., Panasuk, A. F., Rudakowa, S. F., Luriá, E. A., & Ruadkow, I. A. (1974). Precursors for fibroblasts in different populations of hematopoietic cells as detected by the in vitro colony assay method. *Experimental Hematology*, *2*(2), 83–92.

Fundukian, L. J. (2011). *The Gale encyclopedia of medicine* (4th ed.). Cengage Learning.

Ge, Q., Zhang, H., Hou, J., Wan, L., Cheng, W., Wang, X., Dong, D., Chen, C., Xia, J., Guo, J., Chen, X., & Wu, X. (2017). VEGF secreted by mesenchymal stem cells mediates the differentiation of endothelial progenitor cells into endothelial cells via paracrine mechanisms. *Molecular Medicine Reports*, *17*(1), 1667–1675.

Gnecchi, M., He, H., Liang, O. D., Melo, L. G., Morello, F., Mu, H., Noiseux, N., Zhang, L., Pratt, R. E., Ingwall, J. S., & Dzau, V. J. (2005). Paracrine action accounts for marked protection of ischemic heart by Akt-modified mesenchymal stem cells. *Nature Medicine*, *11*(4), 367–368.

Gnecchi, M., He, H., Noiseux, N., Liang, O. D., Zhang, L., Morello, F., Mu, H., Melo, L. G., Pratt, R. E., Ingwall, J. S., & Dzau, V. J. (2006). Evidence supporting paracrine hypothesis for Akt-modified mesenchymal stem cell-mediated cardiac protection and functional improvement. *The FASEB Journal*, *20*(6), 661–669.

Gomes, E. D., Mendes, S. S., Assunção-Silva, R. C., Teixeira, F. G., Pires, A. O., Anjo, S. I., Manadas, B., Leite-Almeida, H., Gimble, J. M., Sousa, N., Lepore, A. C., Silva, N. A., & Salgado, A. J. (2018). Co-transplantation of adipose tissue-derived stromal cells and olfactory ensheathing cells for spinal cord injury repair. *STEM CELLS*, *36*(5), 696–708.

Gomes, E. D., Mendes, S. S., Leite-Almeida, H., Gimble, J. M., Tam, R. Y., Shoichet, M. S., Sousa, N., Silva, N. A., & Salgado, A. J. (2016). Combination of a peptide-modified gellan gum hydrogel with cell therapy in a lumbar spinal cord injury animal model. *Biomaterials*, *105*, 38–51.

Gomes, E. D., Rocha, L. A., Assunção-Silva, R. C., Lima, R., Silva, N. A., & Salgado, A. J. (2020). Cell therapies for spinal cord injury regeneration. In *Spinal Cord Injury (SCI) Repair Strategies* (pp. 157–186). Elsevier.

Goodwin, A. M. (2007). In vitro assays of angiogenesis for assessment of angiogenic and anti-angiogenic agents. *Microvascular Research*, *74*(2–3), 172–183.

Gopinathan, G., Milagre, C., Pearce, O. M. T., Reynolds, L. E., Hodivala-Dilke, K., Leinster, D. A., Zhong, H., Hollingsworth, R. E., Thompson, R., Whiteford, J. R., & Balkwill, F. (2015). Interleukin-6 stimulates defective angiogenesis. *Cancer Research*, *75*(15), 3098–3107.

Gransee, H. M., Zhan, W. Z., Sieck, G. C., & Mantilla, C. B. (2015). Localized delivery of brain-derived neurotrophic factor-expressing mesenchymal stem cells enhances functional recovery following cervical spinal cord injury. *Journal of Neurotrauma*, *32*(3), 185–193.

Grasman, J. M., & Kaplan, D. L. (2017). Human endothelial cells secrete neurotropic factors to direct axonal growth of peripheral nerves. *Scientific Reports*, *7*(1), 1–12.

Grotenhuis, N., De Witte, S. F. H., van Osch, G. J. V. M., Bayon, Y., Lange, J. F., & Bastiaansen-

Jenniskens, Y. M. (2016). Biomaterials influence macrophage–mesenchymal stem cell interaction in vitro. *Tissue Engineering Part A*, *22*(17–18), 1098–1107.

Gu, W., Hong, X., Potter, C., Qu, A., & Xu, Q. (2017). Mesenchymal stem cells and vascular regeneration. *Microcirculation*, *24*(1), 1–15.

Hagen, E. M., & Rekand, T. (2015). Management of neuropathic pain associated with spinal cord injury. *Pain and Therapy*, *4*(1), 51–65.

Haggerty, A. E., Maldonado-Lasunción, I., & Oudega, M. (2018). Biomaterials for revascularization and immunomodulation after spinal cord injury. *Biomedical Materials*, *13*(4), 044105.

Hawryluk, G., Whetstone, W., Saigal, R., Ferguson, A., Talbott, J., Bresnahan, J., Dhall, S., Pan, J., Beattie, M., & Manley, G. (2015). Mean arterial blood pressure correlates with neurological recovery after human spinal cord injury: analysis of high frequency physiologic data. *Journal of Neurotrauma*, *32*(24), 1958–1967.

Haycock, J. W. (2011). 3D cell culture: a review of current approaches and techniques. In *3D Cell Culture: Methods and Protocols, Methods in Molecular Biology* (Vol. 695, pp. 1–15). Humana Press.

He, H., Xu, J., Warren, C. M., Duan, D., Li, X., Wu, L., & Iruela-Arispe, M. L. (2012). Endothelial cells provide an instructive niche for the differentiation and functional polarization of M2-like macrophages. *Blood*, *120*(15), 3152–3162.

Heo, S. C., Jeon, E. S., Lee, I. H., Kim, H. S., Kim, M. B., & Kim, J. H. (2011). Tumor necrosis factor-α-activated human adipose tissue-derived mesenchymal stem cells accelerate cutaneous wound healing through paracrine mechanisms. *Journal of Investigative Dermatology*, *131*(7), 1559–1567.

Horwitz, E. M., Le Blanc, K., Dominici, M., Mueller, I., Slaper-Cortenbach, I., Marini, F. C., Deans, R. J., Krause, D. S., & Keating, A. (2005). Clarification of the nomenclature for MSC: the international society for cellular therapy position statement. *Cytotherapy*, *7*(5), 393–395.

Huang, S. P., Wu, M. S., Shun, C. T., Wang, H. P., Lin, M. T., Kuo, M. L., & Lin, J. T. (2004). Interleukin-6 increases vascular endothelial growth factor and angiogenesis in gastric carcinoma. *Journal of Biomedical Science*, *11*(4), 517–527.

Hupfeld, J., Gorr, I. H., Schwald, C., Beaucamp, N., Wiechmann, K., Kuentzer, K., Huss, R., Rieger, B., Neubauer, M., & Wegmeyer, H. (2014). Modulation of mesenchymal stromal cell characteristics by microcarrier culture in bioreactors. *Biotechnology and Bioengineering*, *111*(11), 2290–2302.

Hur, J. W., Cho, T. H., Park, D. H., Lee, J. B., Park, J. Y., & Chung, Y. G. (2016). Intrathecal transplantation of autologous adipose-derived mesenchymal stem cells for treating spinal cord injury: a

human trial. *Journal of Spinal Cord Medicine*, *39*(6), 655–664.

Hutson, T. H., & Di Giovanni, S. (2019). The translational landscape in spinal cord injury: focus on neuroplasticity and regeneration. *Nature Reviews Neurology*, *15*(12), 732–745.

Hwa Cho, H., Bae, Y. C., & Jung, J. S. (2006). Role of toll-like receptors on human adipose-derived stromal cells. *Stem Cells*, *24*(12), 2744–2752.

James, S. L., Theadom, A., Ellenbogen, R. G., Bannick, M. S., Montjoy-Venning, W., Lucchesi, L. R., Abbasi, N., Abdulkader, R., Abraha, H. N., Adsuar, J. C., Afarideh, M., Agrawal, S., Ahmadi, A., Ahmed, M. B., Aichour, A. N., Aichour, I., Aichour, M. T. E., Akinyemi, R. O., Akseer, N., ... Murray, C. J. L. (2019). Global, regional, and national burden of traumatic brain injury and spinal cord injury, 1990–2016: a systematic analysis for the global burden of disease study 2016. *The Lancet Neurology*, *18*(1), 56–87.

Jensen, C., & Teng, Y. (2020). Is it time to start transitioning from 2d to 3d cell culture? *Frontiers in Molecular Biosciences*, *7*, 1–15.

Jones, T. B. (2014). Lymphocytes and autoimmunity after spinal cord injury. *Experimental Neurology*, *258*, 78–90.

Jung, S., Panchalingam, K. M., Wuerth, R. D., Rosenberg, L., & Behie, L. A. (2012). Large-scale production of human mesenchymal stem cells for clinical applications. *Biotechnology and Applied Biochemistry*, *59*(2), 106–120.

Kaasi, A., & Jardini, A. L. (2016). Bioreactors. In *Reference Module in Materials Science and Materials Engineering* (Issue 2007, pp. 275–296). Elsevier.

Kabu, S., Gao, Y., Kwon, B. K., & Labhasetwar, V. (2015). Drug delivery, cell-based therapies, and tissue engineering approaches for spinal cord injury. *Journal of Controlled Release*, *219*(24), 141–154.

Kaiser, M. G., Haid, R. W., Shaffrey, C. I., & Fehlings, M. G. (2019). Degenerative cervical myelopathy and radiculopathy. In *Degenerative Cervical Myelopathy and Radiculopathy*. Springer International Publishing.

Kao, C.-H., Chio, C.-C., Lin, M.-T., & Yeh, C.-H. (2011). Body cooling ameliorating spinal cord injury may be neurogenesis-, anti-inflammation- and angiogenesis-associated in rats. *The Journal of Trauma: Injury, Infection, and Critical Care*, *70*(4), 885–893.

Kasper, G., Dankert, N., Tuischer, J., Hoeft, M., Gaber, T., Glaeser, J. D., Zander, D., Tschirschmann, M., Thompson, M., Matziolis, G., & Duda, G. N. (2007). Mesenchymal stem cells regulate angiogenesis according to their mechanical environment. *STEM CELLS*, *25*(4), 903–910.

Kermani, P., & Hempstead, B. (2007). Brain-derived neurotrophic factor: a newly described

mediator of angiogenesis. *Trends in Cardiovascular Medicine*, *17*(4), 140–143.

Kern, S., Eichler, H., Stoeve, J., Klüter, H., & Bieback, K. (2006). Comparative analysis of mesenchymal stem cells from bone marrow, umbilical cord blood, or adipose tissue. *Stem Cells*, *24*(5), 1294–1301.

Khan, I. U., Yoon, Y., Kim, A., Jo, K. R., Choi, K. U., Jung, T., Kim, N., Son, Y., Kim, W. H., & Kweon, O.-K. (2018). Improved healing after the co-transplantation of HO-1 and BDNF overexpressed mesenchymal stem cells in the subacute spinal cord injury of dogs. *Cell Transplantation*, *27*(7), 1140–1153.

Kigerl, K. A., Gensel, J. C., Ankeny, D. P., Alexander, J. K., Donnelly, D. J., & Popovich, P. G. (2009). Identification of two distinct macrophage subsets with divergent effects causing either neurotoxicity or regeneration in the injured mouse spinal cord. *Journal of Neuroscience*, *29*(43), 13435–13444.

Kissane, R. W. P., Wright, O., Al'Joboori, Y. D., Marczak, P., Ichiyama, R. M., & Egginton, S. (2019). Effects of treadmill training on microvascular remodeling in the rat after spinal cord injury. *Muscle & Nerve*, *59*(3), 370–379.

Kolte, D., McClung, J. A., & Aronow, W. S. (2016). Vasculogenesis and angiogenesis. In *Translational Research in Coronary Artery Disease* (pp. 49–65). Elsevier.

Krampera, M., Cosmi, L., Angeli, R., Pasini, A., Liotta, F., Andreini, A., Santarlasci, V., Mazzinghi, B., Pizzolo, G., Vinante, F., Romagnani, P., Maggi, E., Romagnani, S., & Annunziato, F. (2006). Role for interferon-γ in the immunomodulatory activity of human bone marrow mesenchymal stem cells. *Stem Cells*, *24*(2), 386–398.

Kruger, E. A., Pires, M., Ngann, Y., Sterling, M., & Rubayi, S. (2013). Comprehensive management of pressure ulcers in spinal cord injury: current concepts and future trends. *The Journal of Spinal Cord Medicine*, *36*(6), 572–585.

Kumar, H., Ropper, A. E., Lee, S. H., & Han, I. (2017). Propitious therapeutic modulators to prevent blood-spinal cord barrier disruption in spinal cord injury. *Molecular Neurobiology*, *54*(5), 3578–3590.

Kwon, Y. W., Heo, S. C., Jeong, G. O., Yoon, J. W., Mo, W. M., Lee, M. J., Jang, I.-H., Kwon, S. M., Lee, J. S., & Kim, J. H. (2013). Tumor necrosis factor-α-activated mesenchymal stem cells promote endothelial progenitor cell homing and angiogenesis. *Biochimica et Biophysica Acta (BBA) - Molecular Basis of Disease*, *1832*(12), 2136–2144.

Lee, J. H., Han, Y. S., & Lee, S. H. (2016). Long-duration three-dimensional spheroid culture

promotes angiogenic activities of adipose-derived mesenchymal stem cells. *Biomolecules and Therapeutics*, *24*(3), 260–267.

Lee, J. Y., Choi, H. Y., & Yune, T. Y. (2015). MMP-3 secreted from endothelial cells of blood vessels after spinal cord injury activates microglia, leading to oligodendrocyte cell death. *Neurobiology of Disease*, *82*, 141–151.

Lee, S. C., Jeong, H. J., Lee, S. K., & Kim, S. J. (2015). Lipopolysaccharide preconditioning of adipose-derived stem cells improves liver-regenerating activity of the secretome. *Stem Cell Research and Therapy*, *6*(1), 1–11.

Lentsch, A. B., & Ward, P. A. (2000). Regulation of inflammatory vascular damage. *The Journal of Pathology*, *190*(3), 343–348.

Li, N., & Hua, J. (2017). Interactions between mesenchymal stem cells and the immune system. *Cellular and Molecular Life Sciences*, *74*(13), 2345–2360.

Lippmann, E. S., Azarin, S. M., Kay, J. E., Nessler, R. A., Wilson, H. K., Al-Ahmad, A., Palecek, S. P., & Shusta, E. V. (2012). Derivation of blood-brain barrier endothelial cells from human pluripotent stem cells. *Nature Biotechnology*, *30*(8), 783–791.

Liu, J., Zhu, P., Song, P., Xiong, W., Chen, H., Peng, W., Wang, S., Li, S., Fu, Z., Wang, Y., & Wang, H. (2015). Pretreatment of adipose derived stem cells with curcumin facilitates myocardial recovery via antiapoptosis and angiogenesis. *Stem Cells International*, *2015*, 1–12.

Maacha, S., Sidahmed, H., Jacob, S., Gentilcore, G., Calzone, R., Grivel, J.-C., & Cugno, C. (2020). Paracrine mechanisms of mesenchymal stromal cells in angiogenesis. *Stem Cells International*, *2020*, 1–12.

Makita, N., Hizukuri, Y., Yamashiro, K., Murakawa, M., & Hayashi, Y. (2015). IL-10 enhances the phenotype of M2 macrophages induced by IL-4 and confers the ability to increase eosinophil migration. *International Immunology*, *27*(3), 131–141.

Maldonado-Lasunción, I., Verhaagen, J., & Oudega, M. (2018). Mesenchymal stem cell-macrophage choreography supporting spinal cord repair. *Neurotherapeutics*, *15*(3), 578–587.

Mantovani, A., Sica, A., Sozzani, S., Allavena, P., Vecchi, A., & Locati, M. (2004). The chemokine system in diverse forms of macrophage activation and polarization. *Trends in Immunology*, *25*(12), 677–686.

Mar, F. M., Bonni, A., & Sousa, M. M. (2014). Cell intrinsic control of axon regeneration. *EMBO Reports*, *15*(3), 254–263.

Martins, L. F., Costa, R. O., Pedro, J. R., Aguiar, P., Serra, S. C., Teixeira, F. G., Sousa, N.,

Salgado, A. J., & Almeida, R. D. (2017). Mesenchymal stem cells secretome-induced axonal outgrowth is mediated by BDNF. *Scientific Reports*, *7*(1), 4153.

Mataliotakis, G. I., & Tsirikos, A. I. (2016). Spinal cord trauma: pathophysiology, classification of spinal cord injury syndromes, treatment principles and controversies. *Orthopaedics and Trauma*, *30*(5), 440–449.

Melchiorri, A. J., Nguyen, B. B., & Fisher, J. P. (2014). Mesenchymal stem cells: roles and relationships in vascularization. *Tissue Engineering Part B: Reviews*, *20*(3), 218–228.

Mendes-Pinheiro, B., Marote, A., Marques, C. R., Teixeira, F. G., Ribeiro, J. C., & Salgado, A. J. (2020). Applications of the stem cell secretome in regenerative medicine. In *Mesenchymal Stem Cells in Human Health and Diseases* (pp. 79–114). Academic Press.

Monteiro, S., Salgado, A. J., & Silva, N. A. (2018). Immunomodulation as a neuroprotective strategy after spinal cord injury. *Neural Regeneration Research*, *13*(3), 423–424.

Mothe, A. J., & Tator, C. H. (2012). Advances in stem cell therapy for spinal cord injury. *Journal of Clinical Investigation*, *122*(11), 3824–3834.

Müller, R., Landmann, G., Béchir, M., Hinrichs, T., Arnet, U., Jordan, X., & Brinkhof, M. W. G. (2017). Chronic pain, depression and quality of life in individuals with spinal cord injury: mediating role of participation. *Journal of Rehabilitation Medicine*, *49*(6), 489–496.

Murphy, K. C., Whitehead, J., Falahee, P. C., Zhou, D., Simon, S. I., & Leach, J. K. (2017). Multifactorial experimental design to optimize the anti-inflammatory and proangiogenic potential of mesenchymal stem cell spheroids. *STEM CELLS*, *35*(6), 1493–1504.

Nagashima, K., Miwa, T., Soumiya, H., Ushiro, D., Takeda-Kawaguchi, T., Tamaoki, N., Ishiguro, S., Sato, Y., Miyamoto, K., Ohno, T., Osawa, M., Kunisada, T., Shibata, T., Tezuka, K., Furukawa, S., & Fukumitsu, H. (2017). Priming with FGF2 stimulates human dental pulp cells to promote axonal regeneration and locomotor function recovery after spinal cord injury. *Scientific Reports*, *7*(1), 13500.

Naito, H., Iba, T., & Takakura, N. (2020). Mechanisms of new blood-vessel formation and proliferative heterogeneity of endothelial cells. *International Immunology*, *32*(5), 295–305.

Ng, M. T. L., Stammers, A. T., & Kwon, B. K. (2011). Vascular disruption and the role of angiogenic proteins after spinal cord injury. *Translational Stroke Research*, *2*(4), 474–491.

Noble, L. J., & Wrathall, J. R. (1989a). Distribution and time course of protein extravasation in the rat spinal cord after contusive injury. *Brain Research*, *482*(1), 57–66.

Noble, L. J., & Wrathall, J. R. (1989b). Correlative analyses of lesion development and functional status after graded spinal cord contusive injuries in the rat. *Experimental Neurology*, *103*(1), 34–40.

O'Donnell, M., Chance, R. K., & Bashaw, G. J. (2009). Axon growth and guidance: receptor regulation and signal transduction. *Annual Review of Neuroscience*, *32*(1), 383–412.

Oliveira, E., Assunção-Silva, R. C., Ziv-Polat, O., Gomes, E. D., Teixeira, F. G., Silva, N. A., Shahar, A., & Salgado, A. J. (2017). Influence of different ECM-like hydrogels on neurite outgrowth induced by adipose tissue-derived stem cells. *Stem Cells International*, *2017*, 1–10.

Oses, C., Olivares, B., Ezquer, M., Acosta, C., Bosch, P., Donoso, M., Léniz, P., & Ezquer, F. (2017). Preconditioning of adipose tissue-derived mesenchymal stem cells with deferoxamine increases the production of pro-angiogenic, neuroprotective and anti-inflammatory factors: potential application in the treatment of diabetic neuropathy. *PLoS ONE*, *12*(5), 1–22.

Ottomanelli, L., & Lind, L. (2009). Review of critical factors related to employment after spinal cord injury: implications for research and vocational services. *The Journal of Spinal Cord Medicine*, *32*(5), 503–531.

Paredes, I., Himmels, P., & Ruiz de Almodóvar, C. (2018). Neurovascular communication during CNS development. *Developmental Cell*, *45*(1), 10–32.

Pill, K., Hofmann, S., Redl, H., & Holnthoner, W. (2015). Vascularization mediated by mesenchymal stem cells from bone marrow and adipose tissue: a comparison. *Cell Regeneration*, *4*(1), 4–8.

Pill, K., Melke, J., Mühleder, S., Pultar, M., Rohringer, S., Priglinger, E., Redl, H. R., Hofmann, S., & Holnthoner, W. (2018). Microvascular networks from endothelial cells and mesenchymal stromal cells from adipose tissue and bone marrow: a comparison. *Frontiers in Bioengineering and Biotechnology*, *6*, 1–10.

Pinho, A. G. (2019). *Impact of the proteic and vesicular secretome of adipose tissue derived stem cells in spinal cord injury*. University of Minho.

Pinho, A. G., Cibrão, J. R., Silva, N. A., Monteiro, S., & Salgado, A. J. (2020). Cell secretome: basic insights and therapeutic opportunities for CNS disorders. *Pharmaceuticals*, *13*(2), 31.

Pires, A. O., Mendes-Pinheiro, B., Teixeira, F. G., Anjo, S. I., Ribeiro-Samy, S., Gomes, E. D., Serra, S. C., Silva, N. A., Manadas, B., Sousa, N., & Salgado, A. J. (2016). Unveiling the differences of secretome of human bone marrow mesenchymal stem cells, adipose tissue-derived stem cells, and human umbilical cord perivascular cells: a proteomic analysis. *Stem Cells and Development*, *25*(14), 1073–1083.

Popa, C., Popa, F., Grigorean, V. T., Onose, G., Sandu, A. M., Popescu, M., Burnei, G., Strambu, V., & Sinescu, C. (2010). Cardiovascular dysfunction following spinal cord injury. *Journal of Medicine*

*and Life*, *3*(3), 275–285.

Ra, J. C., Shin, I. S., Kim, S. H., Kang, S. K., Kang, B. C., Lee, H. Y., Kim, Y. J., Jo, J. Y., Yoon, E. J., Choi, H. J., & Kwon, E. (2011). Safety of intravenous infusion of human adipose tissue-derived mesenchymal stem cells in animals and humans. *Stem Cells and Development*, *20*(8), 1297–1308.

Ribeiro, C. A., Fraga, J. S., Grãos, M., Neves, N. M., Reis, R. L., Gimble, J. M., Sousa, N., & Salgado, A. J. (2012). The secretome of stem cells isolated from the adipose tissue and wharton jelly acts differently on central nervous system derived cell populations. *Stem Cell Research and Therapy*, *3*(3), 18.

Richardson, P. M., McGuinness, U. M., & Aguayo, A. J. (1980). Axons from CNS neurones regenerate into pns grafts. *Nature*, *284*(5753), 264–265.

Rocha, L. A., Gomes, E. D., Afonso, J. L., Granja, S., Baltazar, F., Silva, N. A., Shoichet, M. S., Sousa, R. A., Learmonth, D. A., & Salgado, A. J. (2020a). In vitro evaluation of ASCs and HUVECs co-cultures in 3d biodegradable hydrogels on neurite outgrowth and vascular organization. *Frontiers in Cell and Developmental Biology*, *8*, 489.

Rocha, L. A., Silva, D., Barata-Antunes, S., Cavaleiro, H., Gomes, E. D., Silva, N. A., & Salgado, A. J. (2020b). Cell and tissue instructive materials for central nervous system repair. *Advanced Functional Materials*, *30*(44), 1909083.

Rocha, L. A., Sousa, R. A., Learmonth, D. A., & Salgado, A. J. (2018). The role of biomaterials as angiogenic modulators of spinal cord injury: mimetics of the spinal cord, cell and angiogenic factor delivery agents. *Frontiers in Pharmacology*, *9*, 164.

Rohringer, S., Hofbauer, P., Schneider, K. H., Husa, A.-M., Feichtinger, G., Peterbauer-Scherb, A., Redl, H., & Holnthoner, W. (2014). Mechanisms of vasculogenesis in 3d fibrin matrices mediated by the interaction of adipose-derived stem cells and endothelial cells. *Angiogenesis*, *17*(4), 921–933.

Rooney, G. E., McMahon, S. S., Ritter, T., Garcia, Y., Moran, C., Madigan, N. N., Flügel, A., Dockery, P., O'Brien, T., Howard, L., Windebank, A. J., & Barry, F. P. (2009). Neurotrophic factor–expressing mesenchymal stem cells survive transplantation into the contused spinal cord without differentiating into neural cells. *Tissue Engineering Part A*, *15*(10), 3049–3059.

Rosenstein, J. M., Krum, J. M., & Ruhrberg, C. (2010). VEGF in the nervous system. *Organogenesis*, *6*(2), 107–114.

Ruzicka, J., Urdzikova, L. M., Kloudova, A., Amin, A. G., Vallova, J., Kubinova, S., Schmidt, M. H., Jhanwar-Uniyal, M., & Jendelova, P. (2018). Anti-inflammatory compound curcumin and mesenchymal stem cells in the treatment of spinal cord injury in rats. *Acta Neurobiologiae Experimentalis*, *78*(4),

358–374.

Saldaña, L., Bensiamar, F., Vallés, G., Mancebo, F. J., García-Rey, E., & Vilaboa, N. (2019). Immunoregulatory potential of mesenchymal stem cells following activation by macrophage-derived soluble factors. *Stem Cell Research and Therapy*, *10*(1), 1–15.

Salgado, A. J., Fraga, J. S., Mesquita, A. R., Neves, N. M., Reis, R. L., & Sousa, N. (2010a). Role of human umbilical cord mesenchymal progenitors conditioned media in neuronal/glial cell densities, viability, and proliferation. *Stem Cells and Development*, *19*(7), 1067–1074.

Salgado, A. J., Reis, R. L., Sousa, N., & Gimble, J. M. (2010b). Adipose tissue derived stem cells secretome: soluble factors and their roles in regenerative medicine. *Current Stem Cell Research & Therapy*, *5*(2), 103–110.

Saparov, A., Ogay, V., Nurgozhin, T., Jumabay, M., & Chen, W. C. W. W. (2016). Preconditioning of human mesenchymal stem cells to enhance their regulation of the immune response. *Stem Cells International*, *2016*, 1–10.

Savic, G., Devivo, M. J., Frankel, H. L., Jamous, M. A., Soni, B. M., & Charlifue, S. (2017). Causes of death after traumatic spinal cord injury - a 70-year british study. *Spinal Cord*, *55*(10), 891–897.

Seo, Y., Shin, T.-H., & Kim, H.-S. (2019). Current strategies to enhance adipose stem cell function: an update. *International Journal of Molecular Sciences*, *20*(15), 1–32.

Serra, S. C., Costa, J. C., Assunção-Silva, R. C., Teixeira, F. G., Silva, N. A., Anjo, S. I., Manadas, B., Gimble, J. M., Behie, L. A., & Salgado, A. J. (2018). Influence of passage number on the impact of the secretome of adipose tissue stem cells on neural survival, neurodifferentiation and axonal growth. *Biochimie*, *155*, 119–128.

Shahrezaie, M., Mansour, R. N., Nazari, B., Hassannia, H., Hosseini, F., Mahboudi, H., Eftekhary, M., Kehtari, M., Veshkini, A., Ahmadi Vasmehjani, A., & Enderami, S. E. (2017). Improved stem cell therapy of spinal cord injury using GDNF-overexpressed bone marrow stem cells in a rat model. *Biologicals*, *50*, 73–80.

Shao, J., Zhu, W., Chen, X., Jia, L., Song, D., Zhou, X., Yan, W., & Zhang, Y. (2011). Factors associated with early mortality after cervical spinal cord injury. *Journal of Spinal Cord Medicine*, *34*(6), 555–562.

Shi, Y., Su, J., Roberts, A. I., Shou, P., Rabson, A. B., & Ren, G. (2012). How mesenchymal stem cells interact with tissue immune responses. *Trends in Immunology*, *33*(3), 136–143.

Silva, N. A., Moreira, J., Ribeiro-Samy, S., Gomes, E. D., Tam, R. Y., Shoichet, M. S., Reis, R. L., Sousa, N., & Salgado, A. J. (2013). Modulation of bone marrow mesenchymal stem cell secretome by

ECM-like hydrogels. *Biochimie*, *95*(12), 2314–2319.

Silva, N. A., Sousa, N., Reis, R. L., & Salgado, A. J. (2014). From basics to clinical: a comprehensive review on spinal cord injury. *Progress in Neurobiology*, *114*, 25–57.

Sivanathan, K. N., Gronthos, S., Rojas-Canales, D., Thierry, B., & Coates, P. T. (2014). Interferon-gamma modification of mesenchymal stem cells: implications of autologous and allogeneic mesenchymal stem cell therapy in allotransplantation. *Stem Cell Reviews and Reports*, *10*(3), 351–375.

Soden, R. J., Walsh, J., Middleton, J. W., Craven, M. L., Rutkowski, S. B., & Yeo, J. D. (2000). Causes of death after spinal cord injury. *Spinal Cord*, *38*(10), 604–610.

Song, Y. H., Shon, S. H., Shan, M., Stroock, A. D., & Fischbach, C. (2016). Adipose-derived stem cells increase angiogenesis through matrix metalloproteinase-dependent collagen remodeling. *Integrative Biology*, *8*(2), 205–215.

Spiller, K. L., Anfang, R. R., Spiller, K. J., Ng, J., Nakazawa, K. R., Daulton, J. W., & Vunjak-Novakovic, G. (2014). The role of macrophage phenotype in vascularization of tissue engineering scaffolds. *Biomaterials*, *35*(15), 4477–4488.

Stanfield, C. L. (2012). *Principles of human physiology.* (5th ed.). Pearson.

Staton, C. A., Reed, M. W. R., & Brown, N. J. (2009). A critical analysis of current in vitro and in vivo angiogenesis assays. *International Journal of Experimental Pathology*, *90*(3), 195–221.

Stewart, A. N., Kendziorski, G., Deak, Z. M., Brown, D. J., Fini, M. N., Copely, K. L., Rossignol, J., & Dunbar, G. L. (2017). Co-transplantation of mesenchymal and neural stem cells and overexpressing stromal-derived factor-1 for treating spinal cord injury. *Brain Research*, *1672*, 91–105.

Stewart, P. A., & Wiley, M. J. (1981). Developing nervous tissue induces formation of blood-brain barrier characteristics in invading endothelial cells: a study using quail-chick transplantation chimeras. *Developmental Biology*, *84*(1), 183–192.

Tam, S. J., & Watts, R. J. (2010). Connecting vascular and nervous system development: angiogenesis and the blood-brain barrier. *Annual Review of Neuroscience*, *33*(1), 379–408.

Teixeira, F. G., Carvalho, M. M., Neves-Carvalho, A., Panchalingam, K. M., Behie, L. A., Pinto, L., Sousa, N., & Salgado, A. J. (2015a). Secretome of mesenchymal progenitors from the umbilical cord acts as modulator of neural/glial proliferation and differentiation. *Stem Cell Reviews and Reports*, *11*(2), 288–297.

Teixeira, F. G., Carvalho, M. M., Sousa, N., & Salgado, A. J. (2013). Mesenchymal stem cells secretome: a new paradigm for central nervous system regeneration? *Cellular and Molecular Life*

*Sciences*, *70*(20), 3871–3882.

Teixeira, F. G., Panchalingam, K. M., Anjo, S. I., Manadas, B., Pereira, R., Sousa, N., Salgado, A. J., & Behie, L. A. (2015b). Do hypoxia/normoxia culturing conditions change the neuroregulatory profile of wharton jelly mesenchymal stem cell secretome? *Stem Cell Research and Therapy*, *6*(1), 1–14.

Teixeira, F. G., Panchalingam, K. M., Assunção-Silva, R., Serra, S. C., Mendes-Pinheiro, B., Patrício, P., Jung, S., Anjo, S. I., Manadas, B., Pinto, L., Sousa, N., Behie, L. A., & Salgado, A. J. (2016a). Modulation of the mesenchymal stem cell secretome using computer-controlled bioreactors: impact on neuronal cell proliferation, survival and differentiation. *Scientific Reports*, *6*(1), 27791.

Teixeira, F. G., & Salgado, A. J. (2020). Mesenchymal stem cells secretome: current trends and future challenges. *Neural Regeneration Research*, *15*(1), 75.

Teixeira, F. G., Serra, S. C., & Salgado, A. J. (2016b). Tips on how to collect and administer the mesenchymal stem cell secretome for central nervous system applications. In *Mesenchymal Stem Cells: Methods and Protocols, Methods in Molecular Biology* (Vol. 1416, pp. 457–465). Humana Press.

Thomas, E. D. (2000). Landmarks in the development of hematopoietic cell transplantation. *World Journal of Surgery*, *24*(7), 815–818.

Tjalsma, H., Bolhuis, A., Jongbloed, J. D. H., Bron, S., & van Dijl, J. M. (2000). Signal peptide-dependent protein transport in bacillus subtilis: a genome-based survey of the secretome. *Microbiology and Molecular Biology Reviews*, *64*(3), 515–547.

Tran, H., & Yao, L. (2018). Vascularization in the spinal cord: the pathological process in spinal cord injury and therapeutic approach. In *Glial Cell Engineering in Neural Regeneration* (pp. 111–126). Springer International Publishing.

Tsai, M.-J., Liou, D.-Y., Lin, Y.-R., Weng, C.-F., Huang, M.-C., Huang, W.-C., Tseng, F.-W., & Cheng, H. (2018). Attenuating spinal cord injury by conditioned medium from bone marrow mesenchymal stem cells. *Journal of Clinical Medicine*, *8*(23), 1–13.

Ulndreaj, A., Badner, A., & Fehlings, M. G. (2017). Promising neuroprotective strategies for traumatic spinal cord injury with a focus on the differential effects among anatomical levels of injury. *F1000Research*, *6*, 1–13.

Veneruso, V., Rossi, F., Villella, A., Bena, A., Forloni, G., & Veglianese, P. (2019). Stem cell paracrine effect and delivery strategies for spinal cord injury regeneration. *Journal of Controlled Release*, *300*, 141–153.

Verseijden, F., Posthumus-Van Sluijs, S. J., Pavljasevic, P., Hofer, S. O. P., Van Osch, G. J. V. M., & Farrell, E. (2010). Adult human bone marrow-and adipose tissue-derived stromal cells support the

formation of prevascular-like structures from endothelial cells in vitro. *Tissue Engineering - Part A*, *16*(1), 101–114.

Vismara, I., Papa, S., Rossi, F., Forloni, G., & Veglianese, P. (2017). Current options for cell therapy in spinal cord injury. *Trends in Molecular Medicine*, *23*(9), 831–849.

Vizoso, F., Eiro, N., Cid, S., Schneider, J., & Perez-Fernandez, R. (2017). Mesenchymal stem cell secretome: toward cell-free therapeutic strategies in regenerative medicine. *International Journal of Molecular Sciences*, *18*(9), 1–24.

Wälchli, T., Pernet, V., Weinmann, O., Shiu, J.-Y., Guzik-Kornacka, A., Decrey, G., Yuksel, D., Schneider, H., Vogel, J., Ingber, D. E., Vogel, V., Frei, K., & Schwab, M. E. (2013). Nogo-A is a negative regulator of CNS angiogenesis. *Proceedings of the National Academy of Sciences*, *110*(21), E1943–E1952.

Wälchli, T., Wacker, A., Frei, K., Regli, L., Schwab, M. E., Hoerstrup, S. P., Gerhardt, H., & Engelhardt, B. (2015). Wiring the vascular network with neural cues: a CNS perspective. *Neuron*, *87*(2), 271–296.

Wang, L., Shi, Q., Dai, J., Gu, Y., Feng, Y., & Chen, L. (2017). Increased vascularization promotes functional recovery in the transected spinal cord rats by implanted vascular endothelial growth factor-targeting collagen scaffold. *Journal of Orthopaedic Research*, *17*(3), 127–128.

Wang, M., Zhang, W., Crisostomo, P., Markel, T., Meldrum, K. K., Fu, X. Y., & Meldrum, D. R. (2007). STAT3 mediates bone marrow mesenchymal stem cell VEGF production. *Journal of Molecular and Cellular Cardiology*, *42*(6), 1009–1015.

Wang, W., Huang, X., Lin, W., Qiu, Y., He, Y., Yu, J., Xi, Y., & Ye, X. (2018). Hypoxic preconditioned bone mesenchymal stem cells ameliorate spinal cord injury in rats via improved survival and migration. *International Journal of Molecular Medicine*, *42*(5), 2538–2550.

Wang, X., Cao, K., Sun, X., Chen, Y., Duan, Z., Sun, L., Guo, L., Bai, P., Sun, D., Fan, J., He, X., Young, W., & Ren, Y. (2015). Macrophages in spinal cord injury: phenotypic and functional change from exposure to myelin debris. *Glia*, *63*(4), 635–651.

Watson, P. M. D., Paterson, J. C., Thom, G., Ginman, U., Lundquist, S., & Webster, C. I. (2013). Modelling the endothelial blood-CNS barriers: a method for the production of robust in vitro models of the rat blood-brain barrier and blood-spinal cord barrier. *BMC Neuroscience*, *14*(1), 1.

Watt, S. M., Gullo, F., Van Der Garde, M., Markeson, D., Camicia, R., Khoo, C. P., Zwaginga, J. J., Garde, M. Van Der, Markeson, D., Camicia, R., Khoo, C. P., & Zwaginga, J. J. (2013). The angiogenic properties of mesenchymal stem / stromal cells and their therapeutic potential. *British Medical Bulletin*,

*108*(1), 25–53.

Whetstone, W. D., Hsu, J. Y. C., Eisenberg, M., Werb, Z., & Noble-Haeusslein, L. J. (2003). Blood-spinal cord barrier after spinal cord injury: relation to revascularization and wound healing. *Journal of Neuroscience Research*, *74*(2), 227–239.

Wilhelm, I., Nyúl-Tóth, Á., Suciu, M., Hermenean, A., Krizbai, I. A., & Wilhelm, I. (2016). Heterogeneity of the blood-brain barrier. *Tissue Barriers*, *4*(1), 1–8.

Winkler, E. A., Bell, R. D., & Zlokovic, B. V. (2011). Central nervous system pericytes in health and disease. *Nature Neuroscience*, *14*(11), 1398–1405.

Wobma, H. M., Tamargo, M. A., Goeta, S., Brown, L. M., Duran-Struuck, R., & Vunjak-Novakovic, G. (2018). The influence of hypoxia and IFN-γ on the proteome and metabolome of therapeutic mesenchymal stem cells. *Biomaterials*, *167*(10), 226–234.

Wood, C. R., Al Delfi, I. R. T., Innes, J. F., Myint, P., & Johnson, W. E. B. (2018). Exposing mesenchymal stem cells to chondroitin sulphated proteoglycans reduces their angiogenic and neuro-adhesive paracrine activity. *Biochimie*, *155*, 26–36.

Xie, D., Ju, D., Speyer, C., Gorski, D., & Kosir, M. A. (2016). Strategic endothelial cell tube formation assay: comparing extracellular matrix and growth factor reduced extracellular matrix. *Journal of Visualized Experiments*, *114*, 1–6.

Xu, L., Nirwane, A., & Yao, Y. (2019). Basement membrane and blood-brain barrier. *Stroke and Vascular Neurology*, *4*(2), 78–82.

Yuan, X., Wu, Q., Tang, Y., Jing, Y., Li, Z., & Xiu, R. (2019). Systemic microcirculation dysfunction after low thoracic spinal cord injury in mice. *Life Sciences*, *221*, 47–55.

Zhang, G., Meredith, T. C., & Kahne, D. (2013). On the essentiality of lipopolysaccharide to gram-negative bacteria. *Current Opinion in Microbiology*, *16*(6), 779–785.

Zhang, H.-T., Luo, J., Sui, L.-S., Ma, X., Yan, Z.-J., Lin, J.-H., Wang, Y.-S., Chen, Y.-Z., Jiang, X.-D., & Xu, R.-X. (2009). Effects of differentiated versus undifferentiated adipose tissue-derived stromal cell grafts on functional recovery after spinal cord contusion. *Cellular and Molecular Neurobiology*, *29*(8), 1283–1292.

Zhang, Z., & Guth, L. (1997). Experimental spinal cord injury: Wallerian degeneration in the dorsal column is followed by revascularization, glial proliferation, and nerve regeneration. *Experimental Neurology*, *147*(1), 159–171.

Zhilai, Z., Biling, M., Sujun, Q., Chao, D., Benchao, S., Shuai, H., Shun, Y., & Hui, Z. (2016). Preconditioning in lowered oxygen enhances the therapeutic potential of human umbilical mesenchymal

stem cells in a rat model of spinal cord injury. *Brain Research*, *1642*, 426–435.

Zhou, T., Zheng, Y., Sun, L., Badea, S. R., Jin, Y., Liu, Y., Rolfe, A. J., Sun, H., Wang, X., Cheng, Z., Huang, Z., Zhao, N., Sun, X., Li, J., Fan, J., Lee, C., Megraw, T. L., Wu, W., Wang, G., & Ren, Y. (2019). Microvascular endothelial cells engulf myelin debris and promote macrophage recruitment and fibrosis after neural injury. *Nature Neuroscience*, *22*(3), 421–435.

Zhou, Z., Chen, Y., Zhang, H., Min, S., Yu, B., He, B., & Jin, A. (2013). Comparison of mesenchymal stromal cells from human bone marrow and adipose tissue for the treatment of spinal cord injury. *Cytotherapy*, *15*(4), 434–448.

# 8. Annexes

Table 1A: Statistical analysis of vascular morphogenesis parameters on indirect co-culture.

| Parameter | Groups | Mean ± SD | Statistical significance |
|---|---|---|---|
| Explant Area ($mm^2$) | CTR | 3.09 ± 0.07* | H (3) = 8.251<br>p = 0.041<br>$\eta^2$ = 0.438 |
| | ASCs | 3.33 ± 1.30* | |
| | ASCs (LPS +IFNγ) | 4.34 ± 0.91* | |
| | ASC (IL-10) | 3.37 ± 1.94* | |
| Vessel Area (%) | CTR | 2.34 ± 2.11 | F (3, 4.803) = 3.422<br>p = 0.113<br>$\omega^2$ = 0.312 |
| | ASCs | 7.79 ± 3.13 | |
| | ASCs (LPS +IFNγ) | 6.68 ± 0.33 | |
| | ASC (IL-10) | 6.50 ± 1.86 | |
| Junction Density | CTR | 3.73 ± 3.40 | F (3, 12) = 2.632<br>p = 0.098<br>$\eta^2$ = 0.397 |
| | ASCs | 13.77 ± 6.52 | |
| | ASCs (LPS +IFNγ) | 11.90 ± 1.46 | |
| | ASC (IL-10) | 12.00 ± 6.08 | |
| Total Vessel Length ($mm^{-1}$) | CTR | 0.90 ± 0.79 | F (3, 12) = 3.841<br>p = 0.039<br>$\eta^2$ = 0.490 |
| | ASCs | 3.45 ± 1.43 | |
| | ASCs (LPS +IFNγ) | 2.97 ± 0.20 | |
| | ASC (IL-10) | 2.77 ± 1.14 | |
| Average Vessel Length (mm) | CTR | 0.01 ± 0.09 | F (3, 12) = 1.692<br>p = 0.222<br>$\eta^2$ = 0.297 |
| | ASCs | 0.18 ± 0.04 | |
| | ASCs (LPS +IFNγ) | 0.22 ± 0.07 | |
| | ASC (IL-10) | 0.21 ± 0.09 | |
| End Points | CTR | 14.52 ± 12.65 | F (3, 12) = 5.061<br>p = 0.017<br>$\eta^2$ = 0.559 |
| | ASCs | 47.90 ± 14.74 | |
| | ASCs (LPS +IFNγ) | 37.74 ± 9.27 | |
| | ASC (IL-10) | 20.53 ± 8.64 | |

Table 2A: Multiple comparisons of the vascular morphogenesis parameters on indirect co-culture.

| Parameter | Groups | Multiple comparisons | Statistical significance |
|---|---|---|---|
| Explant Area ($mm^2$) | CTR vs ASCs | Dunn with Bonferroni correction | p = 1.000<br>r = 0.326 |
| | CTR vs ASCs (LPS + IFN-γ) | Dunn with Bonferroni correction | p = 0.033<br>r = 0.693 |
| | CTR vs ASCs (IL-10) | Dunn with Bonferroni correction | p = 1.000<br>r = 0.246 |
| | ASCs vs ASCs (LPS + IFN-γ) | Dunn with Bonferroni correction | p = 0.494<br>r = 0.435 |
| | ASCs vs ASCs (IL-10) | Dunn with Bonferroni correction | p = 1.000<br>r = 0.074 |
| | ASCs (LPS + IFN-γ) vs ASCs (IL-10) | Dunn with Bonferroni correction | p = 0.321<br>r = 0.483 |
| Total Vessel Length ($mm^{-1}$) | CTR vs ASCs | Tukey | p = 0.028<br>d = 2.043 |
| | CTR vs ASCs (LPS + IFN-γ) | Tukey | p = 0.099<br>d = 3.972 |
| | CTR vs ASCs (IL-10) | Tukey | p = 0.150<br>d = 1.837 |
| | ASCs vs ASCs (LPS + IFN-γ) | Tukey | p = 0.902<br>d = 0.445 |
| | ASCs vs ASCs (IL-10) | Tukey | p = 0.768<br>d = 0.525 |
| | ASCs (LPS + IFN-γ) vs ASCs (IL-10) | Tukey | p = 0.992<br>d = 0.250 |
| End Points | CTR vs ASCs | Tukey | p = 0.010<br>d = 2.371 |
| | CTR vs ASCs (LPS + IFN-γ) | Tukey | p = 0.097<br>d = 2.159 |
| | CTR vs ASCs (IL-10) | Tukey | p = 0.181<br>d = 1.894 |
| | ASCs vs ASCs (LPS + IFN-γ) | Tukey | p = 0.589<br>d = 0.801 |
| | ASCs vs ASCs (IL-10) | Tukey | p = 0.356<br>d = 1,090 |
| | ASCs (LPS + IFN-γ) vs ASCs (IL-10) | Tukey | p = 0.975<br>d = 0.386 |

Table 3A: Statistical analysis of vascular morphogenesis parameters on cultures with secretome.

| Parameter | Groups | Mean ± SD | Statistical significance |
|---|---|---|---|
| Explant Area ($mm^2$) | CTR | 2.18 ± 0.41 | F (3, 8) = 2.580<br>p = 0.126<br>$\eta^2$ = 0.492 |
| | ASCs | 2.88 ± 0.15 | |
| | ASCs (LPS +IFNγ) | 2.86 ± 0.26 | |
| | ASC (IL-10) | 2.71 ± 0.49 | |
| Vessel Area (%) | CTR | 10.05 ± 0.79 | F (3, 8) = 2.857<br>p = 0.105<br>$\eta^2$ = 0.517 |
| | ASCs | 7.27 ± 0.64 | |
| | ASCs (LPS +IFNγ) | 9.84 ± 1.90 | |
| | ASC (IL-10) | 7.44 ± 2.19 | |
| Junction Density | CTR | 16.48 ± 8.80 | F (3, 8) = 5.007<br>p = 0.030<br>$\eta^2$ = 0.653 |
| | ASCs | 12.92 ± 1.79 | |
| | ASCs (LPS +IFNγ) | 30.21 ± 8.76 | |
| | ASC (IL-10) | 11.11 ± 4.69 | |
| Total Vessel Length ($mm^{-1}$) | CTR | 4.36 ± 0.92 | F (3, 8) = 4.091<br>p = 0.049<br>$\eta^2$ = 0.605 |
| | ASCs | 3.59 ± 0.49 | |
| | ASCs (LPS +IFNγ) | 5.51 ± 1.08 | |
| | ASC (IL-10) | 3.27 ± 0.82 | |
| Average Vessel Length (mm) | CTR | 0.17 ± 0.04 | F (3, 8) = 9.148<br>p = 0.126<br>$\eta^2$ = 0.774 |
| | ASCs | 0.13 ± 0.02 | |
| | ASCs (LPS +IFNγ) | 0.29 ± 0.08 | |
| | ASC (IL-10) | 0.11 ± 0.03 | |
| End Points | CTR | 67.39 ± 14.84 | F (3, 8) = 0.284<br>p = 0.836<br>$\eta^2$ = 0.096 |
| | ASCs | 67.42 ± 0.96 | |
| | ASCs (LPS +IFNγ) | 64.55 ± 11.29 | |
| | ASC (IL-10) | 72.32 ± 9.28 | |

Table 4A: Multiple comparisons of the vascular morphogenesis parameters on cultures with secretome.

| Parameter | Groups | Multiple comparisons | Statistical significance |
|---|---|---|---|
| Junction Density | CTR vs ASCs | Tukey | p = 0.912<br>d = 0.561 |
| | CTR vs ASCs (LPS + IFN-γ) | Tukey | p = 0.132<br>d = 1.565 |
| | CTR vs ASCs (IL-10) | Tukey | p = 0.763<br>d = 0.762 |
| | ASCs vs ASCs (LPS + IFN-γ) | Tukey | p = 0.053<br>d = 2.737 |
| | ASCs vs ASCs (IL-10) | Tukey | p = 0.987<br>d = 0.510 |
| | ASCs (LPS + IFN-γ) vs ASCs (IL-10) | Tukey | p = 0.033<br>d = 2.733 |
| Total Vessel Length ($mm^{-1}$) | CTR vs ASCs | Tukey | p = 0.696<br>d = 1.052 |
| | CTR vs ASCs (LPS + IFN-γ) | Tukey | p = 0.407<br>d = 1.149 |
| | CTR vs ASCs (IL-10) | Tukey | p = 0.445<br>d = 1.256 |
| | ASCs vs ASCs (LPS + IFN-γ) | Tukey | p = 0.094<br>d = 2.295 |
| | ASCs vs ASCs (IL-10) | Tukey | p = 0.965<br>d = 0.477 |
| | ASCs (LPS + IFN-γ) vs ASCs (IL-10) | Tukey | p = 0.049<br>d = 2.338 |
| Average Vessel Length (mm) | CTR vs ASCs | Tukey | p = 0.733<br>d = 1.330 |
| | CTR vs ASCs (LPS + IFN-γ) | Tukey | p = 0.053<br>d = 2.016 |
| | CTR vs ASCs (IL-10) | Tukey | p = 0.408<br>d = 1.857 |
| | ASCs vs ASCs (LPS + IFN-γ) | Tukey | p = 0.013<br>d = 2.822 |
| | ASCs vs ASCs (IL-10) | Tukey | p = 0.927<br>d = 0.826 |
| | ASCs (LPS + IFN-γ) vs ASCs (IL-10) | Tukey | p = 0.006<br>d = 3.110 |

Table 5A: Statistical analysis of vascular morphogenesis parameters on direct co-cultures.

| Parameter | Groups | Mean ± SD | Statistical significance |
|---|---|---|---|
| Explant Area ($mm^2$) | CTR | 3.03 ± 0.41 | F (3, 9) = 3.898<br>p = 0.049<br>$\eta^2$ = 0.565 |
| | ASCs | 2.19 ± 0.35 | |
| | ASCs (LPS +IFNγ) | 2.62 ± 0.45 | |
| | ASC (IL-10) | 2.14 ± 0.28 | |
| Vessel Area (%) | CTR | 6.18 ± 1.15 | F (3, 9) = 5.245<br>p = 0.023<br>$\eta^2$ = 0.636 |
| | ASCs | 6.53 ± 1.26 | |
| | ASCs (LPS +IFNγ) | 6.66 ± 1.31 | |
| | ASC (IL-10) | 9.68 ± 1.25 | |
| Junction Density | CTR | 4.43 ± 1.59 | F (3, 4.417) = 24.496<br>p = 0.003<br>$\omega^2$ = 0.844 |
| | ASCs | 6.43 ± 1.05 | |
| | ASCs (LPS +IFNγ) | 8.09 ± 3.04 | |
| | ASC (IL-10) | 11.70 ± 0.67 | |
| Total Vessel Length ($mm^{-1}$) | CTR | 2.16 ± 0.43 | F (3, 9) = 3.197<br>p = 0.077<br>$\eta^2$ = 0.516 |
| | ASCs | 1.91 ± 0.35 | |
| | ASCs (LPS +IFNγ) | 1.94 ± 0.42 | |
| | ASC (IL-10) | 2.82 ± 0.50 | |
| Average Vessel Length (mm) | CTR | 0.047 ± 0.005 | F (3, 9) = 7.315<br>p = 0.009<br>$\eta^2$ = 0.708 |
| | ASCs | 0.032 ± 0.003 | |
| | ASCs (LPS +IFNγ) | 0.032 ± 0.006 | |
| | ASC (IL-10) | 0.033 ± 0.005 | |
| End Points | CTR | 91.81 ± 8.26 | F (3, 9) = 6.453<br>p = 0.013<br>$\eta^2$ = 0.683 |
| | ASCs | 122.23 ± 23.19 | |
| | ASCs (LPS +IFNγ) | 125.21 ± 34.75 | |
| | ASC (IL-10) | 177.95 ± 24.61 | |

Table 6A: Multiple comparisons of the vascular morphogenesis parameters on direct co-cultures.

| Parameter | Groups | Multiple comparison | Statistical significance |
|---|---|---|---|
| Explant Area ($mm^2$) | CTR vs ASCs | Tukey | p = 0.067<br>d = 2.240 |
| | CTR vs ASCs (LPS + IFN-γ) | Tukey | p = 0.560<br>d = 0.953 |
| | CTR vs ASCs (IL-10) | Tukey | p = 0.069<br>d = 2.517 |
| | ASCs vs ASCs (LPS + IFN-γ) | Tukey | p = 0.480<br>d = 1.091 |
| | ASCs vs ASCs (IL-10) | Tukey | p = 0.998<br>d = 0.158 |
| | ASCs (LPS + IFN-γ) vs ASCs (IL-10) | Tukey | p = 0.445<br>d = 1.272 |
| Vessel Area (%) | CTR vs ASCs | Tukey | p = 0.982<br>d = 0.288 |
| | CTR vs ASCs (LPS + IFN-γ) | Tukey | p = 0.962<br>d = 0.394 |
| | CTR vs ASCs (IL-10) | Tukey | p = 0.030<br>d = 2.922 |
| | ASCs vs ASCs (LPS + IFN-γ) | Tukey | p = 0.999<br>d = 0.106 |
| | ASCs vs ASCs (IL-10) | Tukey | p = 0.037<br>d = 2.523 |
| | ASCs (LPS + IFN-γ) vs ASCs (IL-10) | Tukey | p = 0.062<br>d = 2.366 |
| Junction Density | CTR vs ASCs | Games-Howell | p = 0.375<br>d = 1.551 |
| | CTR vs ASCs (LPS + IFN-γ) | Games-Howell | p = 0.401<br>d = 1.507 |
| | CTR vs ASCs (IL-10) | Games-Howell | p = 0.022<br>d = 5.974 |
| | ASCs vs ASCs (LPS + IFN-γ) | Games-Howell | p = 0.808<br>d = 0.794 |
| | ASCs vs ASCs (IL-10) | Games-Howell | p = 0.002<br>d = 5.768 |
| | ASCs (LPS + IFN-γ) vs ASCs (IL-10) | Games-Howell | p = 0.391<br>d = 1.641 |
| Average Vessel Length (mm) | CTR vs ASCs | Tukey | p = 0.011<br>d = 3.958 |
| | CTR vs ASCs (LPS + IFN-γ) | Tukey | p = 0.019<br>d = 2.646 |
| | CTR vs ASCs (IL-10) | Tukey | p = 0.024<br>d = 2.839 |
| | ASCs vs ASCs (LPS + IFN-γ) | Tukey | p = 1.000<br>d = 0.074 |

| | | | |
|---|---|---|---|
| | ASCs vs ASCs (IL-10) | Tukey | p = 0.992<br>d = 0.256 |
| | ASCs (LPS + IFN-γ) vs ASCs (IL-10) | Tukey | p = 0.998<br>d = 0.119 |
| End Points | CTR vs ASCs | Tukey | p = 0.410<br>d = 1.626 |
| | CTR vs ASCs (LPS + IFN-γ) | Tukey | p = 0.389<br>d = 1.322 |
| | CTR vs ASCs (IL-10) | Tukey | p = 0.009<br>d = 4.694 |
| | ASCs vs ASCs (LPS + IFN-γ) | Tukey | p = 0.998<br>d = 0.105 |
| | ASCs vs ASCs (IL-10) | Tukey | p = 0.061<br>d = 2.344 |
| | ASCs (LPS + IFN-γ) vs ASCs (IL-10) | Tukey | p = 0.102<br>d = 1.752 |

Table 7A: Statistical analysis of neurite outgrowth on indirect co-culture.

| Parameter | Groups | Mean ± SD | Statistical significance |
|---|---|---|---|
| Neurite Occupied Area ($\mu m^2$) | CTR | 83733.77 ± 82261.85 | F (3, 57) = 1.885<br>p = 0.142<br>$\eta^2$ = 0.090 |
| | ASCs | 156627.25 ± 102552.09 | |
| | ASCs (LPS +IFNγ) | 176156.24 ± 129893.54 | |
| | ASC (IL-10) | 134179.85 ± 138136.77 | |
| Longest Neurite (µm) | CTR | 730.00 ± 502.33 | F (3, 57) = 0.369<br>p = 0.775<br>$\eta^2$ = 0.019 |
| | ASCs | 857.81 ± 349.13 | |
| | ASCs (LPS +IFNγ) | 747.06 ± 386.18 | |
| | ASC (IL-10) | 726.92 ± 355.24 | |

Table 8A: Statistical analysis of the arborization pattern of neurite outgrowth on indirect co-culture.

| Distance (µm) | Groups | Mean ± SD | Statistical significance |
|---|---|---|---|
| 0 | Ctr | 12.47 ± 13.64 | F (3, 57) = 2.293<br>p = 0.088<br>$\eta^2$ = 0.108 |
| | ASCs | 25.06 ± 11.602 | |
| | ASCs (LPS +IFN-γ) | 26.65 ± 22.72 | |
| | ASC (IL-10) | 20.54 ± 15.20 | |
| 100 | Ctr | 22.20 ± 20.71 | F (3, 57) =1.400<br>p = 0.252<br>$\eta^2$ = 0.069 |
| | ASCs | 36.00 ± 17.37 | |
| | ASCs (LPS +IFNγ) | 32.59 ± 21.15 | |
| | ASC (IL-10) | 26.31 ± 22.96 | |
| 200 | Ctr | 18.33 ± 18.09 | F (3, 57) = 1.795<br>p = 0.158<br>$\eta^2$ = 0.086 |
| | ASCs | 32.25 ± 22.57 | |
| | ASCs (LPS +IFNγ) | 33.76 ± 23.84 | |
| | ASC (IL-10) | 22.46 ± 22.98 | |
| 300 | Ctr | 12.27 ± 12.98 | F (3, 57) = 1.810<br>p = 0.156<br>$\eta^2$ = 0.087 |
| | ASCs | 25.50 ± 20.35 | |
| | ASCs (LPS +IFNγ) | 27.35 ± 19.47 | |
| | ASC (IL-10) | 21.62 ± 24.97 | |
| 400 | Ctr | 9.40 ± 10.80 | F (3, 57) = 1.038<br>p = 0.383<br>$\eta^2$ = 0.052 |
| | ASCs | 17.75 ± 17.23 | |
| | ASCs (LPS +IFNγ) | 18.29 ± 15.36 | |
| | ASC (IL-10) | 16.69 ± 19.56 | |
| 500 | Ctr | 6.47 ± 8.18 | F (3, 57) = 1.220<br>p = 0.311<br>$\eta^2$ = 0.060 |
| | ASCs | 12.69 ± 13.43 | |
| | ASCs (LPS +IFNγ) | 13.65 ± 14.76 | |
| | ASC (IL-10) | 8.00 ± 12.07 | |
| 600 | Ctr | 2.87 ± 3.85 | F (3, 57) = 1.632<br>p = 0.192<br>$\eta^2$ = 0.079 |
| | ASCs | 8.00 ± 12.07 | |
| | ASCs (LPS +IFNγ) | 7.12 ± 8.13 | |

| | | | |
|---|---|---|---|
| | ASC (IL-10) | 3.15 ± 4.79 | |
| 700 | Ctr | 3.00 ± 5.13 | F (3, 57) = 0.573<br>p = 0.635<br>$\eta^2$ = 0.029 |
| | ASCs | 4.00 ± 6.63 | |
| | ASCs (LPS +IFNγ) | 5.82 ± 12.95 | |
| | ASC (IL-10) | 2.15 ± 2.85 | |
| 800 | Ctr | 1.07 ± 1.79 | F (3, 57) = 0.872<br>p = 0.461<br>$\eta^2$ = 0.044 |
| | ASCs | 2.19 ± 3.54 | |
| | ASCs (LPS +IFNγ) | 2.59 ± 4.69 | |
| | ASC (IL-10) | 1.08 ± 1.32 | |
| 900 | Ctr | 1.20 ± 1.98 | F (3, 57) = 0.623<br>p = 0.603<br>$\eta^2$ = 0.032 |
| | ASCs | 1.25 ± 3.04 | |
| | ASCs (LPS +IFNγ) | 2.24 ± 4.86 | |
| | ASC (IL-10) | 0.69 ± 1.25 | |
| 1000 | Ctr | 0.93 ± 1.67 | F (3, 57) = 0.306<br>p = 0.821<br>$\eta^2$ = 0.016 |
| | ASCs | 1.13 ± 2.83 | |
| | ASCs (LPS +IFNγ) | 1.35 ± 3.64 | |
| | ASC (IL-10) | 0.46 ± 0.13 | |
| 1100 | Ctr | 0.67 ± 1.18 | F (3, 57) = 0.340<br>p = 0.796<br>$\eta^2$ = 0.018 |
| | ASCs | 0.37 ± 0.89 | |
| | ASCs (LPS +IFNγ) | 0.76 ± 2.33 | |
| | ASC (IL-10) | 0.31 ± 0.75 | |
| 1200 | Ctr | 0.47 ± 1.13 | F (3, 57) = 0.406<br>p = 0.749<br>$\eta^2$ =0.021 |
| | ASCs | 0.37 ± 0.89 | |
| | ASCs (LPS +IFNγ) | 0.47 ± 1.51 | |
| | ASC (IL-10) | 0.08 ± 0.277 | |
| 1300 | Ctr | 0.08 ± 0.99 | F (3, 57) = 0.436<br>p = 0.728<br>$\eta^2$ = 0.022 |
| | ASCs | 0.37 ± 0.89 | |
| | ASCs (LPS +IFNγ) | 0.29 ± 1.21 | |
| | ASC (IL-10) | 0.08 ± 0.277 | |

| | | | |
|---|---|---|---|
| 1400 | Ctr | 0.40 ± 1.12 | F (3, 57) = 0.302<br>p = 0.824<br>$\eta^2$ = 0.016 |
| | ASCs | 0.13 ± 0.34 | |
| | ASCs (LPS +IFNγ) | 0.29 ± 1.21 | |
| | ASC (IL-10) | 0.15 ± 0.56 | |
| 1500 | Ctr | 0.13 ± 0.52 | F (3, 57) = 0.723<br>p = 0.542<br>$\eta^2$ =0.037 |
| | ASCs | 0.00 ± 0.00 | |
| | ASCs (LPS +IFNγ) | 0.06 ± 0.243 | |
| | ASC (IL-10) | 0.00 ± 0.00 | |
| 1600 | Ctr | 0.07 ± 0.26 | F (3, 57) = 1.023<br>p = 0.389<br>$\eta^2$ = 0.051 |
| | ASCs | 0.00 ± 0.00 | |
| | ASCs (LPS +IFNγ) | 0.00 ± 0.00 | |
| | ASC (IL-10) | 0.00 ± 0.00 | |

Table 9A: Statistical analysis of neurite outgrowth on cultures with secretome.

| Parameter | Groups | Mean ± SD | Statistical significance |
|---|---|---|---|
| Neurite Occupied Area ($\mu m^2$) | ASCs | 51109.39 ± 39210.73 | F (2, 21) = 0.877<br>p = 0.431<br>$\eta^2$ = 0.077 |
| | ASCs (LPS +IFNγ) | 41892.52 ± 32157.74 | |
| | ASC (IL-10) | 29097.66 ± 22907.44 | |
| Longest Neurite (μm) | ASCs | 625.00 ± 238.75 | F (2, 21) = 0.889<br>p = 0.426<br>$\eta^2$ = 0.078 |
| | ASCs (LPS +IFNγ) | 552.50 ± 314.786 | |
| | ASC (IL-10) | 443.75 ± 177.155 | |

Table 10A: Statistical analysis of the arborization pattern of neurite outgrowth on cultures with secretome.

| Distance (μm) | Groups | Mean ± SD | Statistical significance |
|---|---|---|---|
| 0 | ASCs | 26.00 ± 42.33 | F (2, 21) = 0.903<br>p = 0.421<br>$\eta^2$ = 0.079 |
| | ASCs (LPS +IFN-γ) | 10.30 ± 10.56 | |
| | ASC (IL-10) | 13.63 ± 13.07 | |
| 100 | ASCs | 15.67 ± 10.63 | F (2, 21) = 2.679<br>p = 0.092<br>$\eta^2$ = 0.203 |
| | ASCs (LPS +IFN-γ) | 7.60 ± 5.54 | |
| | ASC (IL-10) | 7.88 ± 6.24 | |
| 200 | ASCs | 10.50 ± 7.50 | F (2, 21) = 0.040<br>p = 0.961<br>$\eta^2$ = 0.004 |
| | ASCs (LPS +IFN-γ) | 9.20 ± 9.57 | |
| | ASC (IL-10) | 9.88 ± 9.33 | |
| 300 | ASCs | 6.67 ± 5.89 | F (2, 21) = 0.354<br>p = 0.706<br>$\eta^2$ = 0.033 |
| | ASCs (LPS +IFN-γ) | 6.10 ± 5.99 | |
| | ASC (IL-10) | 4.38 ± 4.37 | |
| 400 | ASCs | 5.50 ±4.97 | F (2, 21) =1.199<br>p = 0.321<br>$\eta^2$ = 0.102 |
| | ASCs (LPS +IFN-γ) | 4.00 ± 3.74 | |
| | ASC (IL-10) | 2.38 ± 2.62 | |
| 500 | ASCs | 2.00 ± 2.28 | F (2, 21) = 1.734<br>p = 0.201<br>$\eta^2$ = 0.142 |
| | ASCs (LPS +IFN-γ) | 3.00 ± 3.68 | |
| | ASC (IL-10) | 0.63 ± 0.74 | |
| 600 | ASCs | 0.83 ± 1.17 | F (2, 21) = 0.909<br>p = 0.418<br>$\eta^2$ = 0.080 |
| | ASCs (LPS +IFN-γ) | 1.50 ± 2.84 | |
| | ASC (IL-10) | 0.25 ± 0.46 | |
| 700 | ASCs | 0.50 ± 1.23 | F (2, 21) = 1.056<br>p = 0.366<br>$\eta^2$ = 0.091 |
| | ASCs (LPS +IFN-γ) | 1.60 ± 3.53 | |
| | ASC (IL-10) | 0.00 ± 0.00 | |
| 800 | ASCs | 1.00 ± 2.45 | F (2, 21) = 0.549<br>p = 0.586<br>$\eta^2$ = 0.050 |
| | ASCs (LPS +IFN-γ) | 1.00 ± 2.83 | |
| | ASC (IL-10) | 0.00 ± 0.00 | |

| | | | |
|---|---|---|---|
| 900 | ASCs | 0.17 ± 0.41 | F (2, 21) = 1.011<br>p = 0.381<br>$\eta^2$ = 0.088 |
| | ASCs (LPS +IFN-γ) | 0.70 ± 1.64 | |
| | ASC (IL-10) | 0.00 ± 0.00 | |
| 1000 | ASCs | 0.17 ± 0.41 | F (2, 21) = 0.941<br>p = 0.406<br>$\eta^2$ = 0.082 |
| | ASCs (LPS +IFN-γ) | 0.90 ± 2.23 | |
| | ASC (IL-10) | 0.00 ± 0.00 | |

Table 11A: Statistical analysis of neurite outgrowth on direct co-cultures.

| Parameter | Groups | Mean ± SD | Statistical significance |
|---|---|---|---|
| Neurite Occupied Area ($\mu m^2$) | ASCs | 327453.33 ± 119758.36 | F (2, 13.314) = 0.485<br>p = 0.625<br>$\omega^2$ = 0.047 |
| | ASCs (LPS +IFNγ) | 302429.99 ± 261915.98 | |
| | ASC (IL-10) | 246550.50 ± 180037.69 | |
| Longest Neurite (µm) | ASCs | 1587.50 ± 70.27 | F (2, 10.395) = 0.134<br>p = 0.876<br>$\omega^2$ = 0.081 |
| | ASCs (LPS +IFNγ) | 1555.56 ± 467.34 | |
| | ASC (IL-10) | 1465.63 ± 685.95 | |

Table 12A: Statistical analysis of the arborization pattern of neurite outgrowth on direct co-cultures.

| Distance (µm) | Groups | Mean ± SD | Statistical significance |
|---|---|---|---|
| 0 | ASCs | 91.17 ± 63.50 | F (2, 20) = 0.857<br>p = 0.440<br>$\eta^2$ = 0.079 |
| | ASCs (LPS +IFN-γ) | 68.89 ± 53.48 | |
| | ASC (IL-10) | 53.00 ± 46.73 | |
| 100 | ASCs | 89.67 ± 26.85 | F (2, 20) = 0.493<br>p = 0.618<br>$\eta^2$ = 0.047 |
| | ASCs (LPS +IFN-γ) | 75.67 ± 53.23 | |
| | ASC (IL-10) | 62.75 ± 58.94 | |
| 200 | ASCs | 88.17 ± 37.72 | F (2, 20) = 0.064<br>p = 0.938<br>$\eta^2$ = 0.006 |
| | ASCs (LPS +IFN-γ) | 78.11 ± 65.96 | |
| | ASC (IL-10) | 78.25 ± 62.55 | |
| 300 | ASCs | 73.50 ± 30.97 | F (2, 20) = 0.014<br>p = 0.986<br>$\eta^2$ = 0.001 |
| | ASCs (LPS +IFN-γ) | 69.67 ± 61.05 | |
| | ASC (IL-10) | 69.13 ± 54.41 | |
| 400 | ASCs | 57.50 ± 21.62 | F (2, 20) = 0.165<br>p = 0.849<br>$\eta^2$ = 0.016 |
| | ASCs (LPS +IFN-γ) | 59.56 ± 55.42 | |
| | ASC (IL-10) | 71.25 ± 57.90 | |
| 500 | ASCs | 49.50 ± 22.94 | F (2, 20) = 0.132<br>p = 0.877<br>$\eta^2$ = 0.013 |
| | ASCs (LPS +IFN-γ) | 46.33 ± 44.33 | |
| | ASC (IL-10) | 56.13 ± 43.20 | |
| 600 | ASCs | 39.00 ± 16.04 | F (2, 20) = 0.124<br>p = 0.884<br>$\eta^2$ = 0.012 |
| | ASCs (LPS +IFN-γ) | 37.78 ± 39.16 | |
| | ASC (IL-10) | 45.25 ± 32.53 | |
| 700 | ASCs | 27.83 ± 13.70 | F (2, 20) = 0.261<br>p = 0.773<br>$\eta^2$ = 0.025 |
| | ASCs (LPS +IFN-γ) | 28.89 ± 31.28 | |
| | ASC (IL-10) | 36.88 ± 28.14 | |
| 800 | ASCs | 23.17 ± 14.13 | F (2, 20) = 0.176<br>p = 0.840<br>$\eta^2$ = 0.017 |
| | ASCs (LPS +IFN-γ) | 24.67 ± 27.83 | |

| | | | |
|---|---|---|---|
| | ASC (IL-10) | 30.13 ± 24.35 | |
| 900 | ASCs | 18.83 ± 10.94 | F (2, 20) = 0.016<br>p = 0.984<br>$\eta^2$ = 0.002 |
| | ASCs (LPS +IFN-γ) | 18.78 ± 24.50 | |
| | ASC (IL-10) | 20.25 ± 14.62 | |
| 1000 | ASCs | 14.17 ± 7.23 | F (2, 20) = 0.026<br>p = 0.974<br>$\eta^2$ = 0.003 |
| | ASCs (LPS +IFN-γ) | 15.78 ± 19.43 | |
| | ASC (IL-10) | 15.75 ± 12.05 | |
| 1100 | ASCs | 7.50 ± 4.85 | F (2, 20) = 0.405<br>p = 0.673<br>$\eta^2$ = 0.039 |
| | ASCs (LPS +IFN-γ) | 12.89 ± 15.97 | |
| | ASC (IL-10) | 10.25 ± 8.07 | |
| 1200 | ASCs | 6.00 ± 3.85 | F (2, 20) = 0.299<br>p = 0.745<br>$\eta^2$ = 0.029 |
| | ASCs (LPS +IFN-γ) | 9.44 ± 11.87 | |
| | ASC (IL-10) | 8.50 ± 6.12 | |
| 1300 | ASCs | 4.33 ± 3.08 | F (2, 20) = 0.384<br>p = 0.686<br>$\eta^2$ = 0.037 |
| | ASCs (LPS +IFN-γ) | 7.67 ± 11.87 | |
| | ASC (IL-10) | 8.00 ± 5.90 | |
| 1400 | ASCs | 3.33 ± 1.97 | F (2, 20) = 0.313<br>p = 0.734<br>$\eta^2$ = 0.030 |
| | ASCs (LPS +IFN-γ) | 5.78 ± 8.54 | |
| | ASC (IL-10) | 5.13 ± 3.80 | |
| 1500 | ASCs | 1.67 ± 0.82 | F (2, 20) = 0.578<br>p = 0.570<br>$\eta^2$ = 0.055 |
| | ASCs (LPS +IFN-γ) | 5.00 ± 9.25 | |
| | ASC (IL-10) | 1.13 ± 1.46 | |
| 1600 | ASCs | 0.67 ± 0.82 | F (2, 20) = 0.800<br>p = 0.463<br>$\eta^2$ = 0.074 |
| | ASCs (LPS +IFN-γ) | 2.33 ± 3.97 | |
| | ASC (IL-10) | 1.13 ± 1.46 | |
| 1700 | ASCs | 0.17 ± 0.41 | F (2, 20) = 0.901<br>p = 0.422<br>$\eta^2$ = 0.083 |
| | ASCs (LPS +IFN-γ) | 1.89 ± 3.79 | |
| | ASC (IL-10) | 0.88 ± 1.13 | |

| | | | |
|---|---|---|---|
| 1800 | ASCs | 0.00 ± 0.00 | F (2, 20) = 0.786<br>p = 0.469<br>$\eta^2$ = 0.073 |
| | ASCs (LPS +IFN-γ) | 0.78 ± 1.716 | |
| | ASC (IL-10) | 0.75 ± 1.165 | |
| 1900 | ASCs | 0.00 ± 0.00 | F (2, 20) = 0.791<br>p = 0.467<br>$\eta^2$ = 0.073 |
| | ASCs (LPS +IFN-γ) | 0.67 ± 1.66 | |
| | ASC (IL-10) | 1.00 ± 1.77 | |
| 2000 | ASCs | 0.00 ± 0.00 | F (2, 20) = 0.850<br>p = 0.442<br>$\eta^2$ = 0.078 |
| | ASCs (LPS +IFN-γ) | 0.56 ± 1.13 | |
| | ASC (IL-10) | 0.87 ± 1.73 | |
| 2100 | ASCs | 0.00 ± 0.00 | F (2, 20) = 0.881<br>p = 0.430<br>$\eta^2$ = 0.081 |
| | ASCs (LPS +IFN-γ) | 0.33 ± 0.71 | |
| | ASC (IL-10) | 0.13 ± 0.354 | |
| 2200 | ASCs | 0.00 ± 0.00 | F (2, 20) = 0.761<br>p = 0.480<br>$\eta^2$ = 0.071 |
| | ASCs (LPS +IFN-γ) | 0.22 ± 0.67 | |
| | ASC (IL-10) | 0.00 ± 0.00 | |
| 2300 | ASCs | 0.00 ± 0.00 | F (2, 20) = 0.761<br>p = 480<br>$\eta^2$ = 0.071 |
| | ASCs (LPS +IFN-γ) | 0.22 ± 0.67 | |
| | ASC (IL-10) | 0.00 ± 0.00 | |

Table 13A: Statistical analysis of gene expression relative fold values.

| Gene | Groups | Mean ± SD | Statistical significance |
|---|---|---|---|
| *VEGF* | ASCs | 1.00 ± 0.08 | F (2, 4.287) = 8.097<br>p = 0.035<br>$\omega^2$ = 0.612 |
| | ASCs (LPS +IFNγ) | 1.35 ± 0.13 | |
| | ASC (IL-10) | 1.47 ± 0.42 | |
| *Angiogenin-1* | ASCs | 1.00 ± 0.11 | F (2, 7) = 5.72<br>p = 0.034<br>$\eta^2$ = 0.620 |
| | ASCs (LPS +IFNγ) | 0.67 ± 0.09 | |
| | ASC (IL-10) | 1.00 ± 0.18 | |
| *NGF* | ASCs | 0.95 ± 0.02 | F (2, 7) = 10.020<br>p = 0.009<br>$\eta^2$ = 0.747 |
| | ASCs (LPS +IFNγ) | 0.82 ± 0.05 | |
| | ASC (IL-10) | 1.02 ± 0.08 | |
| *BDNF* | ASCs | 1.00 ± 0.21 | F (2, 7) = 2.47<br>p = 0.154<br>$\eta^2$ = 0.414 |
| | ASCs (LPS +IFNγ) | 0.71 ± 0.07 | |
| | ASC (IL-10) | 0.74 ± 0.21 | |
| *IL-6* | ASCs | 1.00 ± 0.05 | F (2, 7) = 13.542<br>p = 0.004<br>$\eta^2$ = 0.794 |
| | ASCs (LPS +IFNγ) | 1.03 ± 0.04 | |
| | ASC (IL-10) | 1.14 ± 0.25 | |
| *FGF-2* | ASCs | 1.00 ± 0.03 | F (2, 7) = 0.663<br>p = 0.545<br>$\eta^2$ = 0.159 |
| | ASCs (LPS +IFNγ) | 1.34 ± 0.07 | |
| | ASC (IL-10) | 0.99 ± 0.13 | |
| *CXCL1* | ASCs | 1.00 ± 0.12 | F (2, 7) = 1.994<br>p = 0.206<br>$\eta^2$ = 0.363 |
| | ASCs (LPS +IFNγ) | 1.18 ± 0.17 | |
| | ASC (IL-10) | 0.95 ± 0.17 | |
| *CXCL2* | ASCs | 1.00 ± 0.36 | F (2, 7) = 0.943<br>p = 0.434<br>$\eta^2$ = 0.212 |
| | ASCs (LPS +IFNγ) | 1.15 ± 0.31 | |
| | ASC (IL-10) | 0.87 ± 0.13 | |

Table 14A: Multiple comparisons on gene expression relative fold values.

| Gene | Groups | Multiple comparisons | Statistical significance |
|---|---|---|---|
| *VEGF* | ASCs vs ASCs (LPS + IFN-γ) | Games-Howell | p = 0.047<br>d = 3.250 |
| | ASCs vs ASCs (IL-10) | Games-Howell | p = 0.217<br>d = 1.400 |
| | ASCs (LPS + IFN-γ) vs ASCs (IL-10) | Games-Howell | p = 0.877<br>d = 0.330 |
| *Angiogenin-1* | ASCs vs ASCs (LPS + IFN-γ) | Tukey | p = 0.054<br>d = 3.412 |
| | ASCs vs ASCs (IL-10) | Tukey | p = 0.999<br>d = 0.032 |
| | ASCs (LPS + IFN-γ) vs ASCs (IL-10) | Tukey | p = 0.044<br>d = 2.144 |
| *NGF* | ASCs vs ASCs (LPS + IFN-γ) | Tukey | p = 0.022<br>d = 0.303 |
| | ASCs vs ASCs (IL-10) | Tukey | p = 0.925<br>d = 0.022 |
| | ASCs (LPS + IFN-γ) vs ASCs (IL-10) | Tukey | p = 0.010<br>d = 0.206 |
| *IL-6* | ASCs vs ASCs (LPS + IFN-γ) | Tukey | p = 0.008<br>d =6.519 |
| | ASCs vs ASCs (IL-10) | Tukey | p = 0.990<br>d = 0.096 |
| | ASCs (LPS + IFN-γ) vs ASCs (IL-10) | Tukey | p = 0.005<br>d = 3.106 |